Folia Histochemica et Cytobiologica
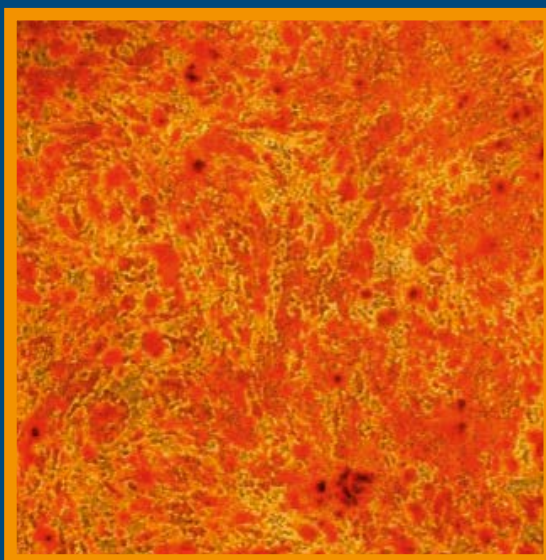
Scientific quarterly devoted to problems of histochemistry, cytochemistry and cell & tissue biology

Folia Histochemica et Cytobiologica

Official Journal of the Polish Society for Histochemistry and Cytochemistry

POLISH SOCIETY FOR HISTOCHEMISTRY AND CYTOCHEMISTRY STATEMENT OF FOLIA HISTOCHEMICA ET CYTOBIOLOGICA EDITORIAL POLICY

Folia Histochemica et Cytobiologica is an international, English-language journal devoted to the rapidly developing fields of histochemistry, cytochemistry, cell and tissue biology.

The Folia Histochemica et Cytobiologica publishes papers that meet the needs and intellectual interests of medical professionals, basic scientists, college and university teachers and students. Prospective authors should read most recent issues of FHC to determine the appropriateness of a possible contribution. However, such an examination does not provide an infallible guide because editorial policy is always under review. Technical correctness is necessary, but it is not the only condition for acceptance. Clarity of exposition and potential interest of the readers are important considerations; it is the reader, not the author, who must receive the benefit of the doubt.

Folia Histochemica et Cytobiologica publishes review articles, original articles, short communications and proceedings of scientific congresses/symposia. Fields of particular interests include development and application of modern techniques in histochemistry and cell biology, cell biology and pathology, cell-microenvironment interactions, tissue organization and pathology.

Manuscripts announcing new theoretical or experimental results, or manuscripts questioning well-established and successful theories, are highly desirable and are a subject for evaluation by specialists. Manuscripts describing original research that clarifies past misunderstandings or allows a broader view of a subject are acceptable. Manuscripts that demonstrate new relations between apparently unrelated areas of fields of interests are appropriate. Manuscripts that show new ways of understanding, demonstrating, or deriving familiar results are also acceptable. Such manuscripts must provide some original cytobiological insight and not just a clever derivation.

Regularly, review or tutorial articles are published, often of a length greater than that of the average article. Most of these articles are a subject of a review; authors planning such articles are asked to consult with the editors at an early stage.

Most readers of a particular article will be specialists in the subject matter presented; the context within which the paper is presented should be established in the order given in Instructions for Authors. Manuscripts must be technically correct and must take proper cognizance of previous work on the same subject regardless of where it may have appeared. Such referencing is especially important for reminders of once well known ideas, proofs, or techniques that may have again become useful to readers. It is the responsibility of the author to provide adequate references; editors and referees will not do the literature search that should have been done by the authors. The references are a matter of review though.

Contributions considered include: Regular Articles (Papers), Short Communications, Review Articles, Conference Proceeding, Book Reviews and Technical Notes, which describe new laboratory methods or substantial improvements of the existing techniques. Regular articles should be about five journal pages or less in length. Short communications are usually confined to the discussion of a single concept and should be about two journal pages in length. Review articles are confined to a broad discussion and should contain the most recent knowledge about the subject.

Instructions concerning the preparation of manuscripts are given in the Information for Authors. Care in following those instructions will permit editors and referees to devote more time to thoughtful evaluation of contributions and will ultimately lead to a better, more interesting Journal.

Copying information, in part or in whole by any means is prohibited without a written permission from the owner.

SUBSCRIPTION

Folia Histochemica et Cytobiologica is available for paper subscription (print on demand).
To read and download articles for free as pdf document, visit http://czasopisma.viamedica.pl/fhc

Publisher: VM Media sp. z o.o. VM Group sp.k., Swietokrzyska St. 73, 80–180 Gdansk, http://www.viamedica.pl, wap.viamedica.pl

Illustration on the cover: *Mineralized nodules present in the culture of rat bone marrow mesenchymal stem cells were visualized by Alizarin red staining* (see: Wang Y *et al.*, pp. 66–73)

© Polish Society for Histochemistry and Cytochemistry

Folia Histochemica et Cytobiologica

Official Journal of the Polish Society for Histochemistry and Cytochemistry

ORIGINAL PAPER

Reactivity of astrocytes in hippocampal CA1 area in rats after administration of habanero peppers

Jadwiga Jaworska-Adamu[1], Aleksandra Krawczyk[1], Karol Rycerz[1], Marcin Golynski[2]

[1]Department of Animal Anatomy and Histology, Faculty of Veterinary Medicine,
University of Life Sciences, Lublin, Poland
[2]Faculty of Biological and Veterinary Sciences, Nicolaus Copernicus University in Torun, Torun,
Poland

Abstract

Introduction. Astrocytes react to microenvironmental changes. Their reactivity is manifested by an increase in glial fibrillary acidic protein (GFAP) and S100β protein levels, hypertrophy and hyperplasia. The aim of the study was to analyse immunoreactive GFAP (GFAP-IR) and S100β (S100β-IR) astrocytes of hippocampal CA1 area in adult rats intragastrically (*i.g.*) treated with habanero peppers.

Material and methods. Brains from 10 control rats (group C) and 10 rats receiving oil suspension of habanero fruits for 7 days (group I-7) or 28 days (group II-28) were used. Antibodies against GFAP and S100β were used for immunohistochemistry. Morphology and distribution of astrocytes was evaluated under light microscope and their density was quantitatively analysed.

Results. In the CA1 hippocampal area of group II-28 rats, GFAP-IR cells with numerous, branched processes were observed. S100β-IR astrocytes had delicate, single processes in comparison with cells without processes observed in groups I-7 and C. In groups I-7 and II-28, GFAP-IR astrocytes' density significantly increased in SR — *stratum radiatum* of hippocampal CA1 area. In group I-7, a density of cells with the expression of S100β was significantly increased in SO — *stratum oriens* layer. In group II-28, the density of S100β-IR astrocytes was decreased.

Conclusions. Habanero peppers administrated to rats, especially for a longer time, caused reactive changes in the astrocytes in hippocampal CA1 area, and thus these glial cells may protect neurons against excitotoxic damage. *(Folia Histochemica et Cytobiologica 2021, Vol. 59, No. 1, 1–7)*

Key words: rat; hippocampus; CA1; astrocytes; GFAP; S100β; capsaicin; IHC

Introduction

Astrocytes of the central nervous system (CNS) are necessary for the proper functioning of the brain. These cells are the structural and metabolic support for neurons. They regulate the extracellular concentration of ions, metabolites, and neurotransmitters in the CNS. Astroglia is also the source of many compounds that affect neuronal and synaptic plasticity, *e.g.* during the induction of long-term potentiation (LTP). In addition, it plays an important role in neurogenesis and synaptogenesis [1–4]. In the course of physiological and pathological processes astrocytes dynamically react to changes in their microenvironment. Their reactivity is manifested by increased expression and synthesis of various proteins, *e.g.* the glial fibrillary acidic protein (GFAP) and S100β protein. Furthermore, overgrowth of cell bodies and cytoplasmic processes (hypertrophy), and glial proliferation (hyperplasia) are observed [5, 6]. Many different endogenous and exogenous factors lead to the reactivity of the astrocytes. Stimulation of the glia is also influenced by diet and living conditions of animals

Correspondence address: Aleksandra Krawczyk, PhD
Department of Animal Anatomy and Histology,
Faculty of Veterinary Medicine,
University of Life Sciences,
Akademicka St. 12, 20–033 Lublin, Poland
e-mail: aleksandra.krawczyk@up.lublin.pl

[7, 8]. In the CA1 area of the hippocampus of mice housed for 8 weeks in the enriched environment, *e.g.* with various toys, tunnels, hideouts, astroglial hypertrophy was observed [8]. Increased synthesis of GFAP and glutamine synthetase (GS) has been shown in the arcuate nucleus and the median eminence in rats treated subcutaneously with capsaicin (CAP) [9]. CAP is an alkaloid contained in habanero peppers (*Capsicum chinense Jacq.*) which, due to spicy taste, are often used as culinary additive. Capsaicin has analgesic, antibacterial and antioxidant characteristics. At low doses, it is characterized by low toxicity, but in large amounts it can have an adverse effect on the body. After intravenous or subcutaneous administration, this alkaloid can be detected in an unchanged form in the CNS. CAP binds to neuronal receptors and astrocytic vanilloid 1 receptor (TRPV1). Some authors suggested that TRPV1 affects the synaptic plasticity in the hippocampal CA1 area [10–13]. Furthermore, it was found that the stimulation of TRPV1 receptor can lead to excessive activity of pyramidal neurons and the induction of seizures. Such a phenomenon is observed in response to a high temperature that activates TRPV1 during fever [11].

The hippocampus controls various mechanisms that affect the animal behaviour. This brain area is involved in learning and memory processes, which depend on *inter alia* induction of LTP. Neurons of hippocampal CA1 area form a characteristic, four-layered arrangement. *Stratum oriens* (SO) contains basket cells and axons of pyramidal neurons which bodies are present in the *stratum pyramidale* (SP), dendrites in the *stratum radiatum* (SR), and their endings are located in the *stratum lacunosum moleculare* (SLM) [14, 15].

So far, intragastric (*i.g.*) administration of habanero peppers, as well as the CAP, has not been studied in hippocampal astroglia. The aim of the study was to carry out morphological and quantitative analyses of GFAP-immunoreactive (GFAP-IR) and S100β-immunoreactive (S100β -IR) astrocytes of hippocampal CA1 area of rats treated intragastrically with habanero peppers at various periods of time.

Material and methods

The experiments were approved by the Second Local Ethics Committee in Lublin (No. 21/2013). A total of 20 male Wistar rats (120–125 g) were used for the study. Animals were housed in an air-conditioned room with a relative humidity of 45–47% and a temperature of 22–23°C in 12 h light/12 h dark cycles. Rats were fed with commercial feed for laboratory animals (LSM, Agropol Motycz Poland) with permanent access to water *ad libitum*. The period of acclimatization before experiments was 16 days, and the duration of experiment was 7 or 28 days. The animals were randomly divided into two study groups which received habanero peppers, i.e. I-7 and II-28, and their respective controls (C-7, C-28). Every 12 h, approx. 0.5 ml of pure peanut oil was administrated to rats in the control groups and rats from groups I-7 and II-28 received the oily suspension of the grounded dried habanero peppers (containing 7.64 mg/d.m. capsaicin and dihydrocapsaicin) at a dose of 0.08 g d.m./kg b.w. After the experiment, all animals were euthanized. Then, the brains were dissected and fixed in buffered 10% formalin (pH 7.0) for 12 h at 4°C. The material was embedded in paraffin blocks using routine histological techniques. For further analyses frontal 6 μm-thick sections containing hippocampus were used (A 4230 μm — A 3750 μm, according to the atlas by König and Klippel) [16].

Staining by the indirect peroxidase-antiperoxidase (PAP) method. Immunochemical reactions were performed on deparaffinised and rehydrated sections prepared from each animal. For the inhibition of the reactivity of endogenous peroxidase 3% H_2O_2 was used for 30 min at room temperature (RT). Then, in order to remove background colouring, sections were treated with 10% goat serum (G9023; SigmaAldrich, St. Louis, MO, USA) for 20 min. A set of antibodies (SigmaAldrich) and reagents diluted in 0.5 M TRIS buffer (TBS) at pH 7.6 according to the manufacturer's instructions were used for the immunostaining. To reveal astrocytic proteins a monoclonal rabbit anti-glial fibrillary acidic protein (GFAP, 1:400 G9269 SigmaAldrich) antibody and mouse anti-S100β protein (1:1000 S2532; SigmaAldrich) antibody were used. Incubation of the material with these antibodies was carried out for 24 h at 4°C. Afterwards, species appropriate secondary IgG — peroxidase antibody (1:400 A9169 SigmaAldrich) was used for 1 h at RT. Diaminobenzidine (DAB, SigmaAldrich) was used as chromogen. Successively, the preparations were counterstained with Mayer's haematoxylin. GFAP-IR and S100β-IR astrocytes of CA1 area were observed and photographed under light microscope Olympus BX 51 (Olympus, Tokyo, Japan) with Olympus Color View IIIu digital camera. Based on the immunoreactivity for GFAP and S100β the morphology of the astrocytes and their distribution in the different layers of the hippocampal CA1 area were analysed [17].

Quantitative and statistical analyses. The mean density of GFAP and S100β immunopositive cells were analysed in layers of hippocampal CA1 area using Cell⌃D programme (Olympus). For each examined protein, 5 sections from each animal were randomly selected. Next, two photomicrographs of the hippocampal CA1 area were taken from each section. A grid of squares of 150 μm × 150 μm

$(22.5 \times 10^{-3}$ mm$^2)$ was imposed on the photographs. The size of the squares was selected in a way that the test area was the same for all layers of the studied regions. Only the squares which entirely covered the studied layer were chosen for counting. GFAP-IR and S100β-IR astrocytes were counted in two randomly chosen squares of the grid. Finally, 100 measurements of GFAP-IR and S100β-IR astrocytes density were collected from each group. Statistical analyses were performed using R 3.0.2 programme. Means were compared by the one-way analysis of variance (ANOVA) and the Tukey HSD post hoc test. The normal distribution of data was assessed using the Shapiro-Wilk test. The data that did not meet the condition of normal distribution was compared using the non-parametric Kruskall-Wallis test. The significance factor of all tests was set to $\alpha = 0.05$.

Results

Microscopic analysis of the GFAP-IR and S100β-IR astrocytes of the hippocampal CA1 area

The duration of the experiment had no effect on the results obtained in the control groups; hence, the data obtained for groups C-7 and C-28 were consolidated and presented together as one control group (C). In the hippocampal CA1 area, all the examined groups of animals (C, I-7 and II-28) showed GFAP-IR and S100β-IR cells. The greatest accumulation of astrocytes expressing both proteins was observed in the SLM (Figs. 1 A–C, 2 A–C). In group II-28 in all layers of the CA1 area GFAP-IR astrocytes were characterized by numerous and branched processes (Fig. 1C). In groups C and I-7 S100β-IR astrocytes without processes were observed in the SO, SP, SR, and SLM of hippocampal CA1 area (Fig. 2 A, B). However, in the group II-28 some part of S100β-IR astrocytes were similar to those observed in groups C and I-7, and the rest of cells had a delicate, branched processes extending from their bodies (Fig. 2C).

Quantitative analyses of GFAP-IR and S100β-IR astrocytes of the hippocampal CA1 area

The density of GFAP-IR astrocytes did not differ significantly between control and I-7, II-28 groups of animals in most layers of the CA1 area of the hippocampus. A statistically significant increase in cell density was demonstrated only in SR of CA1 area in both I-7 and II-28 groups (Fig. 3).

The density of S100β-IR astrocytes was comparable in SP and SR layers of CA1 area in all examined individuals. The density of S100β-IR astrocytes in SO of hippocampal CA1 area was significantly increased in group I-7 rats. However, in the SLM the number of S100β-IR astrocytes significantly decreased in the studied group II-28 of animals (Fig. 4).

Discussion

These studies, carried out with use of antibodies against GFAP and S100β, demonstrated differential reactivity of glia in the hippocampal CA1 area of rats after 7 and 28 days of treatment with habanero
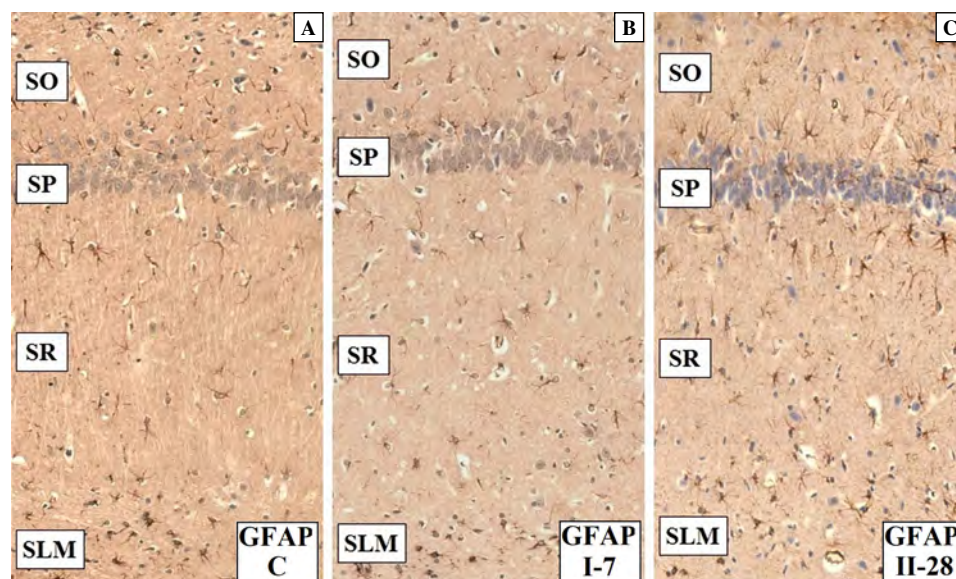

Figure 1. The GFAP-immunoreactive (-IR) astrocytes in rat hippocampal CA1 area of control (**C**), and animals which received habanero pepper for 7 or 28 days (groups I-7, II-28, respectively). SO — *stratum oriens*, SP — *stratum pyramidale*, SR — *stratum radiatum*, SLM — *stratum lacunosum moleculare*. Magnification approx. 200×.
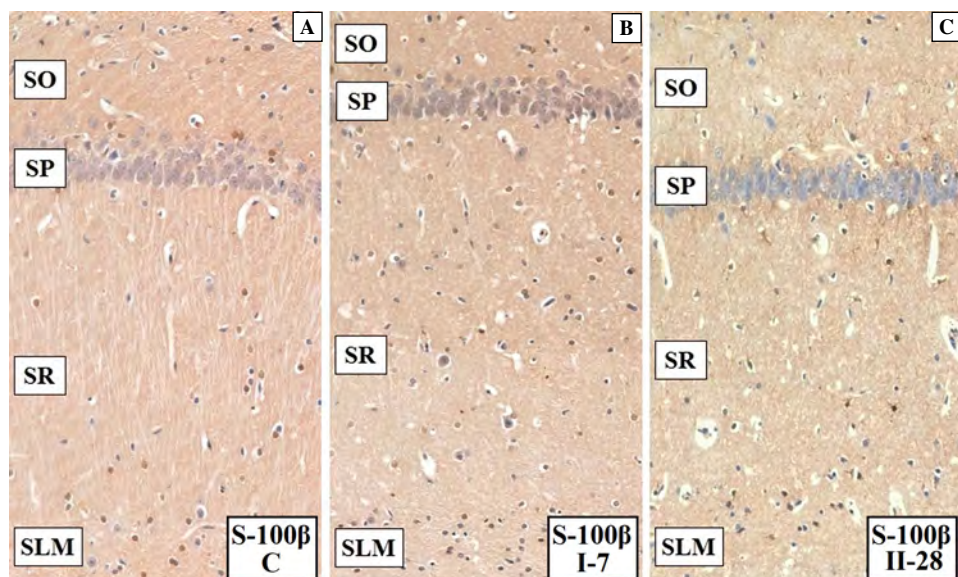
Figure 2. The S100β-IR astrocytes in rat hippocampal CA1 area of control (**C**), I-7 and II-28 groups; Abbreviations as in the legends of Figure 1. Magnification approx. 200×.
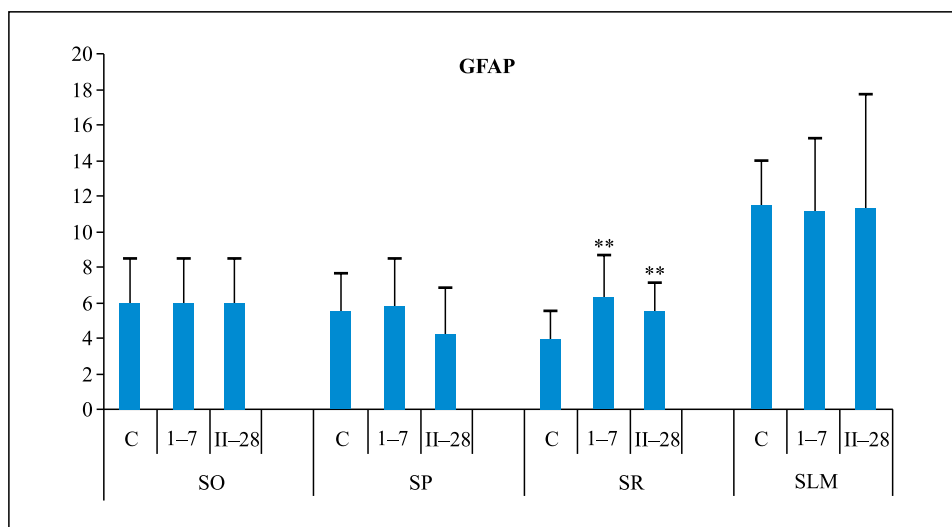
Figure 3. The density of GFAP-IR cells in CA1 area of hippocampus in control (**C**) and experimental (I-7, II-28) rats. Data shows mean density of GFAP-immunopositive cells in the area of 2.5×10^{-3} mm^2 as described in Methods. Bars represent standard deviation; **$p < 0.05$, statistically significant difference between control group and experimental groups (I-7, II-28) (Kruskal-Wallis test). Abbreviations as in the legends of Figure 1.

peppers. The most significant alterations were seen in hippocampal GFAP-IR astrocytes in animals of group II-28. In all layers of CA1 area most cells demonstrated stellate shapes and branched processes. In addition, morphological changes were accompanied by an increase in the density of GFAP-IR astrocytes in layer SR, which was also observed in animals treated with habanero peppers for 7 days. This increase may be a result of the modification of the phenotypic astrocytes in which an overproduction of GFAP, increased for-

mation of intermediate glial filaments and stability of lengthening processes occurred. GFAP is a marker for nearly all of the reactive cells. Nonreactive astroglia contains this protein at a level which is undetectable by immunohistochemical methods [18]. The observed overgrowth of astrocytic processes may be associated with increased activity of CA1 pyramidal neurons. Numerous studies have shown that capsaicin modulates synaptic plasticity of CA1 area pyramidal neurons by the activation of TRPV1 receptors in neurons of CA3

Figure 4. The density of S100β-IR cells in CA1 area of hippocampus in control (**C**) and experimental (I-7, II-28) rats. Data shows mean density of S100β-IR cells in the area of 2.5×10^{-3} mm^2 as described in Methods. Bars represent standard deviation; statistically significant difference between control group and experimental groups (I-7, II-28) related to the same layer: *$p < 0.05$ (ANOVA), **$p < 0.05$ (Kruskal-Wallis). Abbreviations as in the legend to Figure 1.
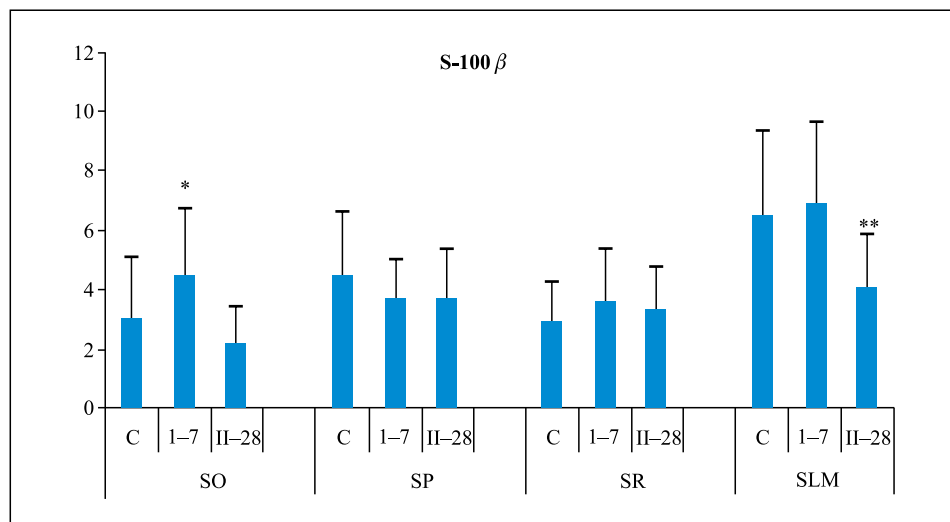
area. Schaffer's collaterals contact with the dendrites of the major cells and interneurons in SR of CA1 area. CAP inhibits the release of glutamate (Glu) from the CA3 neurons to interneurons. However, this alkaloid does not affect the synapses located between the main cells. Therefore, administration of TRPV1 agonists results in a disinhibition of CA1 area pyramidal neurons, an increase in their activation, and thus enhanced induction of LTP [10, 19, 20]. LTP is one of the forms of synaptic plasticity. Initiation and maintenance of LTP are associated with an increase in dendritic branching. Increasing the receptive surface of neurons contributes to the strengthening of excitatory transmission in pyramidal neurons of the CA1 area [21, 22].

Intense neuronal activity leads to an increase in GFAP mRNA and the expression of this protein in astrocytes [23]. GFAP plays an important role in the interactions between astroglia and neuronal cells. Changes in its production affect synaptic functions, Glu and glutamine metabolism, and the concentration of ions [24]. Astrocytic processes limit the spread of neurotransmitters released into the synaptic clefts thereby maintaining proper neurotransmission. Moreover, they are highly mobile and are able to extend in the direction of the newly formed or existing synapses releasing Glu [25]. Synaptogenesis and hyperplasia of glial processes were observed in the rat hippocampal CA1 area, among others, in invoked convulsions model [26]. An abnormal synaptic plasticity which was accompanied by increased

activation of astrocytes was shown during the formation of epileptic focus [26–28]. This is probably related to the necessity of excessive Glu uptake in order to protection of other nerve structures against exitotoxic damage. Transport of glutamate is carried out through specific glial transporter. Some results indicate the colocalization of glial glutamate transporter (GLT-1) with intermediate glial filaments of the astroglia, as well as participation of the cytoskeleton in movement of the transporter along the extensions of the astrocytes [29, 30]. Furthermore, GFAP is involved in anchoring glial glutamate and aspartate transporter (GLAST) in the cell membrane of astrocytes. Hence, it plays an important role in strengthening the transport of glutamate [31]. Glu uptake from the synaptic cleft is modulated, among others, by S100β protein present in the extracellular space and produced by reactive astrocytes [32, 33]. Active release of this protein takes place, *e.g. via* stimulation of the Glu metabotropic receptors from group II (mGluR 3), as shown in the hippocampus of a mouse epilepsy model [34]. Increased secretion of S100β protein to the extracellular space results in a decrease in the number of cells immunoreactive for the protein. This can explain the decreased density of astrocytes observed in our study in the SLM layer of the hippocampal CA1 area of group II-28 of rats. This reaction may be due to the initiation of the mechanisms enhancing the removal of excess glutamate from the newly formed and existing synaptic connections, most likely for neuroprotection [35–38].

To summarise, our findings provide evidence that the habanero pepper administered intragastrically, especially for a longer period of time, affects the activity of hippocampal astrocytes. Increased expression of GFAP and hypertrophy of astrocytic processes is a sign of glial reactivity. This phenomenon may be a part of the mechanisms which allow astrocytes to better control and regulate synaptic microenvironment, and thus protect neurons from excitotoxicity. Structural changes in the astrocytic network could, therefore, play a role in hippocampal synaptic plasticity in animals after the administration of habanero pepper.

References

1. Artinian J, Jordan A, Khlaifia A, et al. Regulation of hippocampal memory by mTORC1 in somatostatin interneurons. J Neurosci. 2019; 39(43): 8439–8456, doi: 10.1523/JNEUROSCI.0728-19.2019, indexed in Pubmed: 31519824.
2. Guerra-Gomes S, Sousa N, Pinto L, et al. Functional roles of astrocyte calcium elevations: from synapses to behavior. Front Cell Neurosci. 2017; 11: 427, doi: 10.3389/fncel.2017.00427, indexed in Pubmed: 29386997.
3. Ota Y, Zanetti AT, Hallock RM. The role of astrocytes in the regulation of synaptic plasticity and memory formation. Neural Plast. 2013; 2013: 185463, doi: 10.1155/2013/185463, indexed in Pubmed: 24369508.
4. Verkhratsky A, Nedergaard M. Physiology of Astroglia. Physiol Rev. 2018; 98(1): 239–389, doi: 10.1152/physrev.00042.2016, indexed in Pubmed: 29351512.
5. Landis DM. The early reactions of non-neuronal cells to brain injury. Annu Rev Neurosci. 1994; 17: 133–151, doi: 10.1146/annurev.ne.17.030194.001025, indexed in Pubmed: 8210172.
6. Siracusa R, Fusco R, Cuzzocrea S. Astrocytes: Role and functions in brain pathologies. Front Pharmacol. 2019; 10: 1114, doi: 10.3389/fphar.2019.01114, indexed in Pubmed: 31611796.
7. Cano V, Valladolid-Acebes I, Hernández-Nuño F, et al. Morphological changes in glial fibrillary acidic protein immunopositive astrocytes in the hippocampus of dietary-induced obese mice. Neuroreport. 2014; 25(11): 819–822, doi: 10.1097/WNR.0000000000000180, indexed in Pubmed: 24911388.
8. Viola GG, Rodrigues L, Américo JC, et al. Morphological changes in hippocampal astrocytes induced by environmental enrichment in mice. Brain Res. 2009; 1274: 47–54, doi: 10.1016/j.brainres.2009.04.007, indexed in Pubmed: 19374889.
9. Okere CO, Waterhouse BD. Capsaicin increases GFAP and glutamine synthetase immunoreactivity in rat arcuate nucleus and median eminence. Neuroreport. 2004; 15(2): 255–258, doi: 10.1097/00001756-200402090-00008, indexed in Pubmed: 15076747.
10. Bennion D, Jensen T, Walther C, et al. Transient receptor potential vanilloid 1 agonists modulate hippocampal CA1 LTP via the GABAergic system. Neuropharmacology. 2011; 61(4): 730–738, doi: 10.1016/j.neuropharm.2011.05.018, indexed in Pubmed: 21645527.
11. Gibson HE, Edwards JG, Page RS, et al. TRPV1 channels mediate long-term depression at synapses on hippocampal interneurons. Neuron. 2008; 57(5): 746–759, doi: 10.1016/j.neuron.2007.12.027, indexed in Pubmed: 18341994.
12. Rycerz K, Krawczyk A, Jaworska-Adamu J, et al. Immunoreactivity of arcuate nucleus astrocytes in rats after intragastric administration of habanero peppers (Capsicum Chinense Jacq.). Pol J Vet Sci. 2016; 19(4): 809–817, doi: 10.1515/pjvs-2016-0102, indexed in Pubmed: 28092615.
13. Thompson RJ. A direct demonstration of functional TRPV1 in Cajal-Retzius cells. J Physiol. 2018; 596(16): 3451–3452, doi: 10.1113/JP276521, indexed in Pubmed: 29920677.
14. El Falougy H, Kubikova E, Benuska J. The microscopical structure of the hippocampus in the rat. Bratisl Lek Listy. 2008; 109(3): 106–110, indexed in Pubmed: 18517132.
15. Knierim JJ. The hippocampus. Curr Biol. 2015; 25(23): R1116–R1121, doi: 10.1016/j.cub.2015.10.049, indexed in Pubmed: 26654366.
16. König JFR, Klippel RAA. stereotactic atlas of the forebrain and lower parts of the brain stem. Williams and Wilkins: Baltimore; 1963.
17. Krawczyk A, Jaworska-Adamu J. Reactivity of astrocytes in the periaqueductal gray matter of rats treated with monosodium glutamate. Folia Histochem Cytobiol. 2020; 58(2): 147–155, doi: 10.5603/FHC.a2020.0010, indexed in Pubmed: 32495938.
18. Kimelberg HK. The problem of astrocyte identity. Neurochem Int. 2004; 45(2-3): 191–202, doi: 10.1016/j.neuint.2003.08.015, indexed in Pubmed: 15145537.
19. Hurtado-Zavala JI, Ramachandran B, Ahmed S, et al. TRPV1 regulates excitatory innervation of OLM neurons in the hippocampus. Nat Commun. 2017; 8: 15878, doi: 10.1038/ncomms15878, indexed in Pubmed: 28722015.
20. Li HB, Mao RR, Zhang JC, et al. Antistress effect of TRPV1 channel on synaptic plasticity and spatial memory. Biol Psychiatry. 2008; 64(4): 286–292, doi: 10.1016/j.biopsych.2008.02.020, indexed in Pubmed: 18405883.
21. Magó Á, Weber JP, Ujfalussy BB, et al. Synaptic plasticity depends on the fine-scale input pattern in thin dendrites of CA1 pyramidal neurons. J Neurosci. 2020; 40(13): 2593–2605, doi: 10.1523/JNEUROSCI.2071-19.2020, indexed in Pubmed: 32047054.
22. Ruan YW, Zou B, Fan Y, et al. Dendritic plasticity of CA1 pyramidal neurons after transient global ischemia. Neuroscience. 2006; 140(1): 191–201, doi: 10.1016/j.neuroscience.2006.01.039, indexed in Pubmed: 16529877.
23. Steward O, Torre ER, Tomasulo R, et al. Neuronal activity up-regulates astroglial gene expression. Proc Natl Acad Sci U S A. 1991; 88(15): 6819–6823, doi: 10.1073/pnas.88.15.6819, indexed in Pubmed: 1862105.
24. Middeldorp J, Hol EM. GFAP in health and disease. Prog Neurobiol. 2011; 93(3): 421–443, doi: 10.1016/j.pneurobio.2011.01.005, indexed in Pubmed: 21219963.
25. Barker AJ, Ullian EM. Astrocytes and synaptic plasticity. Neuroscientist. 2010; 16(1): 40–50, doi: 10.1177/1073858409339215, indexed in Pubmed: 20236948.
26. Hawrylak N, Chang FL, Greenough WT. Astrocytic and synaptic response to kindling in hippocampal subfield CA1. II. Synaptogenesis and astrocytic process increases to in vivo kindling. Brain Res 1993; 603: 309-316. doi: 10.1016/0006-8993(93)91252-n, indexed in Pubmed: 8461983.
27. Armstrong DD. The neuropathology of temporal lobe epilepsy. J Neuropathol Exp Neurol. 1993; 52(5): 433–443, doi: 10.1097/00005072-199309000-00001, indexed in Pubmed: 8360697.
28. Bezprozvanny I, Mattson MP. Neuronal calcium mishandling and the pathogenesis of Alzheimer's disease. Trends Neurosci. 2008; 31(9): 454–463, doi: 10.1016/j.tins.2008.06.005, indexed in Pubmed: 18675468.
29. Shobha K, Vijayalakshmi K, Alladi PA, et al. Altered in-vitro and in-vivo expression of glial glutamate transporter-1 following exposure to cerebrospinal fluid of amyotrophic lateral sclerosis patients. J Neurol Sci. 2007; 254(1-2): 9–16, doi: 10.1016/j.jns.2006.12.004, indexed in Pubmed: 17254611.

30. Zhou J, Sutherland ML. Glutamate transporter cluster formation in astrocytic processes regulates glutamate uptake activity. J Neurosci. 2004; 24(28): 6301–6306, doi: 10.1523/JNEUROSCI.1404-04.2004, indexed in Pubmed: 15254085.

31. Sullivan SM, Sullivan RKP, Miller SM, et al. Phosphorylation of GFAP is associated with injury in the neonatal pig hypoxic-ischemic brain. Neurochem Res. 2012; 37(11): 2364–2378, doi: 10.1007/s11064-012-0774-5, indexed in Pubmed: 22528834.

32. Michetti F, D'Ambrosi N, Toesca A, et al. The S100B story: from biomarker to active factor in neural injury. J Neurochem. 2019; 148(2): 168–187, doi: 10.1111/jnc.14574, indexed in Pubmed: 30144068.

33. Tramontina F, Tramontina AC, Souza DF, et al. Glutamate uptake is stimulated by extracellular S100B in hippocampal astrocytes. Cell Mol Neurobiol. 2006; 26(1): 81–86, doi: 10.1007/s10571-006-9099-8, indexed in Pubmed: 16633903.

34. Sakatani S, Seto-Ohshima A, Shinohara Y, et al. Neural-activity-dependent release of S100B from astrocytes enhances kainate-induced gamma oscillations in vivo. J Neurosci. 2008; 28(43): 10928–10936, doi: 10.1523/JNEUROSCI.3693-08.2008, indexed in Pubmed: 18945900.

35. Abdel-Salam OME, Sleem AA, Sayed MA, et al. Capsaicin exerts anti-convulsant and neuroprotective effects in pentylenetetrazole-induced seizures. Neurochem Res. 2020; 45(5): 1045–1061, doi: 10.1007/s11064-020-02979-3, indexed in Pubmed: 32036609.

36. Donato R. Intracellular and extracellular roles of S100 proteins. Microsc Res Tech. 2003; 60(6): 540–551, doi: 10.1002/jemt.10296, indexed in Pubmed: 12645002.

37. Huang M, Cheng G, Tan H, et al. Capsaicin protects cortical neurons against ischemia/reperfusion injury via down-regulating NMDA receptors. Exp Neurol. 2017; 295: 66–76, doi: 10.1016/j.expneurol.2017.05.001, indexed in Pubmed: 28479337.

38. Yasuda Y, Tateishi N, Shimoda T, et al. Relationship between S100beta and GFAP expression in astrocytes during infarction and glial scar formation after mild transient ischemia. Brain Res. 2004; 1021(1): 20–31, doi: 10.1016/j.brainres.2004.06.015, indexed in Pubmed: 15328028.

ORIGINAL PAPER

VIA MEDICA

Relationship between calcification, atherosclerosis and matrix proteins in the human aorta

Aleksandra Kuzan[1], Jerzy Wisniewski[2], Krzysztof Maksymowicz[3],
Magdalena Kobielarz[4], Andrzej Gamian[1, 5], Agnieszka Chwilkowska[6]

[1]Department of Medical Biochemistry, Faculty of Medicine, Wroclaw Medical University, Wroclaw, Poland

[2]Central Laboratory of Instrumental Analysis, Wroclaw University of Science and Technology, Wroclaw, Poland

[3]Department of Forensic Medicine, Faculty of Medicine, Wroclaw Medical University, Wroclaw, Poland

[4]Department of Mechanics, Materials and Biomedical Engineering, Faculty of Mechanical Engineering, Wroclaw University of Science and Technology, Wroclaw, Poland

[5]Department of Immunology of Infectious Diseases, Hirszfeld Institute of Immunology and Experimental Therapy, Polish Academy of Sciences, Wroclaw, Poland

[6]Department of Molecular and Cellular Biology, Faculty of Pharmacy, Wroclaw Medical University, Wroclaw, Poland

Abstract
Introduction. Extracellular matrix (ECM) proteins have been associated with atherosclerotic complications, such as plaque rupture, calcification and aneurysm. It is not clear what role different types of collagen play in the pathomechanism of atherosclerosis. The aim of the study was to analyze the content of elastin and major types of collagen in the aortic wall and how they associated are with course of atherosclerosis.
Material and methods. In this work we present six biochemical parameters related to ECM proteins and collagen-specific amino acids (collagen type I, III, and IV, elastin, proline and hydroxyproline) analyzed in 106 patients' aortic wall specimens characterized by different degree of atherosclerosis. Liquid Chromatography Electrospray Ionization Tandem Mass Spectrometry (LC/ESI-MS/MS), ELISA and immunohistochemical methods were used. The severity of atherosclerosis was assessed on the six-point scale of the American Heart Association, taking into account the number and location of foam cells, the presence of a fatty core, calcium deposits and other characteristic atherosclerotic features.
Results. The results show that there is a relationship between the content of collagen-specific amino acids and development of atherosclerosis. The degree of atherosclerotic lesions was negatively correlated with the content of proline, hydroxyproline and the ratio of these two amino acids. Calcium deposits and surrounding tissue were compared and it was demonstrated that the ratio of type I collagen to type III collagen was higher in the aortic tissue than in aortic calcification areas, while the ratio of collagen type III to elastin was smaller in the artery than in the calcium deposits.
Conclusions. We suggest that increase in collagen type III presence in the calcification matrix may stem from disorders in the structure of the type I and III collagen fibers. These anomalous fibers are likely to favor accumulation of the calcium salts, an important feature of the process of atheromatosis. *(Folia Histochemica et Cytobiologica 2021, Vol. 59, No. 1, 8–21)*

Key words: atherosclerosis; calcification; collagen type I, III, IV; elastin; proline, hydroxyproline; ELISA; LC/ESI-MS/MS; IHC

Correspondence address: PhD Aleksandra Kuzan
Department of Medical Biochemistry,
Faculty of Medicine, Wrocław Medical University,
Chalubinskiego 10, Wroclaw, Poland
phone: 48 71 784 13 79, fax: 71 784 00 85
e-mail: aleksandra.kuzan@umed.wroc.pl

Introduction

The extracellular matrix (ECM) is a complex network of extracellular molecules, mainly proteins and polysaccharides, interacting with each other and in contact with the majority of cells. Collagen is a struc-

tural and stable protein, with a long half-life span. This protein defines biomechanical properties of the tissues, *e.g.* tensile strength of arteries subjected to a high blood pressure. At the same time it is a protein that is being constantly modified and it is interacting with other tissue proteins. These features are important to providing homeostasis in the arteries and any alteration in that equilibrium can lead to the development of atherosclerosis. Contribution of collagen to the onset of atherosclerosis is complex. It includes formation of the scaffolds for modified lipoproteins, growth factors, advanced glycation end products, it is required for macrophage accumulation, proliferation and migration of smooth muscle cells or clot formation [1, 2]. Collagen molecules are constantly undergoing degradation by matrix metalloproteases (MMPs), released among others by macrophages located in atheromatous plaques, weakening structure of the arteries. Its production may be stimulated or inhibited. Excessive metalloproteinases lead to atherosclerotic plaques being unstable, but their under-expression may lead to collagen accumulating in the form of fibrous caps, which has a significant impact on stiffening of the artery structure [2]. Twenty-eight types of collagen have been identified and described. The types I, III, and IV of collagen were selected here for their predominant presence and for functional importance in formation of the extracellular matrix.

Elastin is another key building block in the connective tissue, particularly important for the arteries' elasticity, allowing their return to original shape after stretching of the blood vessels. Such properties are determined by the presence of intramolecular desmosine bonds formed from three aldehyde derivatives of lysines with unchanged lysine residue. Elastin, in contrast to collagen, represents one genetic type; also, no elastin posttranslational modifications such as hydroxylation of lysines or glycosylation were observed [1].

There has been ongoing effort to establish what role specific types of collagen play and how the ECM proteins contribute to cardiovascular physiology and pathophysiology, particularly within the pathomechanism of atherosclerosis. The reports on ECM's role and on how the content of collagen and elastin in the arteries affects the severity of the atherosclerosis are inconclusive; it is not even clear whether the amount of collagen and elastin increases or decreases with the development of atherosclerosis [3–10]. The aim of this study was to define relationships between different types of collagen (I, III, IV) and elastin in arteries at various stages of atherosclerosis.

Material and methods

Human samples and their classification. The studied biological material consisted of 106 fragments of the abdominal or thoracic aorta sections collected during forensic and medical autopsies performed at the Department of Forensic Medicine of Wroclaw Medical University, Poland. Each sample was from a different patient. The samples came from people who died suddenly, aged 55 ± 15 years (mean ± SD); 73% of them were men and 27% women. A formal requirement for the consent was met and the study was approved by the Bioethics Committee of the Wroclaw Medical University (No 220/2010). The probes were divided into six stages of atherosclerosis, following the American Heart Association scale of Atherosclerosis [11–13]. The classification was carried out independently by two Co-authors (A. K. and A. Ch.). The stages were defined as: I — early lesions, II — fatty streaks, III — pre-atheroma, IV — atheroma, V — fibroatheroma, VI — ruptured lesion, calcified lesion or fibrotic lesion. Samples were subdivided into those in which macroscopically visible calcification were observed (n = 31) and to samples with no visible calcification (n = 49) (in the remaining 26 cases, there were no calcification data available, so they were not analyzed in this respect). Examples of an uncalcified aorta calcified aorta, and an isolated calcium deposit are shown in Figure 1. In the group of calcified samples, in 16 of them a large deposit of calcium was visible so that it was prepared and analyzed independently of the rest of the samples. Samples were subjected to qualitative immunochemical (IHC) staining and quantitative analysis by ELISA (enzyme-linked immunosorbent assay) and liquid chromatography combined with tandem mass spectrometry (LC-ESI-MS/ MS). Reagents, unless indicated otherwise in the text, were purchased from POCH (Gliwice, Poland) and SigmaAldrich (Saint Louis, MO, USA).

Figure 1. Macroscopic view of an uncalcified wall of aorta (**A**), a calcified wall of aorta (**B**) and the isolated calcium deposit (**C**).

Quantification of collagens type I, type III, type IV and elastin content in aortas' fragments by ELISA. The samples about 5 mm × 5 mm × 3 mm were homogenized in extraction buffer (10 mM Tris, 5 mM EDTA, 0.2 M NaCl, pH 7.5) using a homogenizer FastPrep-24® (MP Biomedicals, Santa Ana, CA, USA) and the weight to buffer volume ratio of 100 mg/1 ml was kept constant. The 96-well Maxisorp plates (Nunc®, SigmaAldrich, Darmstadt, Germany) were coated with the homogenates. Standard solutions of collagen type I (Millipore, Billerica, MA, USA, cat. no.: CC050), collagen type III (Millipore, cat. no.: CC054), collagen type IV (Millipore, cat. no.: CC076), elastin (SigmaAldrich, cat. no.: E6902) were tested for the reference. The coating was carried out for 24 h at 4°C. Next, the plates were blocked with 10% skim milk in PBST (PBS — phosphate buffered saline, 0.1% Tween 20) overnight at 4°C. To detect collagens and elastin corresponding antibodies were applied: mouse monoclonal IgG1anti-collagen type I (Novus Biologicals, Abingdon, UK, clone COL1, cat. no.: NB600-450, 1:2000), mouse monoclonal anti-collagen type III (SigmaAldrich, clone FH-7A, cat. no.: C7805, 1:4000), mouse monoclonal anti-collagen type IV (SigmaAldrich, clone COL-94 cat. no.: C1926, 1:2000) or rabbit policlonal anti-elastin (Santa Cruz, Santa Clara, USA, clone H-300, cat. no.: sc-25736, 1:4000). After 2 h incubation secondary monoclonal anti-mouse IgG-HRP (H+L) (JacsonImmuno Research, West Grove, USA, cat. no.: 309-035-082, 1:5000) or anti-rabbit IgG-HRP (H+L) (JacsonImmuno Research, cat. no.: 111-035-045, 1:3000) was applied. After 1.5 h incubation the colorimetric reaction was developed using o-phenylenediamine (SigmaAldrich) and absorbance measured at 450 nm on EnSpire Multimode Plate Reader (Perkin Elmer, Waltham, MA, USA). The concentration of proteins in the homogenates was calculated from the standard curves obtained for individual standard solutions of collagens and elastin.

Immunohistochemistry. Tissue and isolated purified calcium deposit samples were fixed in 4% paraformaldehyde and embedded in paraffin. The paraffin blocks were cut into 5 μm-thick sections. They were next deparaffinized by immersing them in xylene, followed by washing the slides with a series of alcohol dilutions (100%–50% ethanol). To expose the antigen the slides were incubated with proteinase K (Dako, Santa Clara, CA, USA, cat. no.: S3020) for 10 min at 37°C and treated with Real Peroxidase-Blocking Solution (Dako, cat. no.: S2023) for 10 min and Protein Block (Dako, cat. no.: X0909) for 15 minutes. In the following step solutions of antibodies were applied: mouse monoclonal IgG1anti-collagen type I (Novus Biologicals, clone COL1, cat. no.: NB600-450, 1:2000), mouse monoclonal anti-collagen type III antibody (Santa Cruz, clone 3A1, cat. no.: sc-271249, 1:50), mouse anti-collagen type IV (SigmaAldrich, clone COL94, cat. no.: C1926, 1:1000), mouse monoclonal anti-elastin (Santa Cruz,

clone BA-4, cat. no.: sc-58756, 1:50), and slides incubated overnight at 4°C in a humid glass chambers. Finally, the immunocomplexes were visualized using the DAKO LSAB kit + System-HRP), successively with Biotynylated Link Universal, Streptavidin-HRP, DAB (diaminobenzidine) + substrate buffer with DAB + Chromogen, and following the general method guidelines. Delafield hematoxylin was used as the counterstain. Then the slides were immersed and closed with the glass coverslip using DPX (Aqua Medica, Lodz, Poland). The samples were analyzed with the light-field Olympus BX51 microscope (Olympus, Tokyo, Japan). For control of unspecific binding of secondary antibodies we made control incubations by omitting the primary antibody. These control experiments were negative.

Liquid chromatography electrospray ionization tandem mass spectrometry (LC-ESI-MS/MS) analysis. Lipids were removed from the aortic samples by incubating them in the mixture of 30 μL of water and 300 μL of methanol-chloroform (2:1 v/v) and centrifugation at 15 811 rpm, 15 min, 4°C. The precipitate was treated with 380 μL methanol-chloroform-0.2 M HCl (2:1:0.8), followed by centrifugation and lyophilization. Precipitate was suspended in 500 μL of 6M HCl and incubated at 116°C for 18 h. After the hydrolysis samples were dried with nitrogen and the precipitate was triturated with methanol, followed by drying with a stream of nitrogen. The resulting pellets were resuspended in 200 μL of acetonitrile-water (1:1) containing 0.5 μg/mL glycyl-phenylalanine used as internal standard and centrifuged at 12000 rpm (7 min, 20°C). The supernatant was filtered through 0.2 μm syringe filters and then diluted 10-fold with acetonitrile-water (1:1) to reduce the possibility of interfacing the analyte with the matrix. Quantitative measurements of proline (Pro) and hydroxyproline (ProOH) were made using a set of Acquity nanoUPLC Liquid Chromatographs equipped with Waters' Xevo G2 Q-TOF mass spectrometer (Waters, Milford, MA, USA). For the separation of samples, a HSS T3 column (1 × 50 mm; 1.8 μm particle size) was used (Waters). The chromatographic separation was carried out at 80 μL/min. The column was thermostated at 40°C. The total chromatographic separation time, together with the time needed to regenerate the column, was 3 min. The mobile phase components were 0.1% formic acid in acetonitrile (component A) and 0.1% formic acid in water (component B). Spectrometric measurements were performed using an electrospray ion source, in positive ionization mode, and in function MS/MS in high resolution. In order to ensure high accuracy of molecular mass readings, leucine enkephalin was used as internal standard. During the analysis of the fragmentation spectra, the characteristic daughter ions were sought: 70.06 m/z for proline (parent ion: 116.07 m/z; collision energy: 12.5 eV); 86.06 m/z for hydroxyproline (parent ion: 132.06 m/z, collision energy: 12.5 eV) and 120.08 m/z for glycyl-L-phenylalanine (parent ion: 223.10 m/z, collision energy: 19 eV).

Statistical analysis. The statistical analysis was performed using statistical package R for Windows (version 3.1.2) (R Core Team, Vienna, Austria). Correlations of individual parameters were calculated by Spearman correlation method. The Mann-Whitney test was used to investigate the association of individual atherosclerotic scales with protein content. Kruskall-Wallis test with post-hoc analysis of multiple repetitions with Bonferroni correction was used to analyze the association of atherosclerosis with all analyzed biochemical parameters. To compare the average protein content in calcium deposits and arteries, the Fisher test and Student's t-student tests were used. Wilcoxon test was carried out to compare paired data — calcium deposits and non-calcined parts from the same aorta. The analysis of the influence of sex on biochemical parameters was performed using the Mann-Whitney test, and the analysis of the difference between sex and severity of atherosclerosis was performed using a χ^2 test. Significance in all cases was assumed at $p < 0.05$.

Results

Distribution of the studied ECM proteins in aortic wall

Analysis of microscopic specimens with immunohistochemically stained collagen types and elastin (Figs. 2–5) showed localization of the studied proteins.

Type I collagen occurs in all three layers of the aortic wall in patients with lower stages of atherosclerosis, presenting fibers locating between cells (Fig. 2b, c). In samples that originated from people with more advanced atherosclerosis, type I collagen shows the tendency to concentrate, in some samples along the entire width of the artery (Fig. 2h) and in others in the inner layer of the artery (not shown). Similar localization and characteristics can be attributed to type III collagen (Fig. 3). In advanced atherosclerotic plaques type III and IV collagen was found in dense deposits in fibrous cap (Fig. 3g and 4f, g).

In arteries collagen type IV is the major component of the basement membrane of vascular smooth muscle cells (VSMCs) and forms network connecting ECM collagens to these cells. The protein occurs both in the media and intima (Fig. 4). No collagen type IV was observed in tunica adventitia with an exception of the wall of smaller vessels (*vasa vasorum*) (Fig. 4a, b).

In aorta at stage I of atherosclerosis elastin forms strong and pronounced inner or/and outer elastic membranes (Fig. 5, b and c). In third stage of atherosclerosis, called pre-atheroma, and in IV stage of atherosclerosis, the width of the intima is strongly broadened and clear boundary between the intima and the media disappears, as a result of lack
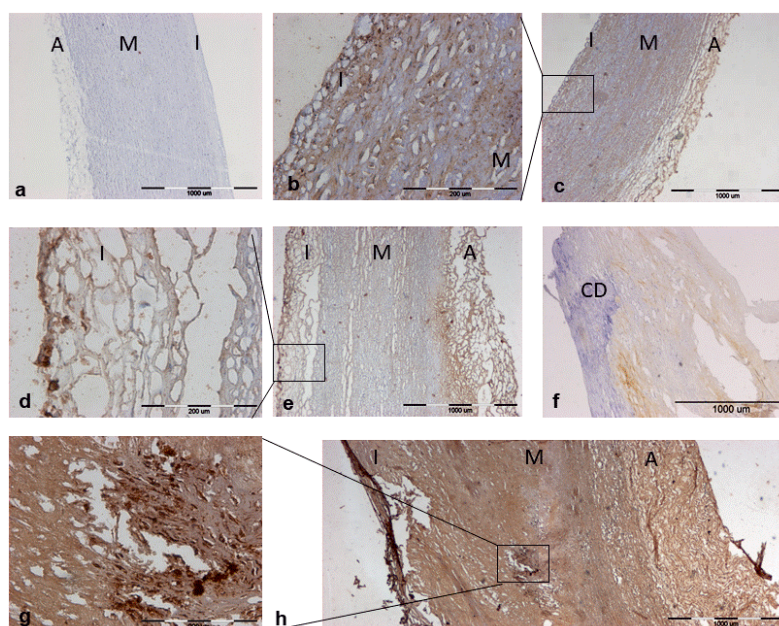
Figure 2. Localization of collagen type I in the wall of aortas at different stages of atherosclerosis. (a) Negative control without primary antibody, stage II; (b, c) Stage I of atherosclerosis; (d, e) III/IV stage of atherosclerosis; (f) calcium deposit; (g, h) V/VI stage of atherosclerosis. Collagen type I was detected by immunohistochemistry and sections were counterstained with hematoxylin (blue-purple) as described in Methods. Abbreviations: I — intima, M — media, A — adventitia, CD — calcium deposit. Scale bars: 1000 μm (a, c, e, f, h) and 200 μm (b, d, g).

Figure 3. Localization of collagen type III in in the wall of aortas at different stages of atherosclerosis. Immunohistochemistry of representative sections with anti-collagen type III antibody (DAB, brown) and with hematoxylin counterstaining (blue-purple). (a–c) I stage of atherosclerosis; (d, e) III/IV stage of atherosclerosis; (f) calcium deposit; (g, h) V/VI stage of atherosclerosis. Abbreviations: I — intima, M — media, A — adventitia, CD — calcium deposit, VV — vasa vasorum. Scale bars 1000 μm (b, e, f, g) and 200 μm (a, c, d, h).

Figure 4. Localization of collagen type IV in the wall of aortas at different stages of atherosclerosis. Immunohistochemistry of representative sections with anti-collagen type IV antibody (DAB, brown) and with hematoxylin counterstaining (blue-purple). (a, b) I stage of atherosclerosis; (c, d) III/IV stage of atherosclerosis; (e) calcium deposit; (f, g) V/VI stage of atherosclerosis. Abbreviations: I — intima, M — media, A — adventitia, CD — calcium deposit, VV — vasa vasorum. Scale bars 1000 μm (b, c, e, f) and 200 μm (a, d, g).

of prominent internal elastic membrane (Fig. 5d). In more advanced stages of atherosclerosis elastin forms pseudomembranes passing between the cells, especially in the media (Fig. 5h, i).

Sections of aortic wall with calcium deposits (Fig. 2f, 4e, 5f) show a trace presence of type I collagen, type IV collagen and elastin; however, type III collagen fibers (Fig. 3f) are present in a relatively large amount.
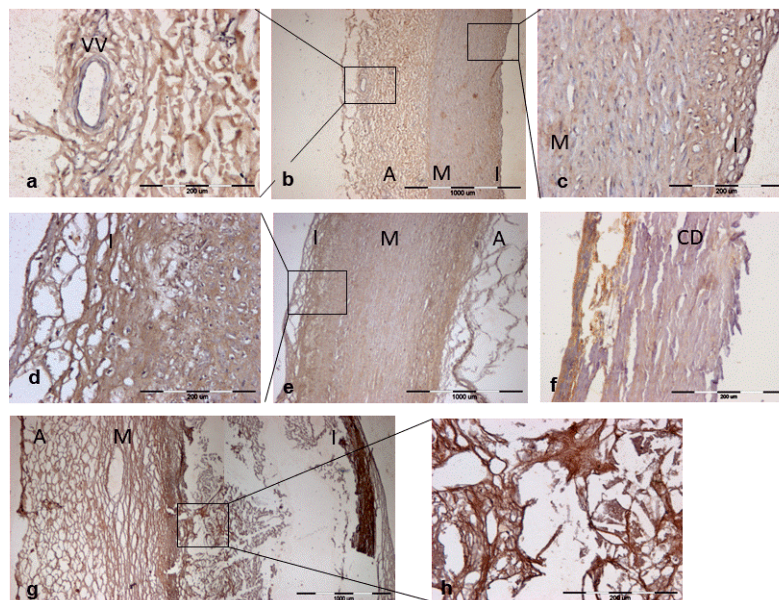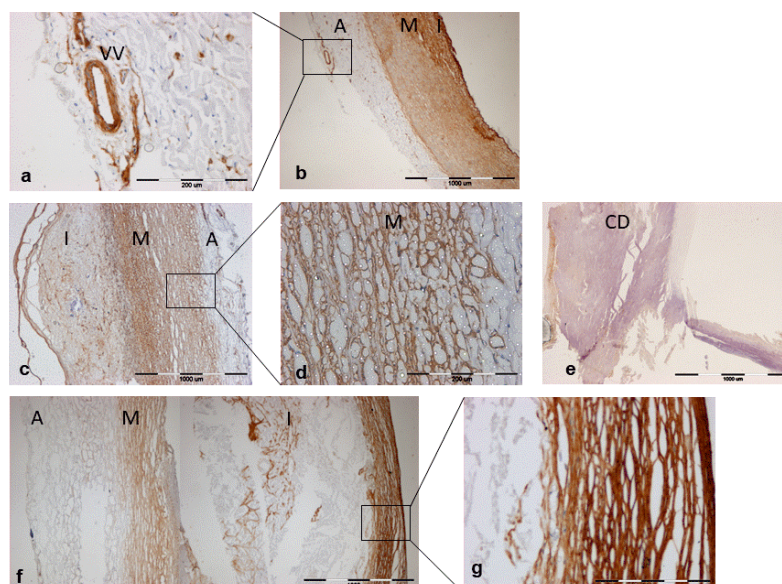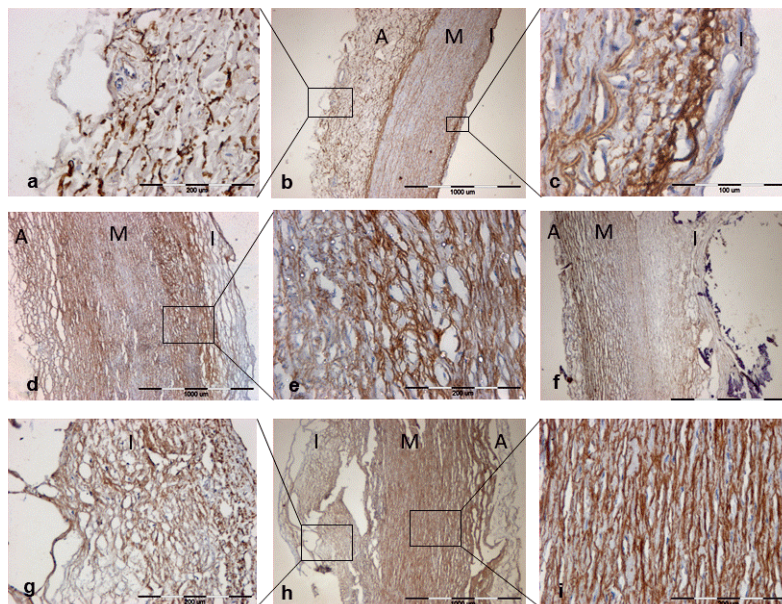
Figure 5. Localization of elastin in the wall of aortas at different stages of atherosclerosis. Immunohistochemistry of representative sections with anti-elastin antibody (DAB, brown) and with hematoxylin counterstaining (blue-purple). (a–c) I stage of atherosclerosis; (d, e) III/IV stage of atherosclerosis; (f) VI stage of atherosclerosis with space formed after preparation-related crushing of calcium deposit; (g–i) V/VI stage of atherosclerosis. Abbreviations: I — intima, M — media, A — adventitia. Scale bars: 1000 μm (b, d, f, h), 200 μm (a, e, g, i) and 100 μm (c).

Analysis of correlations between stage of atherosclerosis and biochemical parameters

We have determined correlations between stage of atherosclerosis and the measured biochemical parameters: as well as between the content of type I and type III collagen, between type I and type IV collagen, between type I collagen and elastin, between type IV collagen and elastin and between type III and type IV collagens. All correlation coefficients were determined as positive and at medium strength (Table 1). We have also observed weak positive correlations between hydroxyproline and type I collagen content and hydroxyproline and total collagen content sum (Table 1).

Consequently, it was expected that the results obtained by ELISA and the LC-ESI-MS/MS methods would converge.

The proline and hydroxyproline concentration in aortic tissue was determined by liquid chromatography coupled with mass spectrometry (LC-ESI-MS/ MS), followed by statistical analysis with both qualitative (Spearman's correlation method, Table 1) and quantitative (Kruskall-Wallis test with repeated post-hoc analysis with Bonferroni correction, Table 2). There were statistically significant associations between degree of atherosclerosis and concentration in arterial tissue of proline content (very weak negative correlation, r = –0.0436), hydroxyproline (weak negative correlation, r = –0.224), proline to hydroxyproline ratio (weak negative correlation, r = –0.391) and age (weak positive correlation, r = –0.353) (Table 1). These data indicate that as the disease progresses, the amino acids present in the collagen, and thus the protein content itself, fall. No statistically significant correlation was observed between the collagen types or elastin and degree of atherosclerosis (Table 1).

Analysis of the influence of sex on biochemical parameters and advanced degree of atherosclerosis

No relationship was observed between the gender and the content of the analyzed ECM proteins. Also, no difference was found between the degree of atherosclerosis between women and men (data not shown).

Analysis of correlations between individual parameters

We have determined a correlation between the following biochemical parameters, *i.e.* between type I and type III collagen, between type I and type IV collagen, between type I collagen and elastin, between type IV collagen and elastin and between type III and type IV collagens. All correlation coefficients were determined as positive and at medium strength (Table 1). We have also observed weak positive correlations between hydroxyproline and type I collagen content and hydroxyproline and collagen sum (Table 1). Consequently, it was expected that the results obtained by ELISA and the LC-ESI-MS/MS methods would converge.

Table 1. Spearman correlation analysis between the studied biochemical parameters in aortic samples and between stage of atherosclerosis (n = 106) as well as between pairs of indicated parameters. Statistically significant results are marked by an asterisk. The levels of collagen type I, III, IV and elastin were measured by ELISA, and the levels of proline and hydroxyproline by LC-ESI-MS/MS.

Pair of parameters	r	p
Collage type I: collagen type III	0.619	< 0.0001*
Collagen type I: collagen IV	0.437	< 0.0001*
Collagen type I: elastin	0.527	< 0.0001*
Collagen type IV: elastin	0.357	0.0002*
Collagen type III: collagen IV	0.612	< 0.0001*
Collagen type III: elastin	0.543	< 0.0001*
Collagen type I: hydroxyproline	0.237	0.0259*
Collagen type III: hydroxyproline	0.175	0.1046
Collagen type IV: hydroxyproline	0.059	0.5822
Elastin: hydroxyproline	0.109	0.322
Sum of the collagens: hydroxyproline	0.214	0.0455*
Collagen type I: stage of atherosclerosis	0.00918	0.9270
Collagen type III: stage of atherosclerosis	–0.178	0.0753
Collagen type IV: stage of atherosclerosis	–0.0915	0.3606
Elastin: stage of atherosclerosis	–0.043	0.6708
Proline: degree of atherosclerosis	–0.0436	< 0.0001*
Hydroxyproline: degree of atherosclerosis	–0.224	0.0391*
Pro/ProOH[a] ratio:degree of atherosclerosis of atherosclerosis	–0.391	0.0002*
Age: degree of atherosclerosis	0.353	0.0003*

[a]Pro, proline, ProOH, hydroxyproline

Comparison of parameters between isolated calcium deposits and uncalcified aortic tissue

The collagens and elastin contents in the sections of the arteries and in the calcium deposits were determined by ELISA and summarized in Table 3. It is noteworthy that in calcium deposits the determined values are several times lower than in arteries, although the percentage content of individual collagens and elastin for both groups of samples remains largely similar (Table 3). Differences in mean values between aortic walls and calcium deposits in the case of individual analyzed parameters are statistically significant except for the difference in the average collagen type III content (Table 3). The greatest difference is observed for type IV collagen — in calcium deposits its percentage is several times lower than in the artery.

Comparison of parameters between calcified samples with and without signs of calcification

In addition to the analysis of depleted calcium deposits, a division was also made between arterial samples based on whether they were calcified or not. We have found that the samples with calcifications are characterized by significantly lower proline content and ratio of proline to hydroxyproline (Table 4). Calcified samples were also derived from significantly older individuals and more advanced atherosclerosis than samples without calcification (Table 4). Comparison of calcium deposits with surrounding tissue revealed that calcium deposits had lower content of the extracellular matrix proteins (collagen type I, IV, elastin) and lower ratio of type I collagen to type III collagen (Table 5). However, in samples with calcium deposits three parameters are statistically higher than in surrounding tissues. They are: the ratio of collagen type I to elastin, the ratio of type III to type IV collagen and the ratio of type III collagen to elastin (Table 5).

Discussion

The structure of collagen and elastin shows a high degree of organization, which in turn determines the biological properties of these proteins. Even a small

Table 2. Results of analysis differences between mean values of the analyzed parameters in aortic samples depending on the severity of atherosclerosis (Kruskall-Wallis test with post-hoc analysis of multiple repetitions with Bonferroni correction). Statistically significant results are marked by an asterisk. The levels of collagen type I, III, IV and elastin were measured by ELISA, and the levels of proline and hydroxyproline by LC-ESI-MS/MS.

Stage of athero-sclerosisis	1	2	3	4	5	6
N	16	22	24	17	14	9
Age [years]						
Mean ± SD	37.19 ± 14.72	54.91± 14.80	58.00± 12.33	65.24± 13.34	54.71± 15.69	61.44± 11.49
p	0.000*					
Collagen type I [μg/mg of tissue]						
Mean ± SD	15.24 ± 9.31	12.77± 5.95	12.86± 6.97	11.73 ± 7.35	16.06± 9.09	13.92± 5.90
p	0.672					
Collagen type III [μg/mg of tissue]						
Mean ± SD	4.45 ± 3.02	3.04 ± 1.60	2.94 ± 1.98	2.87 ± 1.53	3.09 ± 1.50	2.35 ± 0.96
p	0.284					
Collagen type IV [μg/mg of tissue]						
Mean ± SD	3.61± 2.75	3.03± 2.72	2.15 ± 2.25	2.45 ± 1.33	2.75 ± 1.58	2.43 ± 1.54
p	0.199					
Elastin [μg/mg of tissue]						
Mean ± SD	18.93 ± 8.74	12.73 ± 6.70	15.97 ± 6.95	15.53 ± 12.24	20.87 ± 16.52	14.14 ± 7.40
p	0.314					
Sum of collagens type I, III and IV [μg/ml of tissue]						
Mean ± SD	23.57 ± 12.60	19.03 ± 9.00	18.05 ± 9.86	17.38 ± 8.73	22.24 ± 11.01	19.05 ± 7.48
p	0.567					
Proline (Pro) [μg/mg of tissue]						
Mean ± SD	11.32 ± 3.58	13.04 ± 5.25	9.15 ± 3.84	7.87 ± 4.47	8.05 ± 5.46	6.11 ± 4.21
p	0.002 (2 *vs.* 5 p = 0.037; 2 *vs.* 6 p = 0.037)*					
Hydroxyproline (ProOH) [μg/mg of tissue]						
Mean ± SD	5.75 ± 2.45	6.55 ± 3.21	4.62 ± 2.13	4.20 ± 2.20	5.05 ± 3.45	4.13 ± 2.89
p	0.21					
Ratio Pro/ProOH						
Mean ± SD	2.11 ± 0.53	2.08 ± 0.40	2.03 ± 0.36	1.81 ± 0.42	1.67 ± 0.44	1.59 ± 0.45
p	0.008 (2 *vs.* 5 p = 0.11; 2 *vs.* 6 p = 0.12)*					

The results are mean ± SD. The concentration of the studied compound was studied in aortic wall samples as described in Methods.

change in protein structure or in the expression of one of the ECM component, may change the ratio between individual proteins and lead to significant physiological disturbances. It has been postulated that especially aberrations in the structure and amount of collagen types I and III can result in atherosclerosis or hypertensive heart disease [14–17] while changes within the elastin fibers may lead to supraventricular stenosis, hypertension or aneurysm [14]. Our previous study referred to the role of collagen in the arteries in the context of glycation [18] and another one shows that there is a relationship between the content of type II collagen and the degree of atherosclerosis [19]. In the present study the object of interest are other types of fibrillar collagens, *i.e.* type I and type III, type IV collagen and elastin.

Progression of the atherosclerosis, the loss of elasticity and stiffness of the arterial walls, increases with age. These events are probably caused by increase in collagen content in the arteries and loss of elastin [20]. Unfortunately, this hypothesis has not been unequivocally verified. In the literature on the subject

Table 3. Mean content of collagens type I, III, IV and elastin in the samples of aortic wall and in isolated calcium deposits. The levels of collagen type I, III, IV and elastin were measured by ELISA, and the levels of proline and hydroxyproline by LC-ESI-MS/MS.

	Aorta (n = 106)		Calcium deposit (n = 16)		*p*
	Content [µg/mg of tissue]	% of the measured proteins	Content [µg/mg of tissue]	% of the measured proteins	
Collagen type I	13.3 ± 7.44	38.05	7.32 ± 4.57	45.47	0.000*
Collagen type III	3.11 ± 1.97	8.90	2.29 ±1.51	14.22	0.086
Collagen type IV	2.69 ± 2.17	7.70	0.08 ±0.76	0.50	0.000*
Elastin	15.85 ± 10.12	45.35	6.41 ±7.36	39.81	0.000*
Collagen to elastin ratio[a]	1.21:1		1.51:1		

The results are mean ± SD. The content of the studied compound was determined in aortic wall samples as described in Methods. Statistically significant results refer to the difference between arteries and calcium deposits are marked by an asterisk. [a]Ratio of the sum of average collagens' content to average elastin content in aortic wall.

Table 4. Comparison of the patients' age, stage of atherosclerosis, content of extracellular matrix proteins and ratios of selected parameters between aortic samples without with calcium deposits.

	Samples without calcium deposits (n = 49)	Samples with calcium deposits (n = 31)	*p*
Age [years]	49.56 ± 15.07	61.23 ± 12.61	0.00*
Stage of atherosclerosis [I–VI]	2.44 ± 1.29	4.39 ± 1.17	0.00*
Collagen type I [µg/mg of tissue]	13.97 ± 7.77	14.06 ± 7.97	0.99
Collagen type III [µg/mg of tissue]	3.53 ± 2.46	2.78 ± 1.28	0.36
Collagen type IV [µg/mg of tissue]	2.90 ± 2.39	2.28 ± 1.55	0.41
Elastin [µg/mg of tissue]	15.57 ± 8.53	17.94 ± 13.11	0.66
Collagen type I/collagen type III ratio	4.70 ± 2.50	5.39 ± 2.11	0.07
Collagen type I/collagen type IV ratio	7.42 ± 6.66	9.48 ± 9.79	0.25
Collagen type I/elastin ratio	1.69 ± 4.22	1.93 ± 4.03	0.48
Collagen type III/collagen type IV ratio	1.67 ± 1.24	1.67 ± 1.45	0.83
Collagen type III/elastin ratio	0.38 ± 0.75	0.34 ± 0.66	0.02*
Collagen type IV/elastin ratio	0.41 ± 1.33	0.26 ± 0.40	0.14
Proline [µg/mg of tissue]	10.76 ± 4.36	8.17 ± 5.17	0.02*
Hydroksyproline [µg/mg of tissue]	5.65 ± 2.72	4.76 ± 2.84	0.26
Pro/ProOH ratio	1.99 ± 0.39	1.69 ± 0.42	0.00*

The results are mean ± SD. The content of the studied compounds is expressed as µg/mg of tissue. Statistically significant results are marked by an asterisk.

there are contradicting reports, some are showing that with progression of the atherosclerosis collagen concentration increases [3–5], while the other reports describe decreased content of this protein [6, 21]. Such large differences between the results described in the literature are probably due to the fact that each project analyzed a different study group using a variety of methods. It is likely that these differences are also the result of a statistical error related to too small size of a study group. Our study group was exceptionally large for a postmortem human study, so we conclude that the results are reliable. In the present study no particular collagen type has been demonstrated to correlate with atheromatosis (although the data suggests that one of the analyzed type — type III — may be associated with calcification, which sometimes accompanies atherogenesis). The data presented here indicate that there is a negative correlation between the hydroxyproline content, and thus collagen, and degree of atheromatosis. This is a novel observation, as no publication has been found that described the analysis of the content of proline and hydroxyproline in human aortas depending on the degree of atherosclerosis. Only a report by Abdelhalim *et al.* found

Table 5. Comparative analysis of the content of the studied proteins in calcium deposits and surrounding tissue in samples taken from the same vascular wall.

Parameter		Mean ± SD	p
Collagen type I [μg/mg of tissue]	Aorta (n = 16)	16.327 ± 9.1889	0.0093*
	Deposit (n = 16)	6.854 ± 4.5622	
Collagen type III [μg/mg of tissue]	Aorta (n = 16)	3.068 ± 1.3926	0.065
	Deposit (n = 16)	2.301 ± 1.5976	
Collagen type IV [μg/mg of tissue]	Aorta (n = 16)	2.622 ± 1.7534	0.0021*
	Deposit (n = 16)	0.885 ± 0.7587	
Elastin [μg/mg of tissue]	Aorta (n = 16)	23.682 ± 14.6907	0.0001*
	Deposit (n = 16)	6.149 ± 7.2043	
Collagen type I/III ratio	Aorta (n = 16)	5.828 ± 2.2741	0.018*
	Deposit (n = 16)	3.352 ± 1.8551	
Collagen type I/IV ratio	Aorta (n = 16)	11.108 ± 12.4396	0.71
	Deposit (n = 16)	15.682 ± 30.5617	
Collagen type I/elastin ratio	Aorta (n = 16)	0.766 ± 0.3757	0.015*
	Deposit (n = 16)	12.653 ± 30.9017	
Collagen type III/IV ratio	Aorta (n = 16)	1.701 ± 1.8122	0.0042*
	Deposit (n = 16)	4.726 ± 5.2757	
Collagen type III/elastin ratio	Aorta (n = 16)	0.135 ± 0.06409	0.0012*
	Deposit (n = 16)	4.667 ± 8.2404	
Collagen type IV/elastin ratio	Aorta (n = 16)	0.132 ± 0.1144	0.3
	Deposit (n = 16)	2.611 ± 6.0602	

The result are mean ± SD, n = 16. Statistically significant results are marked by an asterisk.

a similar result in rabbits where animals on high fat diets had a reduced aortic hydroxyproline content [22]. Interestingly, although elastic fibers play a key role in the physiological functions of elastic type arteries such as aorta and pulmonary artery, we did not found correlation between elastin content in the wall of aorta and the progress of the atherosclerotic process. Other authors have reported both increased [7] and decreased [1, 8] elastin content in aortic wall during atherogenesis. Perhaps such ambiguous results are again the consequence of a statistical error related to too small size of a study group or individual differences in another study group, although our results indicate the simplest explanation — that there is no direct relationship between the elastin content and the severity of atherosclerosis.

Elastin and collagen have contrasting physical properties and the ratio of collagen to elastin should be of particular interest since it defines mechanical properties of the artery. According to Sakalihasan, the ratio of collagen to elastin in normal aortas is 1.85 : 1; however, it was shown to be higher in the wall of aortic aneurysms [23]. For our samples we have determined an average value of 1.21: 1. In our study the statistical analysis did not show that this parameter for individual samples was related to a degree of atherosclerosis or age. Kong *et al.* [24] reported that ratio of elastin to collagen type III was increased in coronary arteries from patients with acute ischemic heart disease who had a myocardial infarction (the average age of patients with myocardial infarction was 57.4 years and did not differ statistically from the age of control patients). Perhaps the parameter which is the ratio of collagen to elastin is locally significant in specific manifestations of atherosclerosis [25]. For example, it is postulated that the ratio of collagen to elastin in porcine arteries is an accurate predictor of arterial burst pressure [26].

Our description of the distribution of collagens is consistent with earlier reports [27, 28]. Generally, the presence of collagen type I, III and IV was found in samples of a healthy aorta and atherosclerotic lesions, with fibrillar collagens occurring throughout the entire cross-section of aortic wall, and type IV collagen in intima and media as well as in the wall of vascular adventitious vessels. Collagens of all analyzed types have concentrated in the outer layer, forming fibrous cap above highly advanced plaques. In the fat core

itself, however, a decrease in both fibrillar collagen and type IV collagen was observed.

In our project, we also analyzed the phenomenon of calcification. It is a clinically very serious problem that is complex in terms of etiology. It is reported that the formation of calcium deposits occurs in association with dyslipidemia, hypertension, uremia, glycation associated with diabetes, dysregulated mineral metabolism particularly hyperphosphatasemia, chronic oxidative stress, and is associated with a change in expression of fetuin-A and osteoprotegerin. We analyzed the relationship between aortic calcification and selected extracellular matrix proteins composition [29, 30].

Our research shows that in the deposits calcium salts displace organic components therefore ECM protein content in calcium deposits is lower than in soft parts of the arteries what is consistent with our observation. There is generally less proteins in calcium deposits than in the wall of the vessel from which they have been isolated. This is especially true for collagen type I, IV and elastin. Noteworthy is the small difference between the contents of type III collagen in the calcium deposits and in the surrounding tissue. In the deposits, there was also a lower ratio of type I to type III collagen. Microscopic images of the calcium deposit show a prominently higher immunoreactivity of type III collagen fibers compared to trace quantities of elastin, collagen I and IV. Calcium deposits show higher than the surrounding tissue ratio of type I collagen to elastin, type III collagen to type IV collagen, and type III collagen to elastin. It is somewhat intriguing, that for most of the aforementioned parameters that differentiate deposits and surrounding layer, when collagen type III content appears in the denominator, the parameter is higher in the artery, whenever it is present in the numerator, the parameter is lower in the artery than in the calcium deposit. It is also worth mentioning that type III collagen is the only protein of which content is not statistically lower in calcium deposit than in the soft part of the artery. The data point into some relationship between occurrence of this protein and calcification. The collagen type III seems to play a structural role in the deposit and its content exceeds that of the elastin, collagen type I and IV. There have been no other studies describing the role of type III collagen in the calcification of arteries, except for one by Kuga *et al.* [31] asserting that calcification in the abdominal aortic aneurysms was most likely associated with the breakdown of collagen type III fibrils [31]. There are few premises that collagen of this type may have a role in calcification, as it does in other tissues,

such as bones and tendons [32, 33]. As in this study, the results obtained by Lui *et al.* in a calcified tendinopathy model show that the level of collagen in calcified tendon seems to be decreasing, while the ratio of type III to type I collagen is increasing in this tissue [32]. It is well known that type I collagen is the main component of both arteries and tendons. Type III collagen is a protein incorporated in fibrils created by type I collagen. These authors hypothesized that the increase in collagen type III content in tissue undergoing calcification can be linked to abnormalities in the fiber structure — abnormalities that favor accumulation of calcium salts in that area [32]. It is possible that analogous processes govern arterial calcification.

Volk [33] drew attention to the potential impact that type III collagen may have on the osteoblasts differentiation. It is known that apart from soft tissues, high expression of this type of collagen is observed during skeletal embryonic development, and it is also synthesized by osteoblasts in mature bones [34]. When Col3a1 gene was silenced in mice, *i.e.*, type III collagen gene was not expressed, the onset of the Ehlers-Danlos syndrome (EDS) was observed with functional impairment of the soft tissues, disturbed healing, and possibly the bone disorders [35]. It has been found that type III collagen plays a role in the differentiation of osteoblasts, thus conditioning the development of the spongy bone [33]. It is likely that this type of collagen contributes to arterial calcification by differentiating cells from osteoblast-like cells. However, to validate this hypothesis further research is required.

The guiding hypothesis for this research project was that there may be a link between the elastin content and calcification. Such assumption comes from literature reports describing formation of calcium deposits along elastin layers in the wall of an artery (*membrana elastica interna* and *membrana elastica externa)* [36]. This hypothesis is further supported by the reports showing that elastin metabolites can activate calcium deposition in smooth muscle cells [37]. The role of elastin in vascular calcification has also been demonstrated by several other authors in animal models [38–40]. However, the analysis of the data obtained in this study has not shown a statistically significant relationship between the content of elastin, or the ratio of this protein to other ECM components, and the presence of calcification foci. Immunohistochemical staining of the aortic sections also did not show a link between the location and organization of elastin and calcification. Therefore, our results do not support the thesis that elastin plays a causative role in the process of calcium deposition in blood vessels. The lack of such

statistically significant evidence might be related to scarcity of calcified samples and their diversity (among artery segments were samples representing different types of calcification: accompanying atherosclerosis, Mönckeberg's arteriosclerosis, elastocalcinosis). Summarizing, the extracellular matrix of the human aorta consists of nearly 45% of elastin and 55% of collagen, of which the majority are fibrillary collagens type I and III, occurring in all three layers of the artery wall. Type IV collagen accounts for nearly 10% of all abdominal aortic collagen, located in subendothelial basement membrane and also the basement membrane of VSMCs. Quantities of collagen types I, III and IV as well as elastin correlate positively with other analyzed proteins of extracellular matrix. However, in the study described here, there is no relationship between the content of collagen type I, III, IV or elastin and the degree of atherosclerosis. Noteworthy, the weak negative correlation between atherosclerosis and the amount of hydroxyproline is noted, indicating a loss of collagen with the onset of atherogenesis. The results of particular interest are those describing the role of ECM proteins in arterial calcification, and collagen type III playing both structural and regulatory role.

Since patients with the cardiovascular diseases, particularly those caused by atherosclerosis, experience high mortality, there is a pressing need to thoroughly investigate how degenerative lesions in the arteries are being formed. Further studies are also needed to resolve contradictory reports in the literature and unresolved question concerning the role that extracellular matrix proteins may have in atherogenesis and the interplay between various ECM components. Such studies may have a diagnostic value and there are already reports proposing the use of magnetic resonance imaging, positron emission tomography (PET) or single photon emission computed tomography (SPECT) [41, 42] in depicting the ECM changes. According to Järveläinen, Kassam, Zheng and others [14, 43–45] it is possible to influence pharmacologically the matrix protein content in the walls of the blood vessels. Therefore, such diagnostic and therapeutic tools would become indispensable in monitoring the progress of the treatment of cardiovascular diseases.

Funding

Acknowledgements

References

1. Xu J, Shi GP. Vascular wall extracellular matrix proteins and vascular diseases. Biochim Biophys Acta. 2014; 1842(11): 2106–2119, doi: 10.1016/j.bbadis.2014.07.008, indexed in Pubmed: 25045854.

2. Rekhter M. Collagen synthesis in atherosclerosis: too much and not enough. Cardiovasc Res. 1999; 41(2): 376–384, doi: 10.1016/s0008-6363(98)00321-6, indexed in Pubmed: PMID: 10341837.

3. Lan TH, Huang XQ, Tan HM. Vascular fibrosis in atherosclerosis. Cardiovasc Pathol. 2013; 22(5): 401–407, doi: 10.1016/j.carpath.2013.01.003, indexed in Pubmed: 23375582.

4. Geary RL, Wong JM, Rossini A, et al. Expression profiling identifies 147 genes contributing to a unique primate neointimal smooth muscle cell phenotype. Arterioscler Thromb Vasc Biol. 2002; 22(12): 2010–2016, doi: 10.1161/01.atv.0000038147.93527.35, indexed in Pubmed: 12482827.

5. Chiong T, Cheow ESH, WooCC, et al. Aortic wall extracellular matrix proteins correlate with syntax score in patients undergoing coronary artery bypass surgery. Open Cardiovasc Med J. 2016; 10: 48–56, doi: 10.2174/1874192401610010048, indexed in Pubmed: 27347220.

6. Libby P, Aikawa M. Stabilization of atherosclerotic plaques: new mechanisms and clinical targets. Nat Med. 2002; 8(11): 1257–1262, doi: 10.1038/nm1102-1257, indexed in Pubmed: 12411953.

7. Foote CA, Castorena-Gonzalez JA, Ramirez-Perez FI, et al. Arterial stiffening in western diet-fed mice is associated with increased vascular elastin, transforming growth factor-β, and plasma neuraminidase. Front Physiol. 2016; 7: 285, doi: 10.3389/fphys.2016.00285, indexed in Pubmed: 27458385.

8. Asciutto G, Dias NV, Edsfeldt A, et al. Low elastin content of carotid plaques is associated with increased risk of ipsilateral stroke. PLoS One. 2015; 10(3): e0121086, doi: 10.1371/journal.pone.0121086, indexed in Pubmed: 25803692.

9. Shami A, Gonçalves I, Hultgårdh-Nilsson A. Collagen and related extracellular matrix proteins in atherosclerotic plaque development. Curr Opin Lipidol. 2014; 25(5): 394–399, doi: 10.1097/MOL.0000000000000112, indexed in Pubmed: 25137612.

10. Greenwald SE. Ageing of the conduit arteries. J Pathol. 2007; 211(2): 157–172, doi: 10.1002/path.2101, indexed in Pubmed: 17200940.

11. Stary HC, Chandler AB, Dinsmore RE, et al. A definition of advanced types of atherosclerotic lesions and a histological classification of atherosclerosis. A report from the Committee on Vascular Lesions of the Council on Arteriosclerosis, American Heart Association. Arterioscler Thromb Vasc Biol. 1995; 15(9): 1512–1531, doi: 10.1161/01.atv.15.9.1512, indexed in Pubmed: 7670967.

12. Stary HC, Blankenhorn DH, Chandler AB, et al. A definition of the intima of human arteries and of its atherosclerosis-prone regions. A report from the Committee on Vascular Lesions of the Council on Arteriosclerosis, American Heart Association. Arterioscler Thromb. 1992; 12(1): 120–134, doi: 10.1161/01.atv.12.1.120, indexed in Pubmed: 1731855.

13. Stary HC, Chandler AB, Glagov S, et al. A definition of initial, fatty streak, and intermediate lesions of atherosclerosis. A report from the Committee on Vascular Lesions of the Council on Arteriosclerosis, American Heart Association.

Arterioscler Thromb. 1994; 14(5): 840–856, doi: 10.1161/01. atv.14.5.840, indexed in Pubmed: 8172861.

14. Järveläinen H, Sainio A, Koulu M, et al. Extracellular matrix molecules: potential targets in pharmacotherapy. Pharmacol Rev. 2009; 61(2): 198–223, doi: 10.1124/pr.109.001289, indexed in Pubmed: 19549927.

15. Duprez DA, Gross MD, Ix JH, et al. Collagen biomarkers predict new onset of hypertension in normotensive participants: the Multi-Ethnic Study of Atherosclerosis. J Hypertens. 2018; 36(11): 2245–2250, doi: 10.1097/HJH.0000000000001793, indexed in Pubmed: 29782392.

16. Wang H, Liu D, Zhang H. Investigation of the underlying genes and mechanism of macrophage-enriched ruptured atherosclerotic plaques using bioinformatics method. J Atheroscler Thromb. 2019; 26(7): 636–658, doi: 10.5551/jat.45963, indexed in Pubmed: 30643084.

17. Holm Nielsen S, Jonasson L, Kalogeropoulos K, et al. Exploring the role of extracellular matrix proteins to develop biomarkers of plaque vulnerability and outcome. J Intern Med. 2020; 287(5): 493–513, doi: 10.1111/joim.13034, indexed in Pubmed: 32012358.

18. Kuzan A, Chwiłkowska A, Maksymowicz K, et al. Advanced glycation end products as a source of artifacts in immunoenzymatic methods. Glycoconj J. 2018; 35(1): 95–103, doi: 10.1007/s10719-017-9805-4, indexed in Pubmed: 29305778.

19. Kuzan A, Chwiłkowska A, Pezowicz C, et al. The content of collagen type II in human arteries is correlated with the stage of atherosclerosis and calcification foci. Cardiovasc Pathol. 2017; 28: 21–27, doi: 10.1016/j.carpath.2017.02.003, indexed in Pubmed: 28284062.

20. Briones AM, Salaices M, Vila E. Mechanisms underlying hypertrophic remodeling and increased stiffness of mesenteric resistance arteries from aged rats. J Gerontol A Biol Sci Med Sci. 2007; 62(7): 696–706, doi: 10.1093/gerona/62.7.696, indexed in Pubmed: 17634315.

21. Aikawa M, Rabkin E, Okada Y, et al. Lipid lowering by diet reduces matrix metalloproteinase activity and increases collagen content of rabbit atheroma: a potential mechanism of lesion stabilization. Circulation. 1998; 97(24): 2433–2444, doi: 10.1161/01.cir.97.24.2433, indexed in Pubmed: 9641696.

22. Abdelhalim MA, Siddiqi NJ, Alhomida AS, et al. The changes in various hydroxyproline fractions in aortic tissue of rabbits are closely related to the progression of atherosclerosis. Lipids Health Dis. 2010; 9: 26, doi: 10.1186/1476-511X-9-26, indexed in Pubmed: 20214825.

23. Sakalihasan N, Heyeres A, Nusgens BV, et al. Modifications of the extracellular matrix of aneurysmal abdominal aortas as a function of their size. Eur J Vasc Surg. 1993; 7(6): 633–637, doi: 10.1016/s0950-821x(05)80708-x, indexed in Pubmed: 8270064.

24. Kong CH, Lin XY, Woo CC, et al. Characteristics of aortic wall extracellular matrix in patients with acute myocardial infarction: tissue microarray detection of collagen I, collagen III and elastin levels. Interact Cardiovasc Thorac Surg. 2013; 16(1): 11–15, doi: 10.1093/icvts/ivs421, indexed in Pubmed: 23049084.

25. Cantini C, Kieffer P, Corman B, et al. Aminoguanidine and aortic wall mechanics, structure, and composition in aged rats. Hypertension. 2001; 38(4): 943–948, doi: 10.1161/hy1001.096211, indexed in Pubmed: 11641314.

26. Sindram D, Martin K, Meadows JP, et al. Collagen-elastin ratio predicts burst pressure of arterial seals created using a bipolar vessel sealing device in a porcine model. Surg Endosc. 2011; 25(8): 2604–2612, doi: 10.1007/s00464-011-1606-4, indexed in Pubmed: 21404086.

27. Katsuda S, Okada Y, Minamoto T, et al. Collagens in human atherosclerosis. Immunohistochemical analysis using collagen type-specific antibodies. Arterioscler Thromb. 1992; 12(4): 494––502, doi: 10.1161/01.atv.12.4.494, indexed in Pubmed: 1373075.

28. Shekhonin BV, Domogatsky SP, Idelson GL, et al. Relative distribution of fibronectin and type I, III, IV, V collagens in normal and atherosclerotic intima of human arteries. Atherosclerosis. 1987; 67(1): 9–16, doi: 10.1016/0021-9150(87)90259-0, indexed in Pubmed: 3314885.

29. Jing L, Li L, Ren X, et al. Role of sortilin and matrix vesicles in Nε-carboxymethyl-lysine-induced diabetic atherosclerotic calcification. Diabetes Metab Syndr Obes. 2020; 13: 4141–4151, doi: 10.2147/DMSO.S273029, indexed in Pubmed: 33177854.

30. Tsai CH, Lin LY, Lin YH, et al. Abdominal aorta calcification predicts cardiovascular but not non-cardiovascular outcome in patients receiving peritoneal dialysis: A prospective cohort study. Medicine (Baltimore). 2020; 99(37): e21730, doi: 10.1097/MD.0000000000021730, indexed in Pubmed: 32925715.

31. Kuga T, Esato K, Zempo N, et al. Detection of type III collagen fragments in specimens of abdominal aortic aneurysms. Surg Today. 1998; 28(4): 385–390, doi: 10.1007/s005950050146, indexed in Pubmed: 9590702.

32. Lui PPY, Chan LS, Lee YW, et al. Sustained expression of proteoglycans and collagen type III/type I ratio in a calcified tendinopathy model. Rheumatology (Oxford). 2010; 49(2): 231–239, doi: 10.1093/rheumatology/kep384, indexed in Pubmed: 19955224.

33. Volk SW, Shah SR, Cohen AJ, et al. Type III collagen regulates osteoblastogenesis and the quantity of trabecular bone. Calcif Tissue Int. 2014; 94(6): 621–631, doi: 10.1007/s00223-014-9843-x, indexed in Pubmed: 24626604.

34. Asgari M, Latifi N, Heris HK, et al. In vitro fibrillogenesis of tropocollagen type III in collagen type I affects its relative fibrillar topology and mechanics. Sci Rep. 2017; 7(1): 1392, doi: 10.1038/s41598-017-01476-y, indexed in Pubmed: 28469139.

35. Busch A, Hoffjan S, Bergmann F, et al. Vascular type Ehlers-Danlos syndrome is associated with platelet dysfunction and low vitamin D serum concentration. Orphanet J Rare Dis. 2016; 11(1): 111, doi: 10.1186/s13023-016-0491-2, indexed in Pubmed: 27488172.

36. Stary HC, Chandler AB, Dinsmore RE, et al. A definition of advanced types of atherosclerotic lesions and a histological classification of atherosclerosis. A report from the Committee on Vascular Lesions of the Council on Arteriosclerosis, American Heart Association. Circulation. 1995; 92(5): 1355–1374, doi: 10.1161/01.cir.92.5.1355, indexed in Pubmed: 7648691.

37. Lee JS, Basalyga DM, Simionescu A, et al. Elastin calcification in the rat subdermal model is accompanied by up-regulation of degradative and osteogenic cellular responses. Am J Pathol. 2006; 168(2): 490–498, doi: 10.2353/ajpath.2006.050338, indexed in Pubmed: 16436663.

38. Qin X, Corriere MA, Matrisian LM, et al. Matrix metalloproteinase inhibition attenuates aortic calcification. Arterioscler Thromb Vasc Biol. 2006; 26(7): 1510–1516, doi: 10.1161/01.ATV.0000225807.76419.a7, indexed in Pubmed: 16690876.

39. Pereira L, Lee SY, Gayraud B, et al. Pathogenetic sequence for aneurysm revealed in mice underexpressing fibrillin-1. Proc Natl Acad Sci U S A. 1999; 96(7): 3819–3823, doi: 10.1073/pnas.96.7.3819, indexed in Pubmed: 10097121.

40. Bailey M, Pillarisetti S, Jones P, et al. Involvement of matrix metalloproteinases and tenascin-C in elastin calcification. Cardiovasc Pathol. 2004; 13(3): 146–155, doi: 10.1016/S1054-8807(04)00009-2, indexed in Pubmed: 15081471.

41. Reimann C, Brangsch J, Colletini F, et al. Molecular imaging of the extracellular matrix in the context of atherosclerosis. Adv Drug Deliv Rev. 2017; 113: 49–60, doi: 10.1016/j.addr.2016.09.005, indexed in Pubmed: 27639968.

42. Chen W, Cormode DP, Vengrenyuk Y, et al. Collagen-specific peptide conjugated HDL nanoparticles as MRI contrast agent to evaluate compositional changes in atherosclerotic plaque regression. JACC Cardiovasc Imaging. 2013; 6(3): 373–384, doi: 10.1016/j.jcmg.2012.06.016, indexed in Pubmed: 23433925.

43. Kassam HA, Bahnson EM, Cartaya A, et al. Pharmacokinetics and biodistribution of a collagen-targeted peptide amphiphile for cardiovascular applications. Pharmacol Res Perspect. 2020; 8(6): e00672, doi: 10.1002/prp2.672, indexed in Pubmed: 33090704.

44. Zheng J, Li Q, He L, et al. Protocatechuic Acid Inhibits Vulnerable Atherosclerotic Lesion Progression in Older Apoe-/- Mice. J Nutr. 2020; 150(5): 1167–1177, doi: 10.1093/jn/nxaa017, indexed in Pubmed: 32047914.

45. Tomosugi N, Yamamoto S, Takeuchi M, et al. Effect of Collagen Tripeptide on Atherosclerosis in Healthy Humans. J Atheroscler Thromb. 2017; 24(5): 530–538, doi: 10.5551/jat.36293, indexed in Pubmed: 27725401.

ORIGINAL PAPER

VM
VIA MEDICA

miR-140-5p inhibits the proliferation, migration and invasion of vascular smooth muscle cells by suppressing the expression of NCKAP1

Qing Ma, Jiancheng Liu, Chunbo Li, Dong Wang

Cardiovascular Surgery, Tangshan Gongren Hospital, Tangshan, Hebei Province, 063000, China

Abstract

Introduction. The occurrence of aortic dissection is related to the proliferation and metastasis of vascular smooth muscle cells. In our present study, we found that the expression of miR-140-5p was inhibited in the wall of abdominal aorta of aortic dissection patients. However, the mechanism of miR-140-5p in the development of aortic dissection is unclear.

Material and methods. We detected the expression of miR-140-5p and NCK Associated Protein 1 (NCKAP1) in blood vessel of aortic dissection patients and normal people by PCR. Next, we established the miR-140-5p over-expression and miR-140-5p inhibition vascular smooth muscle cells (CRL-1999 cells). The BrdU assays, wound healing assays and transwell assays were performed to detect the proliferation and invasion ability of these cells. Finally, luciferase reporter assay was performed to detect the relationship between miR-140-5p and NCKAP1.

Results. The expression of miR-140-5p was suppressed in blood vessel of aortic dissection patients, and the levels of NCKAP1 in those tissues were upregulated. Overexpression of miR-140-5p inhibited the proliferation, migration and invasion of vascular smooth muscle cells. miR-140-5p targeted and suppressed the expression of NCKAP1.

Conclusions. miR-140-5p repressed the proliferation, migration and invasion of vascular smooth muscle cells by targeting and inhibiting the expression of NCKAP1. Furthermore, the results of our study suggest new strategies and targets for the clinical treatment of arterial dissection. *(Folia Histochemica et Cytobiologica 2021, Vol. 59, No. 1, 22–29)*

Key words: aortic dissection; miR-140-5p; NCKAP1; vascular smooth muscle cells; proliferation; invasion

Introduction

Aortic dissection is a cardiovascular disease induced by blood entering the middle layer of the vessel wall and the formation of swelling [1]. Aortic dissection is a serious life-threatening cardiovascular disease. In addition to vascular endothelial damage, it can also Cause serious complications [2]. At present, the effective treatment of aortic dissection is mainly surgery. However, statistical data showed that the mortality rate of postoperative period is still 9–30% [3]. Therefore,

there is a need to determine the molecular mechanism of aortic dissection to develop the new therapeutic treatments. The application of drugs intervening in the disease's pathomechanism combined with surgery is expected to further improve the survival rate of patients. Furthermore, as the component of aortic vessel wall, the lesion of vascular smooth muscle cells (VSMCs) was considered as the important reasons for the onset of aortic dissection [4]. The VSMCs of aortic wall mainly showed low differentiation, strong proliferation and metastasis [5]. In addition, the large amount of extracellular matrix secreted by VSMCs also promotes their proliferation and invasion [6]. These effects of VSMCs attenuate the stability of the blood vessel wall, which in turn may induce the occurrence of aortic dissection [7].

Correspondence address: Dong Wang,
Cardiovascular Surgery, Tangshan Gongren Hospital, No. 27, Wenhua Road, Tangshan City, Hebei Province, China
phone: 86+03152305089, e-mail: wangdongwd12345@163.com

Non-coding RNA is a type of RNA that does not translate into protein. Recent studies have found that non-coding RNA played a crucial role during the physiological process of cell differentiation, apoptosis, proliferation and metabolism [8, 9]. Other research also revealed that miRNA was related to the occurrence and development of aortic dissection [10]. On the other hand, the overexpression of miRNA-30a promoted the development of aortic dissection [11]. Our results showed that levels of miR-140-5p were also downregulated in the VSMCs during the development of aortic dissection. However, the function of miR-140-5p during the development of aortic dissection and its molecular mechanism are unclear. Therefore, we explored the effect of miR-140-5p on the development of aortic dissection in an in the culture of VSMCs. Our findings suggest that miR-140-5p has the potential to suppress the aortic dissection by restricting the proliferation and metastasis of vascular smooth muscle cells.

Material and methods

Collection of tissue samples. Samples of ascending aorta tissue (10 samples of aortic dissection patients and 7 samples of normal people, all these patients were 35 years old, half of the patients was male and others were female, 3 normal people were male and others were female) were collected from the hospital and used for the detection. These samples were collected during the clinical operation. Then we used liquid nitrogen to freeze these samples, and then we used a mortar to grind these samples. Finally, Trizol (Thermo Fisher Scientific, Waltham, MA, USA) was applied to extract RNA and protein from these samples. This experiment has been approved by the Ethics Committee of Tangshan Gongren Hospital, Tangshan, China. All the operation of this study followed the World Medical Association Declaration of Helsinki [12].

Cell culture and transfection. Human aortic vascular smooth muscle cell line (CRL-1999) was applied for the experiments in this study. CRL-1999 cell line was acquired from the ATCC (Manassas, VA, USA). All the cells were incubated in 37°C humid atmosphere with 5% CO_2 in RPMI-1640 medium (Hyclone, Logan, UT, USA) supplemented with the 10% fetal bovine serum (FBS, Gibco, Gaithersburg, MD, USA). Furthermore, the inhibitor and mimic of miR-140-5p were obtained from the Genechem (Shanghai, China) and applied for the transfection of these cells. Plasmids used in this assay were obtained from the Genechem. Polybrene was mixed with the lentivirus (with the ratio of 1:7) containing the inhibitor and mimic of miR-140-5p and applied to promote the efficiency of transfection. Subsequently, the mixed lentivirus medium was co-cultured with these cells for 12 hours to complete the transfection. Since the plasmid vector contained antibiotic resistance genes, we used media supplemented with puromycin (1mg/mL, Thermo Fisher Scientific) to culture these cells in subsequent experiments to screen for successfully transfected cells.

Bromodeoxyuridine (BrdU) incorporation assay. CRL-1999 cells were incubated with $10 \mu m$ bromodeoxyuridine (BrdU) (Sigma, Burbank CA, USA) for 4 hours in the incubator. Next, these cells were rinsed with the PBS buffer (phosphate-buffered saline) and fixed with 4% formaldehyde. Then, these cells were washed with PBS again and incubated with the 4N HCl containing 1% Triton X-100 for 15 min. Next, anti-BrdU antibodies (SigmaAldrich) were diluted with PBS and incubated with the cells. At last, these cells were incubated with anti-mouse IgG-Cy3 (SigmaAldrich) in the dark and the fluorescence was detected by spectrophotometer (Aoxi Company, Shanghai, China).

Cell counting kit-8 (CCK-8). Before the assays, CRL-1999 cells were plated into four 96 well plates. After the adhesion (0, 24, 48 and 72 hours) of these cells, the CCK-8 (Dojindo, Kumamoto, Japan) was diluted with the RPMI-medium (1:10) and incubated with the cells at 37°C for 1 hour. Then, the absorbance of these cells was detected by spectrophotometer (Aoxi Company). And the absorbance of these cells reflected the proliferation of these cells.

Wound healing assays. CRL-1999 cells were plated in the 6 well plates before the experiment. After adhesion was reached, the cells were cultured with the serum-free medium for 12 h. Then, the scratch was created with the pipette tip. The scratch was photographed with inverted microscope (Olympus, Tokyo, Japan) after 0 and 24 h. The width of the scratch was measured with the Image J software (National Institutes of Health, Bethesda, MD, USA).

Transwell assay. CRL-1999 cell line was cultured with the medium without FBS serum for 12 h. In addition, the matrix gel (10 mg/mL, BD, USA) was diluted with the FBS-free medium (with the ratio of 1:10) and added into the upper layer of the $8 \mu m$ Boyden chamber (Corning, NY, USA). Cells were seeded into the upper layer of the chamber. The medium containing FBS was added into the lower layer of the chamber. Then, Boyden chamber was placed in the incubator for 24 h. Then, cells that pass through the aperture were stained with the crystal violet (Thermo Fisher Scientific) and photographed with inverted microscope.

RT-PCR. Total RNA was collected with the Trizol (Thermo Fisher Scientific). Then, the reverse transcription kit (Takara, Shiga, Japan) was used for the reverse transcription of RNA. Next, ABI7500 system (Thermo Fisher Scientific) was used for the amplification of cDNA and the relative levels of the target genes were analyzed with the $2^{-\Delta\Delta Ct}$ method [13]. The primers used in this study were listed in Table 1.

Table 1. Primers used for the qPCR

Gene	Forward primer	Reverse primer
miR-140-5p	5'-TGCGGCAGTGGTTTTACCCTATG-3'	5'-CCAGTGCAGGGTCCGAGGT-3'
U6	5'-TGCGGGTGCTCGCTTCGGCAGC-3'	5'-CCAGTGCAGGGTCCGAGGT-3'

Western blotting. Total protein was extracted by RIPA buffer (Beyotime, Beijng, China). Then, protein concentration was determined by BCA method (Beyotime). After that, proteins were segregated by 10% SDS-PAGE gel (Beyotime). Next, PVDF membranes were used for the adsorption of these proteins. Then, 5% skim milk powder (BD, USA) was prepared for the blocking of these membranes. After that, these membranes were hatched by primary antibodies. The primary antibodies used in this research included MMP-2 (Abcam, ab51075), MMP-9 (Abcam, ab76003), NCKAP1 (Abcam, ab126061) and β-actin (Abcam, ab8226). In the second day, these membranes were hatched with the second antibody (Abcam, ab6721). These primary and second antibodies were diluted with the antibody diluent (Beyotime) with the ratio (1:1000). Finally, the bands were emerged with the enhanced chemiluminescence reagents (Pierce, Rockford, IL, USA).

Luciferase reporter assays. CRL-1999 cells were cultured in the 6 well plates. Next, psiCHECKTM-2 vector (Genechem) contained the cloned miR-140-5p binding site of NCKAP1 (NCKAP1-wild type) was co-transfected with mimics NC or miR-140-5p mimics by Lipofectamine^{2000} transfection reagent. The psiCHECKTM-2 vector containing a mutant sequence of miR-140-5p binding site (3'-untranslated region of NCKAP1), named NCKAP1-mutation (Mut), was established with QuickChange Site-Directed Mutagenesis Kit (Stratagene, La Jola, CA, USA). Fluorescence intensity was detected with the luciferase Reporter Assay Kit (Promega, Fitchburg, WI, USA) after the transfection.

Statistical analysis. GraphPad Prism 6.0 software (GraphPad Software Inc., San Diego, CA, USA) was used for analyzing of the data. And data was displayed as mean ± standard deviation (SD) in this paper. All the experiments were repeated for three times. The linear regression was used for the analysis of the expression between miR-140-5p and NCKAP1. Student's t test was applied for the analyzed of the data in this paper. And there is the statistically significant difference between the two groups until the values of p was less than 0.05.

Results

miR-140-5p inhibited proliferation of vascular smooth muscle cells

To detect the efficacy of miR-140-5p on development of aortic dissection, we detected the expression of miR-140-5p in blood vessel wall of aortic dissection
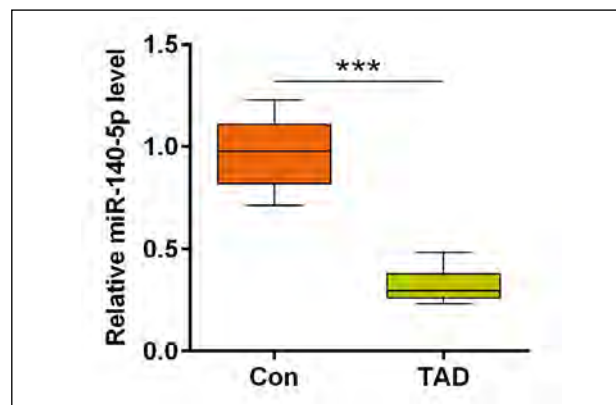

Figure 1. The expression of miR-140-5p was inhibited in blood vessel tissues of aortic dissection patients. The expression of miR-140-5p in vessel tissues of aortic dissection patients and normal vessel tissues was detected with the RT-PCR as described in Methods. Con, tissue from aorta's wall of normal subjects; TAD, tissue from the wall of aortic dissection patients. ***$p < 0.001$.

patients and normal vascular tissues. According to the results (Fig. 1), we revealed that the levels of miR-140-5p were decreased during the occurrence and development of aortic dissection. Next, lentivirus contained the plasmids of overexpression miR-140-5p or miR-140-5p shRNA were applied to upregulate or downregulate miR-140-5p in CRL-1999 cells, respectively. Then the CCK-8 assay was applied for the detection of the viability of these cells. The results in Figure 2A showed that the viability of these cells was repressed after the overexpression of miR-140-5p and enhanced after the inhibition of miR-140-5p. Similarly, results (Fig. 2B) of BrdU assays also showed that overexpression of miR-140-5p suppressed the proliferation of these cells. Furthermore, the inhibition of miR-140-5p promoted the proliferation of these cells. Results of this part revealed that miR-140-5p suppressed the proliferation and viability of vascular smooth muscle cells.

miR-140-5p suppressed the migration and invasion of vascular smooth muscle cells

Next, we detected the migration of CRL-1999 cells by wound healing assays. The results (Fig. 3A) showed that the healing rate of scratches was slower when the expression of miR-140-5p was promoted in these cells. However, the healing rate was faster when the levels
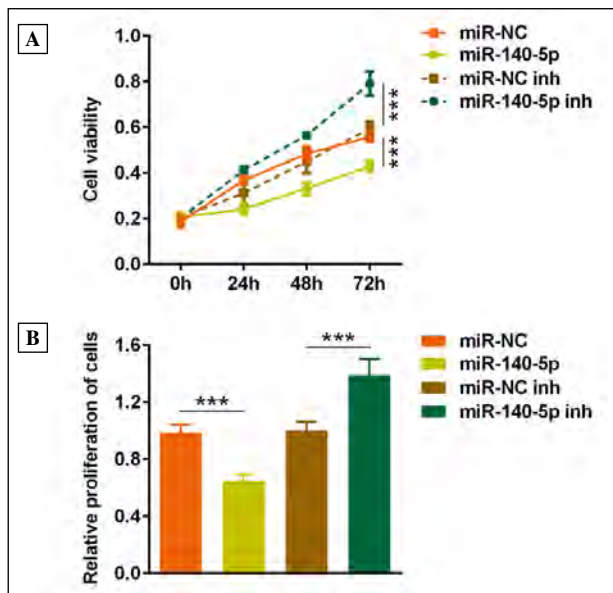
Figure 2. Overexpression of miR-140-5p inhibited the proliferation of vascular smooth muscle cells. **A.** The cell viability of vascular smooth muscle cells was detected with the CCK-8 assay. **B.** Proliferation of vascular smooth muscle cells was determined with BrdU assay. ***$p < 0.001$.

of miR-140-5p were inhibited. In addition, results (Fig. 3B) of transwell showed that the quantity of invasion cells was reduced after overexpression of miR-140-5p. However, the number of invasion cells was promoted after inhibition of miR-140-5p in CRL-1999 cells. Furthermore, the results (Fig. 3C) of western blotting showed that the expression of MMP-2 and MMP-9 was inhibited after overexpression of miR-140-5p. However, the levels of MMP-2 and MMP-9 were upregulated after inhibition of miR-140-5p. And these results suggested that miR-140-5p restricted the migration and invasion of vascular smooth muscle cells.

miR-140-5p targeted and restricted the expression of NCKAP1 in vascular smooth muscle cells

By querying Targetscan database (targetscan, http://www.targetscan.org/vert_72/), we found that miR-140-5p had the potential to bind to the 3'-UTR of NCKAP1. The results (Fig. 4A) of RT-PCR also showed that the expression of NCKAP1 was promoted in blood vessel wall of aortic dissection patients compared to the normal tissues. And the results (Fig. 4B)

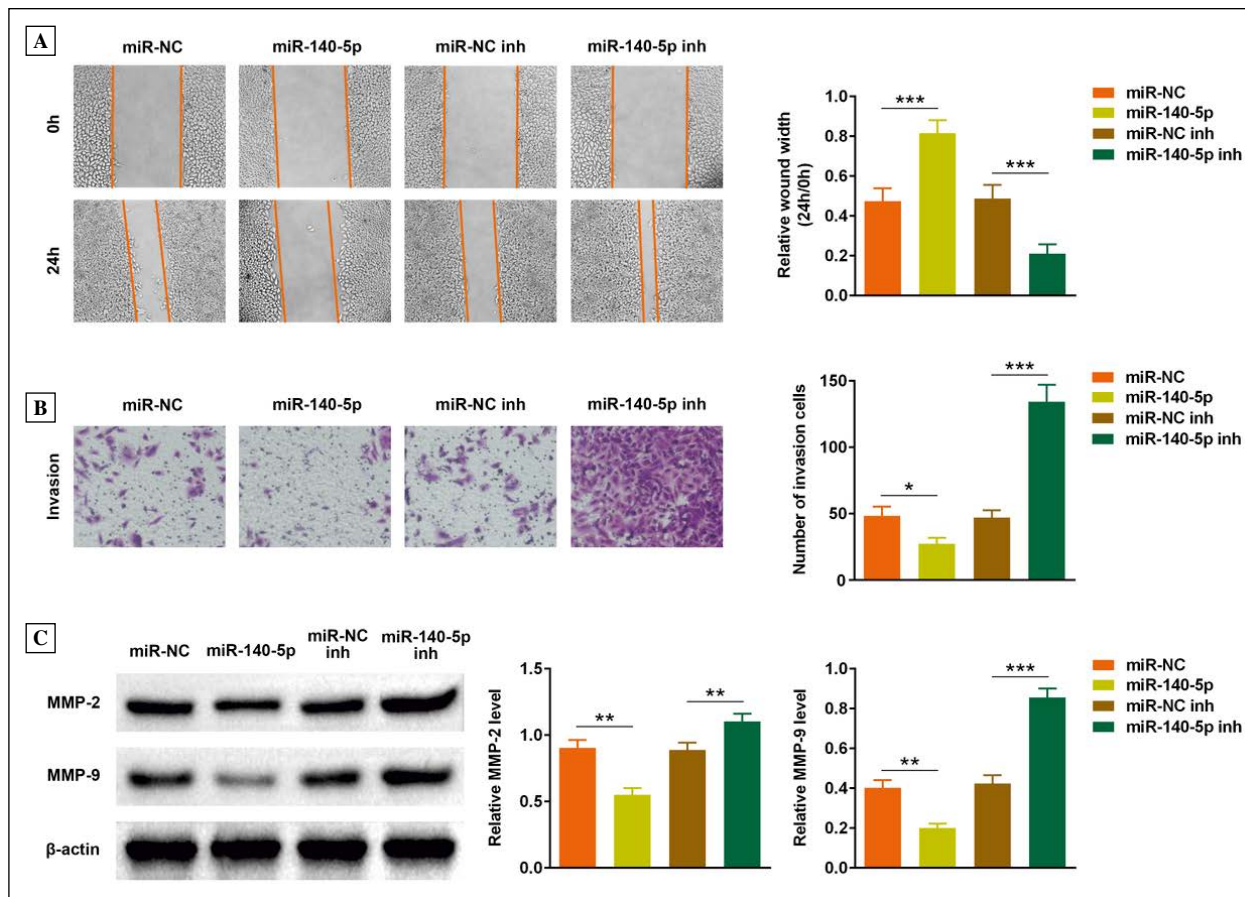**Figure 3.** Overexpression of miR-140-5p inhibited the migration and invasion of vascular smooth muscle cells. **A.** The migration of vascular smooth muscle cells was detected by the wound healing assay. **B.** Invasion of vascular smooth muscle cells was determined with transwell assay. **C.** The expression of MMP-2 and MMP-9 were detected by western blotting. *$p < 0.05$, **$p < 0.01$, ***$p < 0.001$.
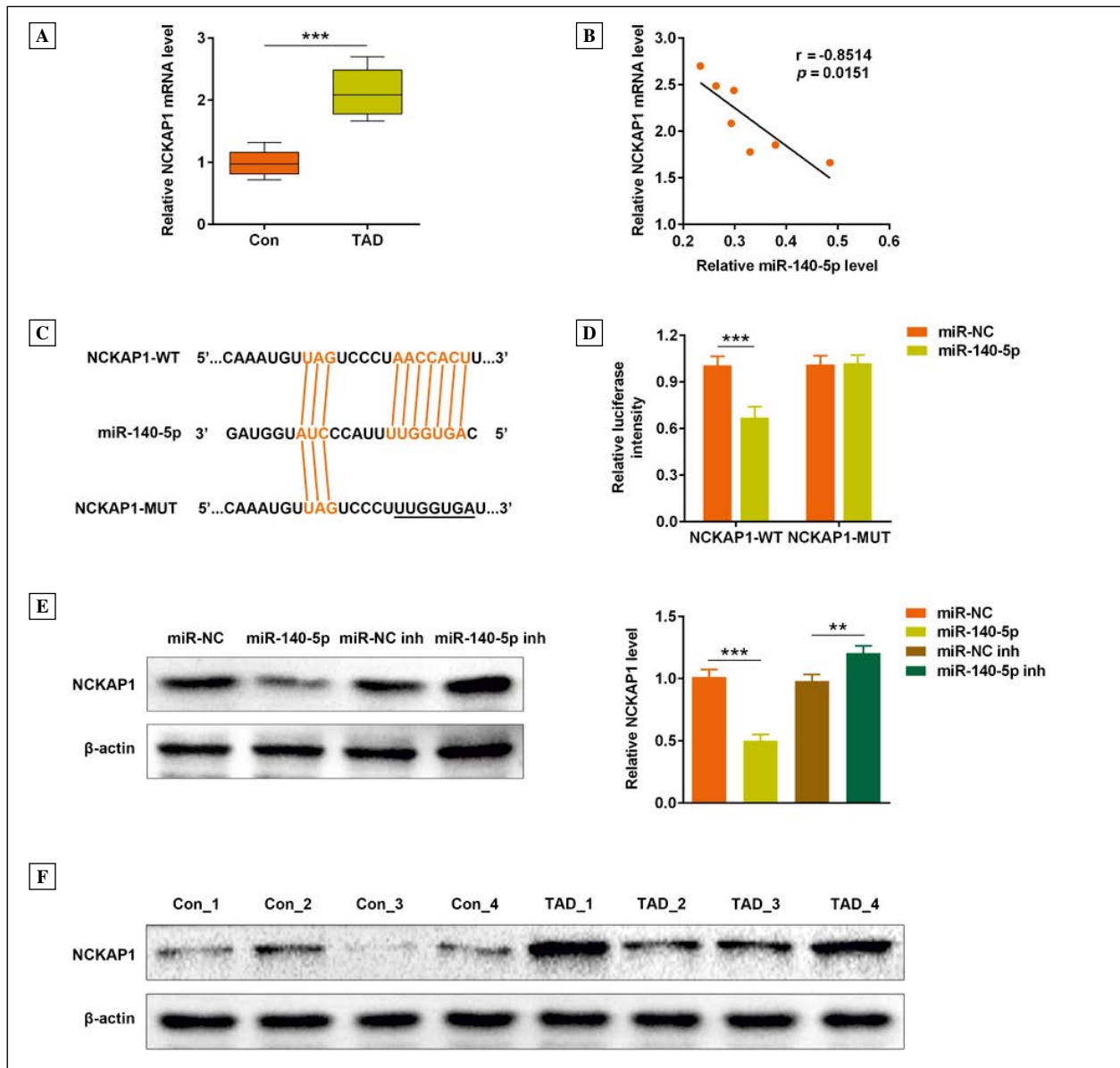
Figure 4. miR-140-5p targeted and inhibited the expression of NCKAP1 in vascular smooth muscle cells. **A.** The expression of NCKAP1 in clinical samples was detected with the RT-PCR. **B.** Linear regression analysis was performed to detect the relationship between miR-140-5p and NCKAP1. **C.** Target region between miR-140-5p and NCKAP1 was depicted. **D.** The fluorescence intensity of vascular smooth muscle cells was measured with the spectrophotometer. **E.** Western blotting was performed to detect the expression of NCKAP1 in vascular smooth muscle cells after the overexpression or inhibition of miR-140-5p. **F.** The expression of NCKAP1 in vessel tissues of aortic dissection patients and normal vessel tissues was detected with western blotting. **$p < 0.01$, ***$p < 0.001$.

of linear-regression analysis also showed that the expression of NCKAP1 was negatively correlated with the levels of miR-140-5p. Results of luciferase reporter assay also showed that the fluorescence intensity was suppressed in the NCKAP1 wild type and miR-140-5p overexpression system. However, there was no difference of the fluorescence between the negative control and miR-140-5p overexpression group after the mutation of 3'-UTR of NCKAP1 (Fig. 4C and Fig.

4D). Next, the expression of NCKAP1 in miR-140-5p overexpression and suppression CRL-1999 cells was determined by western blotting. The results (Fig. 4E) revealed that the level of NCKAP1 was repressed when the expression of miR-140-5p was promoted in these cells. Moreover, expression of NCKAP1 was enhanced when the expression of miR-140-5p was suppressed in CRL-1999 cells. Finally, we also found that the expression of NCKAP1 was upregulated in
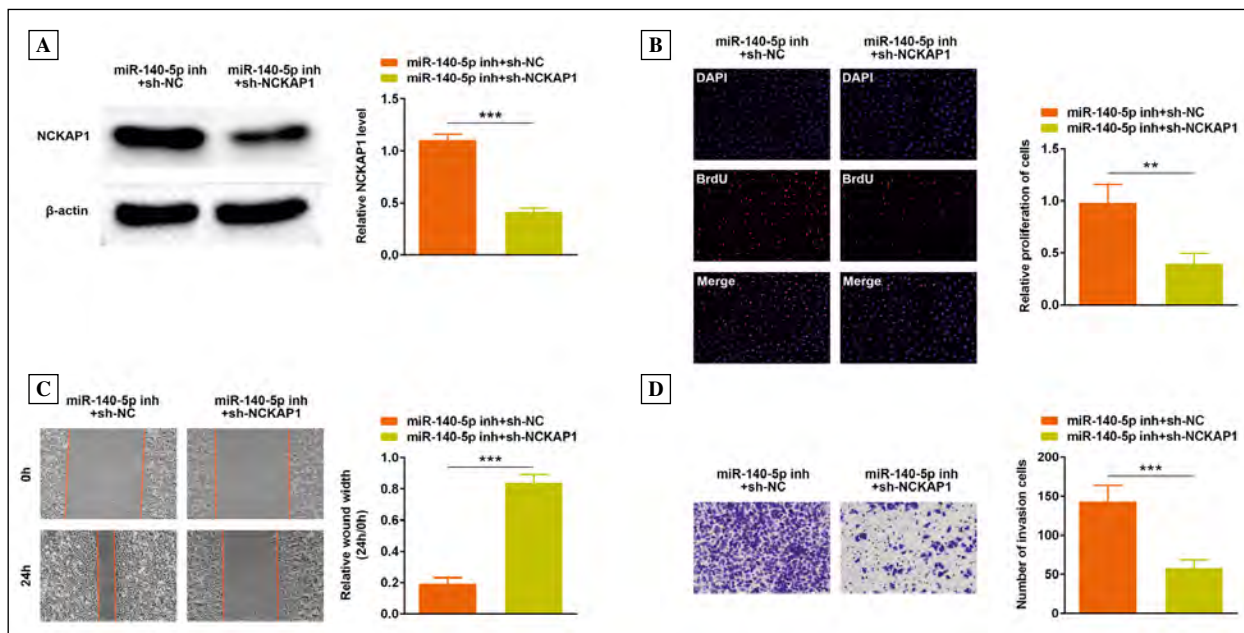
Figure 5. Suppression of NCKAP1 repressed the proliferation, migration and invasion of miR-140-5p inhibition vascular smooth muscle cells. **A.** The expression of NCKAP1 was detected by western blotting. **B.** BrdU assay was performed to detect the proliferation of vascular smooth muscle cells. **C.** Wound healing assay was conducted to detect the migration of vascular smooth muscle cells. **D.** Invasion of vascular smooth muscle cells was determined with the transwell assay. ******$p < 0.01$, *******$p < 0.001$.

arterial vascular wall of aortic dissection patients compared to the normal tissues (Fig. 4F).

Repression of NCKAP1 restricted the proliferation, migration and invasion of miR-140-5p inhibition vascular smooth muscle cells

In this part, we suppressed the expression of NCKAP1 in miR-140-5p inhibition vascular smooth muscle cells. The results (Fig. 5A) showed that the protein levels of NCKAP1 were decreased in the cells transfected with sh-NCKAP1. And the results (Fig. 5B) of BrdU assays showed that the proliferation of CRL-1999 cells was inhibited after the suppression of NCKAP1. Finally, wound healing and transwell assays were performed to explore the changing of migration and invasion of CRL-1999 cells after the repression of NCKAP1. According to the results (Fig. 5C and Fig. 5D), the migration and invasion of the miR-140-5p inhibition CRL-1999 cells were inhibited after the suppression of NCKAP1. These results also implied that the effects of miR-140-5p/NCKAP1 axis on the proliferation, migration and invasion of vascular smooth cells.

Discussion

Weakening of the arterial wall often induced the formation of aortic dissection. And the main feature of aortic dissection is the separation of the aortic media induced by blood flow [14]. And the development of aortic dissection may induce the occurrence of the aortic aneurysm [15]. However, the specific molecular mechanism of aortic dissection is still unclear.

Furthermore, vascular smooth muscle cell is the main cell type in the media layer of the aorta. And the existent of vascular smooth muscle cell played an important role in maintaining the normal physiological function of the aortic wall [1, 16]. In addition, previous research revealed that the EZH2 could affect the development of aortic dissection by regulating the autophagy of vascular smooth muscle cells [17]. Some studies also suggested that proliferation and metastasis of vascular smooth muscle cells were correlated to the development of vascular disease [18, 19]. For instance, miR-146a-5p promoted the development of aortic dissection by enhancing the proliferation and migration of vascular smooth muscle cells [20]. However, there is also research revealed that the proliferation of VSMCs led to the occurrence of plaque of blood vessels and did not induce the aortic dissection [21]. Most of these results from the previous studies suggested that the intensive proliferation and migration of vascular smooth muscle cell promoted the occurrence and development of aortic dissection. In addition, some studies also pointed out that miR-140-5p repressed the proliferation of human pulmonary artery smooth muscle cells [22, 23]. Similarly, we also found that the expression

of miR-140-5p was downregulated in arterial wall of aortic dissection patients. In addition, overexpression of miR-140-5p repressed the proliferation and migration of vascular smooth muscle cells. All these results suggested that miR-140-5p restricted the proliferation, migration and invasion of vascular smooth muscle cell. And the results of our study implied that higher levels of miR-140-5p might have the potential to repress the development of the aortic dissection by suppressing the proliferation, migration and invasion of vascular smooth muscle cells.

On the other hand, miRNAs could affect the expression of target genes by binding to the 3'-UTR of the these genes [24]. By querying the database, we found that miR-140-5p has potential to bind to and affect the expression of NCKAP1. NCKAP1 is localized along the lamellipodia and associated with the migration of multiple types of cells [25]. Another study also revealed that the expression of NCKAP1 promoted the metastasis of breast tumor cells and induced poor prognosis of these patients [26]. Previous study suggested that miR-214 repressed the proliferation, migration and invasion of vascular smooth muscle cells by inhibiting the expression of NCKAP1. In this study, we revealed that miR-140-5p targeted and suppressed the expression of NCKAP1. And the expression of NCKAP1 was also upregulated in the arterial wall of aortic dissection patients. Furthermore, repression of NCKAP1 restricted the proliferation, migration and invasion of miR-140-5p inhibition vascular smooth muscle cells. These results also indicated that NCKAP1 was played a crucial role during the development of aortic dissection. And the results in our study suggested that NCKAP1 can enhance the proliferation and invasion of multiple types of cells. Above all, in this study, we revealed that miR-140-5p inhibited the proliferation, migration and invasion of vascular smooth muscle cells by decreasing of the levels of NCKAP1. And results also implied that miR-140-5p has the potential to impede the development of aortic dissection. Moreover, the results of our research offered new targets and strategy of the clinic treatment of aortic dissection.

Acknowledgements

Not applicable.

Funding

Not applicable.

Competing interests

The authors state that there are no conflicts of interest to disclose.

Ethics approval

Ethical approval was obtained from the Ethics Committee of Tangshan Gongren Hospital.

Statement of Informed Consent

Written informed consent was obtained from a legally authorized representative(s) for anonymized patient information to be published in this article.

Availability of data and materials

All data generated or analyzed during this study are included in this published article.

Authors' contributions

Qing Ma and Jiancheng Liu designed the study, supervised the data collection, Chunbo Li analyzed the data, interpreted the data, Dong Wang prepare the manuscript for publication and reviewed the draft of the manuscript. All authors have read and approved the manuscript.

References

1. Golledge J, Eagle K. Acute aortic dissection. Lancet. 2008; 372(9632): 55–66, doi: 10.1016/s0140-6736(08)60994-0, indexed in Pubmed: PMID: 18603160.
2. Parthenakis F, Koutalas E, Patrianakos A, et al. Diagnosing acute aortic syndromes: The role of specific biochemical markers. Int J Cardiol. 2010; 145(1): 3–8, doi: 10.1016/j.ijcard.2010.04.022, indexed in Pubmed: 20483494.
3. Pagni S, Ganzel B, Trivedi J, et al. Early and midterm outcomes following surgery for acute type A aortic dissection. J Card Surg. 2013; 28(5): 543–549, doi: 10.1111/jocs.12170, indexed in Pubmed: 23909254.
4. Mészáros I, Mórocz J, Szlávi J, et al. Epidemiology and clinicopathology of aortic dissection. Chest. 2000; 117(5): 1271–1278, doi: 10.1378/chest.117.5.1271, indexed in Pubmed: 10807810.
5. Wei X, Sun Y, Wu Y, et al. Downregulation of Talin-1 expression associates with increased proliferation and migration of vascular smooth muscle cells in aortic dissection, BMC Cardiovasc Disord. 2017; 17: 162, doi: 10.1186/s12872-017-0588-0, indexed in Pubmed: 28637452.
6. Hao H, Gabbiani G, Bochaton-Piallat ML. Arterial smooth muscle cell heterogeneity. Arterioscler Thromb Vasc Biol. 2003; 23(9): 1510–1520, doi: 10.1161/01.atv.0000090130.85752.ed, indexed in Pubmed: PMID: 12907463.
7. Salabei J, Hill B. Implications of autophagy for vascular smooth muscle cell function and plasticity. Free Radic Biol Med. 2013; 65: 693–703, doi: 10.1016/j.freeradbiomed.2013.08.003, indexed in Pubmed: 23938401.
8. Jin YY, Wang JF, Wang XJ, et al. Roles of non-coding RNA in pancreatic islet development and functioning. Zhongguo Yi Xue Ke Xue Yuan Xue Bao. 2014; 36: 691–696, doi: 10.3881/j.issn.1000-503X.2014.06.025, indexed in Pubmed: 25556748.
9. Schwarzer A, Emmrich S, Schmidt F, et al. The non-coding RNA landscape of human hematopoiesis and leukemia, Nat Commun. 2017; 8 (1): 218, doi: 10.1038/s41467-017-00212-4, indexed in Pubmed: 28794406.

10. Wang Y, Dong CQ, Peng GY, et al. MicroRNA-134-5p Regulates media degeneration through inhibiting VSMC phenotypic switch and migration in thoracic aortic dissection. Molecular Therapy - Nucleic Acids. 2019; 16: 284–294, doi: 10.1016/j.omtn.2019.02.021, indexed in Pubmed: 30951965.

11. Yu Y, Shi E, Gu T, et al. Overexpression of microRNA-30a contributes to the development of aortic dissection by targeting lysyl oxidase. J Thorac Cardiovasc Surg. 2017; 154(6): 1862–1869, doi: 10.1016/j.jtcvs.2017.06.019, indexed in Pubmed: 28711328.

12. World Medical Association Declaration of Helsinki: ethical principles for medical research involving human subjects. J Am Coll Dent. 2014; 81: 14–18, indexed in Pubmed: 25951678.

13. Walton T, Li G, McCulloch T, et al. Quantitative RT-PCR analysis of estrogen receptor gene expression in laser microdissected prostate cancer tissue. Prostate. 2009; 69(8): 810–819, doi: 10.1002/pros.20929, indexed in Pubmed: 19189301.

14. Takeda N, Komuro I. Genetic basis of hereditary thoracic aortic aneurysms and dissections. J Cardiol. 2019; 74(2): 136–143, doi: 10.1016/j.jjcc.2019.03.014, indexed in Pubmed: 31000321.

15. Martino ADe, Morganti R, Falcetta G, et al. Acute aortic dissection and pregnancy: Review and meta analysis of incidence, presentation, and pathologic substrates. J Card Surg. 2019; 34(12): 1591–1597, doi: 10.1111/jocs.14305, indexed in Pubmed: 31794127.

16. Barbour J, Spinale F, Ikonomidis J. Proteinase systems and thoracic aortic aneurysm progression. J Surg Res. 2007; 139(2): 292–307, doi: 10.1016/j.jss.2006.09.020, indexed in Pubmed: 17292415.

17. Li R, Yi X, Wei X, et al. EZH2 inhibits autophagic cell death of aortic vascular smooth muscle cells to affect aortic dissection. Cell Death Dis. 2018; 9: 180, doi: 10.1038/s41419-017-0213-2, indexed in Pubmed: 29416002.

18. Choi M, Lee I, Kim G, et al. Regulation of PDGF signalling and vascular remodelling by peroxiredoxin II. Nature. 2005; 435(7040): 347–353, doi: 10.1038/nature03587, indexed in Pubmed: 15902258.

19. Hopkins P. Molecular biology of atherosclerosis. Physiol Rev. 2013; 93(3): 1317–1542, doi: 10.1152/physrev.00004.2012, indexed in Pubmed: 23899566.

20. Xue L, Luo S, Ding H, et al. Upregulation of miR-146a-5p is associated with increased proliferation and migration of vascular smooth muscle cells in aortic dissection. J Clin Lab Anal. 2019; 33: e22843, doi: 10.1002/jcla.22843, indexed in Pubmed: 30779466.

21. Clément M, Chappell J, Raffort J, et al. Vascular smooth muscle cell plasticity and autophagy in dissecting aortic aneurysms. Arterioscler Thromb Vasc Biol. 2019; 39(6): 1149–1159, doi: 10.1161/atvbaha.118.311727, indexed in Pubmed: 30943775.

22. Rothman A, Arnold N, Pickworth J, et al. MicroRNA-140-5p and SMURF1 regulate pulmonary arterial hypertension. J Clin Invest. 2016; 126(7): 2495–2508, doi: 10.1172/jci83361, indexed in Pubmed: 27214554.

23. Zhang Y, Xu J. miR-140-5p regulates hypoxia-mediated human pulmonary artery smooth muscle cell proliferation, apoptosis and differentiation by targeting Dnmt1 and promoting SOD2 expression. Biochem Biophys Res Commun. 2016; 473(1): 342–348, doi: 10.1016/j.bbrc.2016.03.116, indexed in Pubmed: 27021683.

24. Loginov VI, Rykov SV, Fridman MV, et al. Methylation of miRNA genes and oncogenesis. Biochemistry (Moscow). 2015; 80(2): 145–162, doi: 10.1134/s0006297915020029, indexed in Pubmed: 25756530.

25. Nakao S, Platek A, Hirano S, et al. Contact-dependent promotion of cell migration by the OL-protocadherin–Nap1 interaction. J Cell Biol. 2008; 182(2): 395–410, doi: 10.1083/jcb.200802069, indexed in Pubmed: 18644894.

26. Lomakina M, Lallemand F, Vacher S, et al. Arpin downregulation in breast cancer is associated with poor prognosis. Br J Cancer. 2016; 114(5): 545–553, doi: 10.1038/bjc.2016.18, indexed in Pubmed: 26867158.

ORIGINAL PAPER

VIA MEDICA

Potential of miR-25-3p in protection of chondrocytes: emphasis on osteoarthritis

Xiao He[1], Lili Deng[2]

[1]The Joint Surgical Center, Chenzhou No. 1 People's Hospital, Chenzhou, Hunan 423000, China
[2]Pediatric Intensive Care Unit, Chenzhou No. 1 People's Hospital, Chenzhou, Hunan 423000, China

Abstract

Introduction. Osteoarthritis (OA) is the most prevailing musculoskeletal dysfunction triggered by lesions in synovial membranes and articular cartilage. MicroRNAs (miRNAs) have emerged as crucial regulators participated in many biological processes, such as osteoarthritis. This study was undertaken to address the role of miR-25-3p in the apoptosis of rat chondrocytes under an OA-like condition and its underlying mechanism.
Material and methods. OA cellular model was established in rat chondrocytes by TNF-α induction. Then, qRT-PCR and Western blotting were utilized for evaluation of the expressions of miR-25-3p and insulin-like growth factor-binding protein 7 (IGFBP7), CCK-8 assay for inspection of chondrocyte viability, flow cytometry for assessment of cell apoptosis rate, Western blotting for the detection of cleaved caspase-3 level and dual-luciferase reporter gene assay for verification of the targeting relationship between miR-25-3p and IGFBP7.
Results. The miR-25-3p expression was decreased and IGFBP7 was elevated in TNF-α-induced rat chondrocytes. The miR-25-3p inhibited chondrocyte apoptosis and IGFBP7 promoted apoptosis as evidenced by enhanced cell viability and suppressed cell apoptosis in OA chondrocytes after miR-25-3p overexpression or IGFBP7 knockdown. The miR-25-3p facilitated chondrocyte viability and repressed cell apoptosis in OA by negatively regulating IGFBP7.
Conclusions. MiR-25-3p negatively regulates IGFBP7 to promote chondrocyte proliferation and restrain chondrocyte apoptosis. Our findings suggest that the regulation of IGFBP7 by miR-25-3p may emerge as a novel therapeutic regimen for OA. *(Folia Histochemica et Cytobiologica 2021, Vol. 59, No. 1, 30–39)*

Key words: miR-25-3p; insulin-like growth factor-binding protein 7; osteoarthritis; chondrocyte; proliferation; apoptosis

Introduction

Osteoarthritis (OA) has been defined as a chronic joint malady featured by degeneration of ligaments and articular cartilage, thickening of subchondral bone and generation of osteophytes [1, 2]. The prevalence of OA worldwide is staggeringly high with an estimated over 250 million people affected and with a lifetime risk for worsening to knee OA of approximately 40% [3]. Chondrocyte, a primary cell type of articular cartilage which occupies approximately 1% of total cartilage volume, is essential for retaining the dynamic equilibrium between catabolism and anabolism of the extracellular matrix in articular cartilage and has been deemed as one of the indispensable regulators of OA pathogenesis [4, 5]. Declining cell number and cell viability of chondrocytes is implicated in the progression and advancement of OA [6]. Thus, the prevention of chondrocyte apoptosis and the promotion of chondrocyte proliferation may be potential therapeutic strategies for OA treatment.

MicroRNAs (miRNAs) play roles in a variety of physiological functions and disease processes by mediating cleavage and destabilization of mRNA [7].

Correspondence address: Xiao He
The Joint Surgical Center,
Chenzhou No. 1 People's Hospital, No. 102, Luojiajin,
Beihu District, Chenzhou, Hunan 423000, China
phone: +86-15973507312, e-mail: hexiao8211@163.com

Zhixi Duan *et al.* have illustrated that miR-15a-5p motivates the degeneration and proliferation of chondrocytes through PTHrP inhibition [8]. Another study describes that the promotion of chondrocyte apoptosis and suppression of chondrocyte proliferation in OA can be caused by miR-181 [9]. These studies emphasize the possibility that miRNAs are associated with OA pathogenesis. In neurons, miR-25-3p was shown to suppress epileptiform discharges by hampering apoptosis and oxidative stress [10]. Besides, miR-25 possesses an inhibitory effect on sepsis-induced cardiomyocyte apoptosis [11]. However, the definite mechanism of miR-25-3p in the apoptosis of chondrocytes remains largely unexplored. Serving as a low-affinity insulin growth factor binder, insulin-like growth factor-binding protein 7 (IGFBP7) may confer significant protective effects on bone metabolism [12]. In breast cancer, IGFBP7 can block cancer cell growth through induction of apoptosis and senescence [13]. Additionally, the elevated IGFBP7 expression in human OA chondrocytes has been recently reported [14]. Accordingly, IGFBP7 may represent an up-and-coming target during the therapy of apoptosis-related OA. Herein, this study presented that miR-25-3p was significantly suppressed and IGFBP7 was remarkably elevated in TNF-α-induced rat chondrocytes. Overexpression of miR-25-3p significantly enhanced cell viability and inhibited cell apoptosis in rat chondrocytes *in vitro*. Interestingly, we corroborated that miR-25-3p regulates IGFBP7 by directly targeting the 3'-UTR of IGFBP7. Our findings suggest that the regulation of IGFBP7 by miR-25-3p may emerge as a novel therapeutic regimen for OA.

Materials and methods

Ethical statement. The experimental scheme was authorized by the Research Ethics Committee of Chenzhou No. 1 People's Hospital. All procedures involving animals were in compliance with the Guide for the Care and Use of Laboratory Animals.

Cell culture. Male Wistar rats (140 ± 10 g) were supplied by Laboratory Animal Center, Chinese Academy of Sciences (Beijing, China). Rats were anesthetized and sacrificed by cervical dislocation. Then chondrocytes were isolated from cartilage tissues of rats under sterile conditions. In brief, cartilage was digested with trypsin (Thermo, Waltham, MA, USA) at 37°C for 30 min and then with 0.2% type II collagenase (Thermo) for 3 h at 37°C. Five min of shaking every 1 h in a constant temperature container was necessary until the fragments were digested. When cartilage mass was visible to the naked eye in floccule shape, isolated chondrocytes were observed under an inverted microscope. Cell digestion was terminated by exposure to fetal bovine serum (FBS, Gibco, Carlsbad, CA) and stroking with a pipette tip. After that, cells were filtrated (200 mesh), centrifuged (1,500 rpm × 10 min) and washed 3 × with phosphate-buffered saline (PBS). Cells were cultured with Dulbecco's modified Eagle medium (DMEM) containing 10% of FBS and 1% of penicillin/streptomycin (Solarbio, Beijing, China) in an incubator (Thermo) at 37°C in 5% CO_2. After 48 h of incubation, the culture medium was changed to remove the non-adherent cells, followed by replacement every other day. Cell morphology and adherent growth were recorded under an inverted microscope. The passage was conducted after the cell adherence to 85% ~ 90%. The chondrocytes of the 3rd to 5th generation were utilized in the experiments. Identification of chondrocytes was performed using toluidine blue staining and immunofluorescent staining of type II collagenase.

Toluidine blue staining [15]. The adherent chondrocytes were digested to prepare a cell suspension, and then cells (1 × 10^5/mL) were seeded into six-well plates for incubation. When cells were completely attached and the cell confluence reached approximately 80%, the culture medium was discarded before the cells were washed 3 × in PBS. Cells in each well were fixed in 4% paraformaldehyde (2 mL) in refrigerator at 4°C for 1 h, followed by three times of PBS washing, exposure to 1 mL of toluidine blue (an appropriate stain for detecting aggrecan, Sangon Biotech, Shanghai, China) at room temperature for 1 h, and toluidine blue was removed after washing 3 × with PBS. The inverted microscope was utilized for observation of the cells.

Immunofluorescent staining. Cells (1 × 10^5/mL) were placed on disposable confocal dishes for incubation, prior to three times of PBS rinsing, 30 min of fixation in 2 mL of 4% paraformaldehyde at room temperature, 3× of PBS rinsing, 20 min of permeation with 1 mL of 0.1% TritonX-100 solution at room temperature and 3 × of PBS rinsing. After that, cells were blocked with 1 mL of 10% goat serum (Zsbio, Beijing, China) at room temperature for 30 min. Cells were incubated with primary antibody (1 mL) against 10% goat serum-diluted rabbit anti-type II collagen (ab34712, 1:200, Abcam, Cambridge, MA, USA) overnight in the dark at 4°C, and then washed 3× with PBS. Following incubation with the secondary antibody (1 mL) against 10% goat serum-diluted Alexa Fluor (ab150077, 1:500, Abcam) at 37°C for 1 h and washing 3× with PBS, cells were immersed in 1 mL of DAPI (SigmaAldrich, Merck KGaA, Darmstadt, Germany) at room temperature for 2 min, followed by washing 3× with PBS. Images were captured by a laser scanning confocal microscopy (200×, green light: wavelength of 543 nm, blue light: wavelength of 458 nm, Olympus OLS5000, Tokyo, Japan) after the cells were covered with 1 mL of anti-fading mounting medium.

Establishment of OA cellular model. TNF-α is a commonly used stimulus to establish OA cellular models [16]. In the present study, 20 ng/mL of TNF-α (PeproTech, Rocky Hill,

Table 1. Primers' sequences

Name		Sequences (5'-3')
miR-25-3p	Forward	CATTGCACTTGTCTCGGTCTGA
	Reverse	GCTGTCAACGATACGCTACGTAACG
U6	Forward	UUCUCCGAACGUGUCACGUTT
	Reverse	UGACACGUUCGGAGAATT
IGFBP7	Forward	CGAGCAAGGTCCTTCCATAGT
	Reverse	GGTGTCGGGATTCCGATGAC
GAPDH	Forward	GGAGCGAGATCCCTCCAAAAT
	Reverse	GGCTGTTGTCATACTTCTCATGG

NJ, USA) was used to stimulate chondrocytes. Briefly, cells were immersed in culture medium with 20 ng/mL of TNF-α for 6 h, and then the medium was changed into normal culture medium for 24 h of additional culture. Cells in the OA group were treated with 20 ng/mL of TNF-α for 6 h of OA modeling, and cells in the Sham group were cultured in normal medium. To determine expression levels of the studied molecules and functional tests, cells were seeded onto six-well plates and exposed to the Lipofectamine 2000 reagent for cell transfection. After that, cells were cultured in normal medium for 24 h prior to 6 h of 20 ng/mL TNF-α treatment, and then the medium containing TNF-α was replaced with normal medium for 24 h of additional incubation. Then the levels of miR-25-3p and IGFBP7 were measured as described below.

Cell transfection and grouping. The miR-25-3p mimic, mimic-NC (100 nM), miR-25-3p inhibitor, inhibitor-NC (100 nM), pcDNA3.1-IGFBP7 and pcDNA3.1 (2 μg) were supplied by GenePharma (Shanghai, China). When cell confluence reached 70% ~ 80%, cell transfection was performed according to the introduction provided with the Lipofectamine 2000 kit (Invitrogen, Carlsbad, CA, USA). Cells were transfected with above plasmids and accordingly grouped into the miR-25-3p mimic group, mimic-NC group, miR-25-3p inhibitor group, inhibitor-NC group, pcDNA3.1-IGFBP7 group, pcDNA3.1 group and Blank group.

Quantitative reverse transcription polymerase chain reaction (qRT-PCR). Total RNA was obtained from chondrocytes by utilizing TRIzol (Invitrogen). Reverse transcription was performed with the reverse transcription kit (TaKaRa, Tokyo, Japan). All operations were conducted based on the manufacturer's instructions. The expression of gene was inspected by LightCycler 480 qPCR instrument (Roche, Indianapolis, IN, USA), and reaction condition was instructed by the fluorescence quantitative PCR kit (SYBR Green Mix, Roche Diagnostics). The real-time PCR program was as follows: 95°C for 10 s, followed by 45 cycles of 95°C for 5 s, 60°C for 10 s and 72°C for 10 s.

A final extension was performed at 72°C for 5 min. The experiments were done in triplicate. The internal reference was GAPDH and data analysis utilized 2$^{-\Delta\Delta Ct}$ method. The formula is as follows: $\Delta\Delta Ct = [Ct_{(target\ gene)} - Ct_{(reference\ gene)}]_{experimental\ group} - [Ct_{(target\ gene)} - Ct_{(reference\ gene)}]_{control\ group}$. The primer sequences are presented in Table 1.

Western blotting. Cells were lysed with RIPA lysate (Beyotime Biotechnology, Shanghai, China) to obtain protein samples. After the protein concentration was analyzed by a BCA kit (Beyotime), the corresponding volume of protein was added to the loading buffer (Beyotime) and mixed. The solution containing proteins was placed in a boiling-water bath for 5 min of denaturation. Electrophoresis was conducted for 30 min at 80 V and then for 1 ~ 2 h at 120 V once bromphenol blue reached the separation gel. Then, the proteins were transferred onto membranes at 220 mA for 120 min in an ice-bath. The membranes were rinsed 1 ~ 2 min with washing solution and sealed in the blocking solution at room temperature for 60 min. After blocking, the membranes were incubated with the primary antibodies against GAPDH (5174S, 1:1000, Cell Signaling, Boston, USA), IGFBP7 (ab74169, 1:1000, Abcam) and cleaved caspase-3 (ab49822, 1:1000, Abcam) overnight at 4°C on a shaking table. Following incubation, the membranes were washed 3 × with washing solution for 10 min before incubation with horseradish peroxidase-labeled goat anti-rabbit IgG (1:5000, Beijing ComWin Biotech Co., Ltd., Beijing, China) for 1 h at room temperature. The membranes were washed 3x for 10 min and exposed to developing liquid for color development. Then chemiluminescence imaging analysis system (Bio-rad, Hercules, CA, USA) was utilized for observation.

Flow cytometry. One milliliter of cell suspension was seeded onto a six-well plate (5 × 10⁵ cells/well) and cultured in an incubator at 37°C in 5% CO$_2$. After 24 h, adherent cells were digested by trypsin, washed with precooled PBS twice (2,000 rpm, 5 min) and re-suspended with 1 mL of Annexin V binding buffer. Flow cytometry (flow cytometer, FACSCalibur, BD Biosciences) was utilized to assess cell apoptosis after

cell exposure to 10 μL of propidium iodide (PI) and 5 μL of Annexin V-FITC for 30 min at room temperature in the dark. The experiments were done in triplicate.

CCK-8 assay. The cell viability was measured with CCK-8 assay kit (CCK-8, Merck KGaA). One hundred microliters of cell suspension in each well of 96-well plates (1,500 cells /well) was incubated at 37°C in 5% CO_2. After 24 h of pre-incubation, 10 μL of CCK-8 was added for 2 h of additional incubation. The absorbance (optical density, OD) at the wavelength of 450 nm was determined by using a microplate reader, and the experiment was repeated 3×. The absorbance value A was measured and the proliferation rate was reckoned. Proliferation rate (%) = [A$_{(transfection\ group)}$-A$_{(Control)}$]/ /[A$_{(Blank\ group)}$-A$_{(Control)}$] × 100%. A$_{(transfection\ group)}$: absorbance value of cells subjected to cell transfection and CCK-8 solution; A$_{(Control)}$: absorbance value of cells incubated with culture medium and CCK-8 solution; A$_{(Blank\ group)}$: absorbance value of cells without cell transfection but incubated with CCK-8 solution.

Dual-luciferase reporter gene assay. The TargetScan (http://www.targetscan.org/vert_72/) was used to predict the binding site of miR-25-3p and IGFBP7. The mutated and wild type sequences in the binding site of miR-25-3p and IGFBP7 were determined in accordance with the predicted results (mut-IGFBP7, wt-IGFBP7) and cloned into luciferase expression vectors (pGL3-Basic). Then the vectors were cotransfected with miR-25-5p (0, 50 nM, 300 nM, Gene Pharma, Shanghai, China) into HEK293T cells. After cell transfection, HEK293T cells were incubated with 100 μL of cell lysis buffer on a shaking table at room temperature for 20 min to lyse the cells. Firefly luciferase activity or Renilla luciferase activity was measured after cell suspension exposure to 50 μL of luciferase reaction solution (Promega, Madison, WI, USA) or 50 μL of Stop&Glo reagent (Promega). The relative activity was calculated as the ratio of firefly luciferase activity to Renilla luciferase activity. Renilla luciferase activity was regarded as the internal control. Three replicates were set for this test.

Statistical analysis. Statistical analysis was conducted by utilizing GraphPad Prism 5 software (GraphPad Software Inc., San Diego, CA, USA). Student's *t*-test was adopted for the comparison between two groups. Dunnett's multiple comparisons test for comparisons among multiple groups, and the Pearson correlation coefficient was applied to assess the correlation among parameters. *P* values of significance were at *p* < 0.05.

Results

Identification of rat chondrocytes and OA cellular model

The morphology of isolated rat chondrocytes was identified by an inverted microscopy. As depicted in Figure 1A, the rat chondrocytes are grown adherent to the wall, arranged in an irregularly rounded or polygonal pattern and covered the bottom of dishes. Toluidine blue staining of aggrecan secreted by rat chondrocytes exhibited that the cell membrane and cytoplasm of chondrocytes were in blue-purple and the nuclei were in dark purple with obvious nucleoli (Fig. 1B). Results of immunofluorescent staining of specific type II collagenase secreted by rat chondrocytes expounded that the addition of specific type II collagen antibodies stained the cytoplasm to green, and DAPI stained nucleus to blue (Fig. 1C). These data indicated that the cells isolated from rat knee joints are chondrocytes.

After TNF-α stimulation for OA modeling, CCK-8 assay, flow cytometry and Western blotting were adopted to evaluate the model establishment. These results manifested that the OA group had suppressed proliferation rate (Fig. 1D, *p* < 0.01), elevated apoptosis rate (Fig. 1E, *p* < 0.01) and enhanced cleaved caspase-3 expression (Fig. 1F, *p* < 0.01) when compared with the Sham group. The above results proved that the cells isolated and extracted in this experiment are primary rat chondrocytes from the knee joint, and the apoptosis of chondrocytes could be induced by TNF-α. The successfully established OA cellular models could be used for subsequent experiments.

miR-25-3p facilitates cell proliferation and represses apoptosis in TNF-α-induced chondrocytes

To ascertain the role of miR-25-3p in cell apoptosis and proliferation under the OA-like condition, rat chondrocytes were transfected with miR-25-3p mimic, miR-25-3p inhibitor as well as corresponding negative controls. qRT-PCR described that OA modeling decreased the expression of miR-25-3p in rat chondrocytes (Fig. 2A, *p* < 0.05, *vs.* sham group). Transfection with miR-25-3p mimic heightened miR-25-3p level (Fig. 2B, *p* < 0.05, *vs.* mimic-NC group), while transfection with miR-25-3p inhibitor inhibited miR-25-3p expression in the rat chondrocytes (Fig. 2B, *p* < 0.05, *vs.* inhibitor-NC group), suggesting that miR-25-3p mimic and inhibitor have good transfection efficiencies and can be used in the subsequent experiments.

CCK-8 assay and flow cytometry were performed to further identify the effect of miR-25-3p on the activity of TNF-α-induced rat chondrocytes, and results revealed that the OA + miR-25-3p mimic group possessed elevated cell proliferation rate (Fig. 2C, *p* < 0.05) and repressed cell apoptosis (Fig. 2D, *p* < 0.05) in comparison to the OA + mimic NC group, while the fall in cell proliferation (Fig. 2C, *p* < 0.05) and the rise in cell apoptosis (Fig. 2D, *p* < 0.05) were observed in OA + miR-25-3p inhibitor group when compared with the OA + inhibitor NC group. No significant
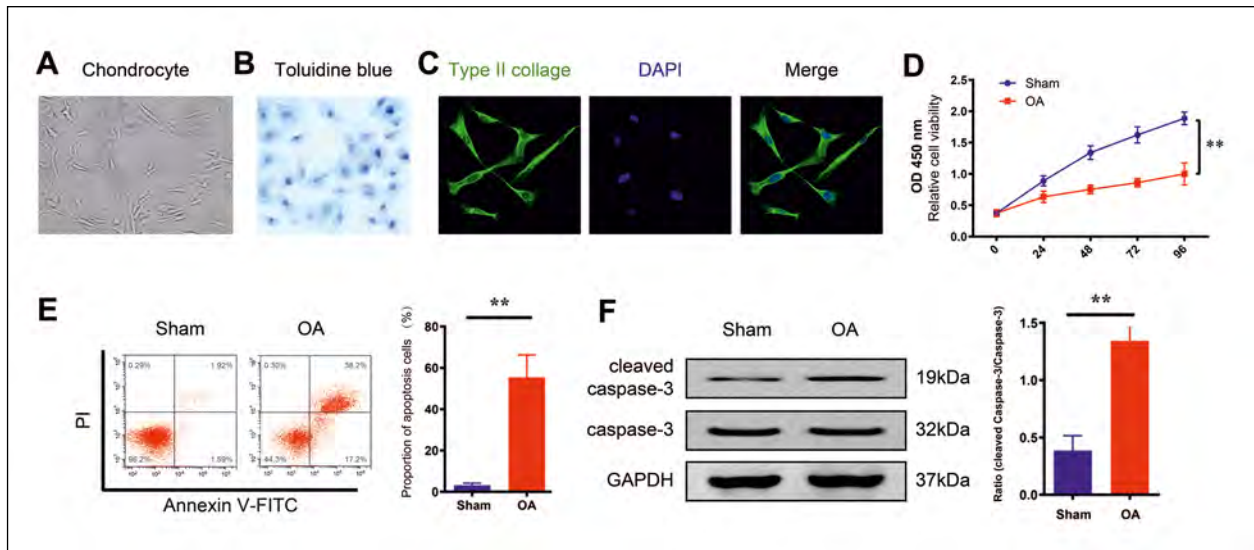
Figure 1. Isolation of rat chondrocytes and establishment of osteoarthritis (OA) cellular model. **A.** The morphology of rat chondrocytes was observed by inverted microscopy, Scale bar indicates 100 μm. **B.** Toluidine blue staining (purple, 100×). **C.** Type II collagen staining (green, 200×), and DAPI staining (blue, 200×). The cell proliferation rate was determined by CCK-8 assay **(D)**, cell apoptosis rate was assessed by flow cytometry **(E)** and protein level of cleaved caspase-3 was measured by Western blotting **(F)**. ******$p < 0.01$.

differences among the OA group, OA + mimic NC group and OA + inhibitor NC group were noted with regard to those indices ($p > 0.05$).

Western blotting showed that the OA + miR-25-3p mimic group had decreased cleaved caspase-3 protein expression (Fig. 2E, $p < 0.05$, *vs.* OA + mimic NC group), whereas the OA + miR-25-3p inhibitor group had increased cleaved caspase-3 (Fig. 2E, $p < 0.05$, *vs.* OA + inhibitor NC group). These findings illustrated that miR-25-3p can enhance viability of rat chondrocytes and suppress apoptosis of TNF--α-induced chondrocytes.

TNF-α-induced chondrocyte apoptosis is promoted by IGFBP7

This study was undertaken to explore the role of IGFBP7 in OA. Analyses of qRT-PCR and Western blotting manifested that the mRNA and protein levels of IGFBP7 were increased in rat chondrocytes following TNF-α induction (Fig. 3A, $p < 0.05$, *vs.* sham group). Additionally, overexpression of IGFBP7 heightened IGFBP7 expression (Fig. 3B, $p < 0.05$, *vs.* pcDNA3.1 group), while knockdown of IGFBP7 diminished IGFBP7 expression (Fig. 3B, $p < 0.05$, *vs.* si-NC group). These results indicated good transfection efficiencies of si-IGFBP7 and pcD-NA3.1-IGFBP7.

Results of CCK-8 assay, flow cytometry and Western blotting revealed that transfection with pcD-NA3.1-IGFBP7 elevated cell apoptosis (Fig. 3D,

$p < 0.05$, *vs.* OA + pcDNA3.1 group) and protein level of cleaved caspase-3 (Fig. 3E, $p < 0.05$), along with decreased cell viability (Fig. 3C, $p < 0.05$) of rat chondrocytes, while transfection with si-IGFBP7 had opposite findings (Fig. 3C–E, $p < 0.05$, OA + si-IGFBP7 group *vs.* OA + si-NC group). There were no remarkable differences in these factors among the OA, OA + si-NC and OA + pcDNA3.1 groups. Collectively, IGFBP7 can accelerate TNF-α-induced chondrocyte apoptosis and inhibit cell proliferation.

miR-25-3p negatively mediates IGFBP7

The aforementioned results have addressed that miR-25-3p and IGFBP7 play opposite roles in the regulation of chondrocyte viability and apoptosis. Subsequently, whether miR-25-3p can regulate IGFBP7 in chondrocytes needs to be investigated. Prediction by the online biological software StarBase 2.0 displayed that miR-25-3p had a binding site with IGFBP7. Dual-luciferase reporter gene assay exhibited that the luciferase activity of HEK293T cells in the IGFBP7 3'-UTR WT group was decreased by transfection of miR-25-3p mimic in a dose dependent manner (Fig. 4A, $p < 0.05$). While transfection with miR-25-3p mimic had no significant impact on the luciferase activity of HEK293T cells in the IGFBP7 3'-UTR MUT group, indicating the binding of miR-25-3p and IGFBP7. qRT-PCR and Western blotting further corroborated this finding. Transfection with miR-25-3p mimic suppressed IGFBP7 in rat chon-
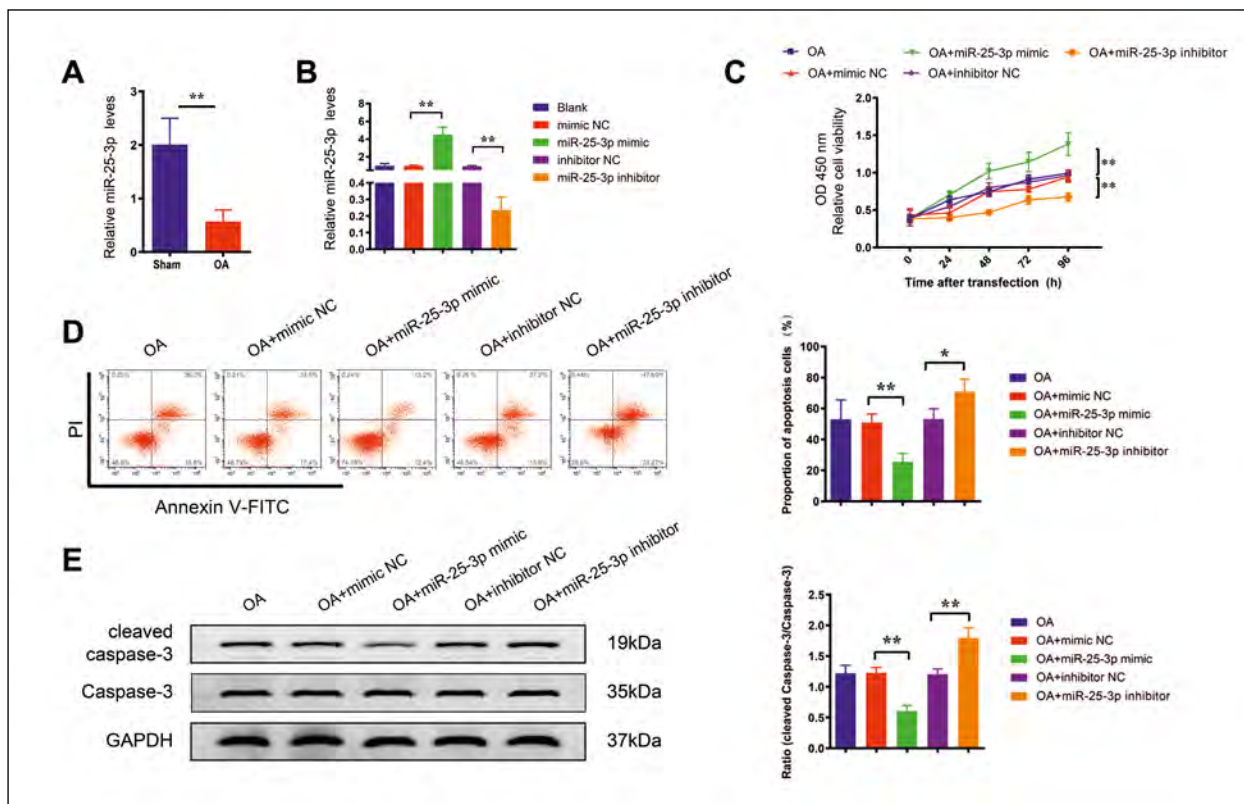
Figure 2. MiR-25-3p enhances the viability and reduces the apoptosis of TNF-α-induced rat chondrocytes. qRT-PCR detection of miR-25-3p expression in rat chondrocytes after OA modeling (**A**) and the transfection efficiency of miR-25-3p mimic and inhibitor (**B**). CCK-8 assay was used to measure the effect of miR-25-3p on chondrocyte viability (**C**). The role of miR-25-3p in cell apoptosis after OA modeling was determined by flow cytometry (**D**). Western blotting was utilized to detect the effect of miR-25-3p on protein expression of cleaved caspase-3 after TNF-α induction (**E**). *$p < 0.05$, **$p < 0.01$, OA — osteoarthritis.

drocytes (Fig. 4B–C, $p < 0.05$, miR-25-3p mimic group vs. mimic NC group), whereas transfection with miR-25-3p inhibitor raised IGFBP7 level (Fig. 4B–C, $p < 0.05$, miR-25-3p inhibitor group vs. inhibitor NC group). Taken together, miR-25-3p may negatively regulate IGFBP7.

miR-25-3p negatively targets IGFBP7 to inhibit the apoptosis of TNF-α-induced rat chondrocytes
It will be further verified whether miR-25-3p could exert its effect on chondrocyte apoptosis by regulating IGFBP7. CCK-8 assay, flow cytometry and Western blotting uncovered that there were increased cell viability (Fig. 5A, $p < 0.05$), repressed cell apoptosis (Fig. 5B, $p < 0.05$) and decreased cleaved caspase-3 expression (Fig. 5C, $p < 0.05$) in the OA + miR-25-3p mimic group rather than in the OA group or OA + miR-25-3p mimic + pcDNA3.1-IGFBP7 group. Furthermore, overexpression of IGFBP7 in OA chondrocytes heightened cell apoptosis rate, increased cleaved caspase-3 expression, and diminished cell viability (Fig. 5A–C, $p < 0.05$, OA group vs. OA +

pcDNA3.1-IGFBP7 group), while following exposure to miR-25-3p mimic revered these trends (Fig. 5A–C, $p < 0.05$, OA + pcDNA3.1-IGFBP7 group vs. OA + miR-25-3p mimic + pcDNA3.1-IGFBP7 group). These data implicated that miR-25-3p may negatively target IGFBP7 to promote proliferation and restrain apoptosis of rat chondrocytes induced by TNF-α.

Discussion

OA, typified by joint space narrowing and a degenerative loss of cartilage integrity, is a dominant reason for disability, pain, and shortening of adult working life [17]. Interestingly, there is evidence showing that apoptosis is progressively recognized as a crucial driver of OA cartilage pathology [18, 19]. Dysregulated gene expression in chondrocytes is implicated in the apoptosis and proliferation of chondrocytes, emphasizing the functional role of miRNAs in controlling chondrocyte apoptosis and development of OA [9, 20]. In the present study, the chondrocytes were isolated from cartilage tissues of rats under sterile con-
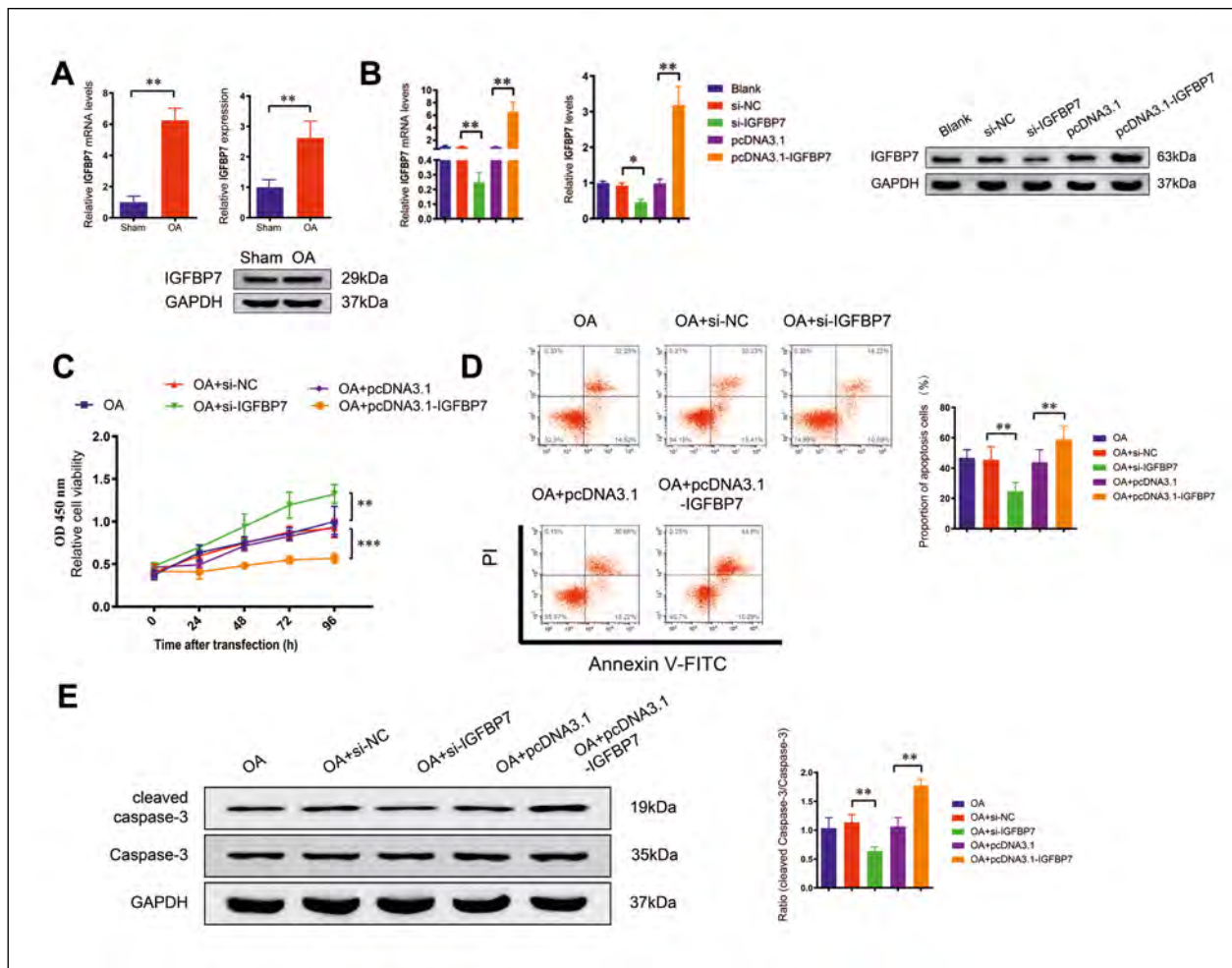
Figure 3. IGFBP7 pushes the apoptosis of TNF-α-induced rat chondrocytes. **A.** The IGFBP7 expression in chondrocytes after OA modeling was determined by qRT-PCR and Western blotting. **B.** The transfection efficiencies of si-IGFBP7 and pcDNA3.1-IGFBP7 were measured by qRT-PCR. CCK-8 assay was used for the assessment of chondrocyte viability **(C)**, flow cytometry for determination of cell apoptosis after OA modeling **(D)**, and Western blotting for measurement of cleaved caspase-3 protein expression after TNF-α induction (E).*$p < 0.05$,**$p < 0.01$, ***$p < 0.001$; OA — osteoarthritis.

ditions, cell cultures were established and then cells were induced with TNF-α. Subsequently, the effects of miR-25-3p on the proliferation and apoptosis of chondrocytes were researched in this study to reveal OA etiology. The results from our study suggested that miR-25-3p represses the apoptosis and promotes the proliferation of rat chondrocytes under the OA-like condition by IGFBP7 suppression.

Initially, we identified that the morphology of isolated cells shared some characteristics with chondrocytes. Furthermore, these findings were further supported by the results of toluidine blue staining of aggrecan and immunofluorescent staining of specific type II collagenase, which suggested that the isolated cells from rats are chondrocytes. Then, the chondrocytes were exposed to 20 ng/mL of TNF-α to induce OA in

chondrocytes. A series of analyses demonstrated that TNF-α induction caused apoptosis of chondrocytes, indicating successful OA cellular model. The expression of miR-25-3p was significantly decreased in the in vitro OA model. This has been previously suggested by a bioinformatical analysis of the osteoarthritis-associated miRNA [21–25]. Additionally, miR-25-3p was found to interfere with the proliferation and apoptosis of chondrocytes under the OA-like condition. As a member of the miR-106b-25 cluster, miR-25 has been identified to be abnormally expressed in various types of tumor and to confer functional roles during a variety of tumor-related processes, including tumorigenesis and cancer cell migration, proliferation and metastasis [26]. For example, miR-25-3p functions as an oncogenic miRNA in osteosarcoma by targeting
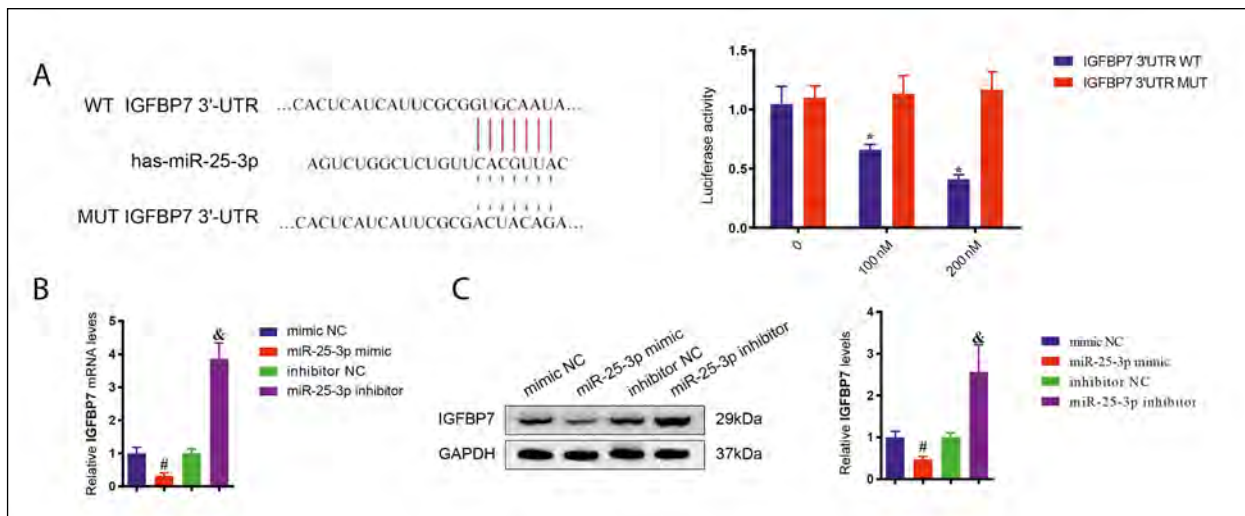
Figure 4. IGFBP7 is negatively regulated by miR-25-3p in rat chondrocytes. **A.** Left: the binding site and mutation site of IGFBP7 and miR-25-3p; right: the binding of miR-25-3p to IGFBP7 displayed by dual-luciferase reporter gene assay. The regulation of miR-25-3p on the mRNA and protein levels of IGFBP7 was exhibited by qRT-PCR (**B**) and Western blotting (**C**). *$p < 0.05$ compared to IGFBP7 3'UTR WT group; #$p < 0.05$ compared to mimic NC group. &$p < 0.05$ compared to inhibitor NC group. WT — wild type; NC — negative control; UTR — untranslated region.
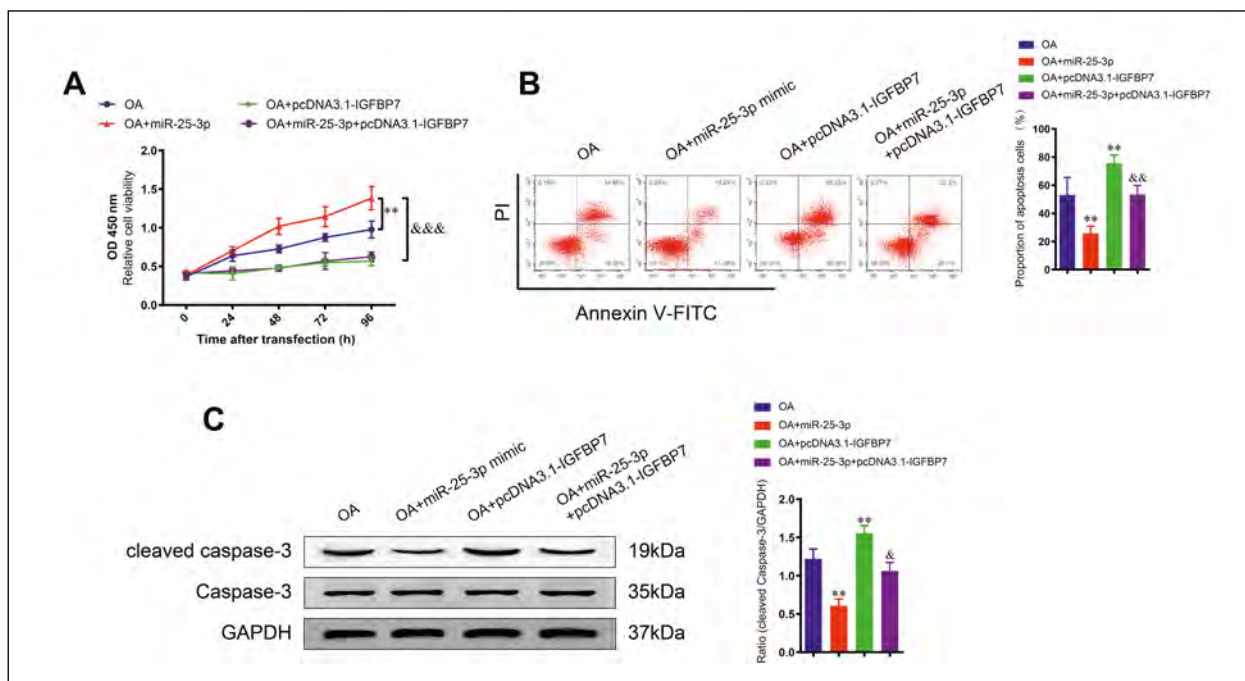
Figure 5. MiR-25-3p inhibits the apoptosis of TNF-α-induced rat chondrocytes by suppressing IGFBP7. CCK-8 assay was utilized for inspection of chondrocyte proliferation rate (**A**), flow cytometry for detection of cell apoptosis rate (**B**) and Western blotting for assessment of cleaved caspase-3 expression (**C**). **$p < 0.01$ compared to OA group; &$p < 0.05$, &&$p < 0.01$, &&&$p < 0.001$ compared to OA + miR-25-3p group; OA — osteoarthritis.

Merlin, and may serve as a potential therapeutic target for osteosarcoma [27]. Previously, miR-25 was expounded to involve in the metastasis and proliferation of non-small cell lung cancer by targeting the LATS2//YAP pathway [28]. Moreover, in triple-negative breast cancer, the biological effects of miR-25-3p on cell apoptosis and proliferation through BTG2 mediation and subsequent activation of AKT and ERK-MAPK pathway were also elucidated in a recent study [29]. In agreement with recent studies, we found that

miR-25-3p facilitated proliferation and suppressed apoptosis of TNF-α-induced chondrocytes. Our finding was subsequently corroborated by the loss and gain of miR-25-3p function, which addressed that overexpression of miR-25-3p enhanced cell viability, decreased cell apoptosis and diminished cleaved caspase-3, while knockdown of miR-25-3p promoted cell apoptosis and repressed cell proliferation.

The second novel observation of this study that has not been reported before is the finding of a possible role of IGFBP7 in the pathomechanisms of OA because we showed that there is a reciprocal relationship between the expression of miR-25-3p and IGFBP7 in the TNF-α-induced OA model. In the current study, the expression level of IGFBP7 was found to be increased in rat chondrocytes following TNF-α induction. IGFBP7 is a protein secreted from the IGFBP family [30]. In this study, IGFBP7 conferred crucial effects on the biological behaviors of TNF-α-induced rat chondrocytes. A lot of experiments illustrated that IGFBP7 facilitated TNF-α-induced chondrocyte apoptosis and inhibited cell proliferation. The previous study has illustrated that IGFBP7 restrains thyroid carcinoma cell proliferation through suppressing cell cycle progression and AKT activity [31]. IGFBP7 is reported to trigger the apoptosis of acute myeloid leukemia cell and to synergize with chemotherapy in suppressing leukemia cells [32]. Additionally, IGFBP7 may exert a therapeutic role in estrogen deficiency-induced osteoporosis [12]. With regard to these evidences, we ensured that IGFBP7 plays an indispensable role in the proliferation and apoptosis of TNF-α-induced rat chondrocytes. Subsequently, the online biological software StarBase 2.0 predicted that IGFBP7 was a target gene of miR-25-3p. Subsequently, dual-luciferase reporter gene assay verified that miR-25-3p can target the 3'-UTR of IGFBP7. Toward this end, gene cotransfection for rescue assay was arranged, and we discovered that miR-25-3p can promote cell growth and repress cell apoptosis in TNF-α-induced rat chondrocytes by targeting IGFBP7.

In conclusion, these data signified that miR-25-3p/IGFBP7 axis may possess a positive effect on mediating the pathologic response to apoptosis for chondrocytes. Furthermore, our study provides evidence that miR-25-3p suppresses the apoptosis of rat chondrocytes and promotes cell proliferation by targeting IGFBP7. This study may be useful for future research on targeting miR-25-3p in the treatment of OA. However, there exists a limitation in our study. These findings were only observed in vitro and will be validated in an animal model in future experiments. An investigation with larger sample sizes are needed to provide a deeper insight regarding which pathways miR-25-3p

modulates to affect the proliferation and apoptosis of OA chondrocytes. More and more methods have been shown to be effective in treating OA [33–35]. Therefore, it is still vital to explore new potential treatment strategies for OA progression.

Acknowledgements

Conflicts of interests

The authors declare there is no conflict of interest regarding the publication of this paper.

Funding

References

1. Qiong J, Xia Z, Jing L, et al. Synovial mesenchymal stem cells effectively alleviate osteoarthritis through promoting the proliferation and differentiation of meniscus chondrocytes. Eur Rev Med Pharmacol Sci. 2020; 24(4): 1645–1655, doi: 10.26355/eurrev_202002_20338, indexed in Pubmed: 32141530.

2. Zou L, Liu J, Lu H. Influence of protein kinase RIPK4 expression on the apoptosis and proliferation of chondrocytes in osteoarthritis. Mol Med Rep. 2018; 17(2): 3078–3084, doi: 10.3892/mmr.2017.8209, indexed in Pubmed: 29257245.

3. Charlier E, Deroyer C, Ciregia F, et al. Chondrocyte dedifferentiation and osteoarthritis (OA). Biochem Pharmacol. 2019; 165: 49–65, doi: 10.1016/j.bcp.2019.02.036, indexed in Pubmed: 30853397.

4. Charlier E, Relic B, Deroyer C, et al. Insights on molecular mechanisms of chondrocytes death in osteoarthritis. Int J Mol Sci. 2016; 17(12), doi: 10.3390/ijms17122146, indexed in Pubmed: 27999417.

5. Yang Bo, Ni J, Long H, et al. IL-1β-induced miR-34a up-regulation inhibits Cyr61 to modulate osteoarthritis chondrocyte proliferation through ADAMTS-4. J Cell Biochem. 2018; 119(10): 7959–7970, doi: 10.1002/jcb.26600, indexed in Pubmed: 29236314.

6. Wang X, Guo Y, Wang C, et al. MicroRNA-142-3p inhibits chondrocyte apoptosis and inflammation in osteoarthritis by targeting HMGB1. Inflammation. 2016; 39(5): 1718–1728, doi: 10.1007/s10753-016-0406-3, indexed in Pubmed: 27447821.

7. Miao G, Zang X, Hou H, et al. Bax Targeted by miR-29a regulates chondrocyte apoptosis in osteoarthritis. Biomed Res Int. 2019; 2019: 1434538, doi: 10.1155/2019/1434538, indexed in Pubmed: 30993110.

8. Duan ZX, Huang P, Tu C, et al. MicroRNA-15a-5p regulates the development of osteoarthritis by targeting PTHrP in chondrocytes. Biomed Res Int. 2019; 2019: 3904923, doi: 10.1155/2019/3904923, indexed in Pubmed: 30949498.

9. Wu XF, Zhou ZH, Zou J. MicroRNA-181 inhibits proliferation and promotes apoptosis of chondrocytes in osteoarthritis

by targeting PTEN. Biochem Cell Biol. 2017; 95(3): 437–444, doi: 10.1139/bcb-2016-0078, indexed in Pubmed: 28177757.

10. Li R, Wen Y, Wu B, et al. MicroRNA-25-3p suppresses epileptiform discharges through inhibiting oxidative stress and apoptosis via targeting OXSR1 in neurons. Biochem Biophys Res Commun. 2020; 523(4): 859–866, doi: 10.1016/j.bbrc.2020.01.050, indexed in Pubmed: 31954517.

11. Yao Y, Sun F, Lei M. miR-25 inhibits sepsis-induced cardiomyocyte apoptosis by targetting PTEN. Biosci Rep. 2018; 38(2), doi: 10.1042/BSR20171511, indexed in Pubmed: 29440462.

12. Ye C, Hou W, Chen Mo, et al. IGFBP7 acts as a negative regulator of RANKL-induced osteoclastogenesis and oestrogen deficiency-induced bone loss. Cell Prolif. 2020; 53(2): e12752, doi: 10.1111/cpr.12752, indexed in Pubmed: 31889368.

13. Benatar T, Yang W, Amemiya Y, et al. IGFBP7 reduces breast tumor growth by induction of senescence and apoptosis pathways. Breast Cancer Res Treat. 2012; 133(2): 563–573, doi: 10.1007/s10549-011-1816-4, indexed in Pubmed: 21997538.

14. Aki T, Hashimoto Ko, Ogasawara M, et al. A whole-genome transcriptome analysis of articular chondrocytes in secondary osteoarthritis of the hip. PLoS One. 2018; 13(6): e0199734, doi: 10.1371/journal.pone.0199734, indexed in Pubmed: 29944724.

15. Gao ZQ, Guo X, Duan C, et al. Altered aggrecan synthesis and collagen expression profiles in chondrocytes from patients with Kashin-Beck disease and osteoarthritis. J Int Med Res. 2012; 40(4): 1325–1334, doi: 10.1177/147323001204000411, indexed in Pubmed: 22971484.

16. Kayal RA, Siqueira M, Alblowi J, et al. TNF-alpha mediates diabetes-enhanced chondrocyte apoptosis during fracture healing and stimulates chondrocyte apoptosis through FOXO1. J Bone Miner Res. 2010; 25(7): 1604–1615, doi: 10.1002/jbmr.59, indexed in Pubmed: 20200974.

17. Pearson MJ, Philp AM, Heward JA, et al. Long intergenic noncoding RNAs mediate the human chondrocyte inflammatory response and are differentially expressed in osteoarthritis cartilage. Arthritis Rheumatol. 2016; 68(4): 845–856, doi: 10.1002/art.39520, indexed in Pubmed: 27023358.

18. Li Y, Li S, Luo Y, et al. LncRNA PVT1 regulates chondrocyte apoptosis in osteoarthritis by acting as a sponge for miR-488-3p. DNA Cell Biol. 2017; 36(7): 571–580, doi: 10.1089/dna.2017.3678, indexed in Pubmed: 28520497.

19. Tan Li, Harper L, McNulty MA, et al. High-fat diet induces endoplasmic reticulum stress to promote chondrocyte apoptosis in mouse knee joints. FASEB J. 2020; 34(4): 5818–5826, doi: 10.1096/fj.201902746R, indexed in Pubmed: 32124494.

20. Chen J, Wu X. MicroRNA-103 contributes to osteoarthritis development by targeting Sox6. Biomed Pharmacother. 2019; 118: 109186, doi: 10.1016/j.biopha.2019.109186, indexed in Pubmed: 31302420.

21. Wang Xi, Ning Y, Zhou B, et al. Integrated bioinformatics analysis of the osteoarthritis-associated microRNA expression signature. Mol Med Rep. 2018; 17(1): 1833–1838, doi: 10.3892/mmr.2017.8057, indexed in Pubmed: 29138855.

22. Coutinho de Almeida R, Ramos YFM, Mahfouz A, et al. RNA sequencing data integration reveals an miRNA interactome of osteoarthritis cartilage. Ann Rheum Dis. 2019; 78(2): 270–277, doi: 10.1136/annrheumdis-2018-213882, indexed in Pubmed: 30504444.

23. Li H, Bai B, Wang J, et al. Identification of key mRNAs and microRNAs in the pathogenesis and progression of osteoarthritis using microarray analysis. Mol Med Rep. 2017; 16(4): 5659–5666, doi: 10.3892/mmr.2017.7251, indexed in Pubmed: 28849222.

24. Yu C, Chen WP, Wang XH. MicroRNA in osteoarthritis. J Int Med Res. 2011; 39(1): 1–9, doi: 10.1177/147323001103900101, indexed in Pubmed: 21672302.

25. Kolhe R, Hunter M, Liu S, et al. Gender-specific differential expression of exosomal miRNA in synovial fluid of patients with osteoarthritis. Sci Rep. 2017; 7(1): 2029, doi: 10.1038/s41598-017-01905-y, indexed in Pubmed: 28515465.

26. Wang M, Yang YOu, Jin Q, et al. Function of miR-25 in the invasion and metastasis of esophageal squamous carcinoma cells and bioinformatical analysis of the miR-106b-25 cluster. Exp Ther Med. 2018; 15(1): 440–446, doi: 10.3892/etm.2017.5358, indexed in Pubmed: 29250158.

27. Rao HC, Wu ZK, Wei Sd, et al. MiR-25-3p serves as an oncogenic MicroRNA by downregulating the expression of merlin in osteosarcoma. Cancer Manag Res. 2020; 12: 8989–9001, doi: 10.2147/CMAR.S262245, indexed in Pubmed: 33061594.

28. Wu T, Hu H, Zhang T, et al. miR-25 Promotes Cell Proliferation, Migration, and Invasion of Non-Small-Cell Lung Cancer by Targeting the LATS2/YAP Signaling Pathway. Oxid Med Cell Longev. 2019; 2019: 9719723, doi: 10.1155/2019/9719723, indexed in Pubmed: 31316723.

29. Chen H, Pan H, Qian Yi, et al. MiR-25-3p promotes the proliferation of triple negative breast cancer by targeting BTG2. Mol Cancer. 2018; 17(1): 4, doi: 10.1186/s12943-017-0754-0, indexed in Pubmed: 29310680.

30. Chen D, Siddiq A, Emdad L, et al. Insulin-like growth factor-binding protein-7 (IGFBP7): a promising gene therapeutic for hepatocellular carcinoma (HCC). Mol Ther. 2013; 21(4): 758–766, doi: 10.1038/mt.2012.282, indexed in Pubmed: 23319057.

31. Zhang Le, Lian R, Zhao J, et al. IGFBP7 inhibits cell proliferation by suppressing AKT activity and cell cycle progression in thyroid carcinoma. Cell Biosci. 2019; 9: 44, doi: 10.1186/s13578-019-0310-2, indexed in Pubmed: 31183073.

32. Verhagen HJ, de Leeuw DC, Roemer MGm, et al. IGFBP7 induces apoptosis of acute myeloid leukemia cells and synergizes with chemotherapy in suppression of leukemia cell survival. Cell Death Dis. 2014; 5: e1300, doi: 10.1038/cddis.2014.268, indexed in Pubmed: 24967962.

33. Yang Q, Zhou Y, Cai P, et al. Downregulation of microRNA-23b-3p alleviates IL-1β-induced injury in chondrogenic CHON-001 cells. Drug Des Devel Ther. 2019; 13: 2503–2512, doi: 10.2147/DDDT.S211051, indexed in Pubmed: 31440033.

34. Yu Y, Zhao J. Modulated Autophagy by MicroRNAs in osteoarthritis chondrocytes. Biomed Res Int. 2019; 2019: 1484152, doi: 10.1155/2019/1484152, indexed in Pubmed: 31205933.

35. Jeon OkH, Wilson DR, Clement CC, et al. Senescence cell-associated extracellular vesicles serve as osteoarthritis disease and therapeutic markers. JCI Insight. 2019; 4(7), doi: 10.1172/jci.insight.125019, indexed in Pubmed: 30944259.

ORIGINAL PAPER

Keratin 17 knockdown suppressed malignancy and cisplatin tolerance of bladder cancer cells, as well as the activation of AKT and ERK pathway

Chen Li, HongWei Su, CongGang Ruan, Xiang Dong Li

Department of Urology, The First Affiliated Hospital of Hebei North University, Zhangjiakou City, Hebei Province, 075000, China

Abstract
Introduction. Bladder cancer (BCa) is one the most common urinary system malignancies and approximately one quarter of diagnosis is invasive muscle-invasive BCa. Accumulating evidence revealed that keratin 17 (KRT17) is closely related to the prognosis and progression of various tumors including a recent study also implying the potential role of KRT17 in the diagnosis of BCa. However, the specific role of KRT17 in BCa remains to be elucidated.
Material and methods. The expression of KRT17 in 5637 BCa cells and SV-HUC-1 normal human urothelial cells was detected using quantitative real-time PCR (qRT-PCR) and western blot. Short hairpin RNA targeting KRT17 was used to knockdown KRT17 in BCa cells. The colony formation was assessed and the proliferation of cells was studied by Cell Counting Kit-8 (CCK-8). Invasion and epithelial-mesenchymal transition (EMT) capacity of BCa cells were assessed using transwell assay and western blot, respectively. Cisplatin sensitivity of cancer cells was measured by evaluating the cell viability using CCK-8 assay. The downstream pathway of KRT17 was explored by western blot.
Results. The expression of KRT17 was elevated in BCa cells in comparison with the normal human urothelial cell at the mRNA and protein levels. The *in vitro* assays demonstrated that KRT17 interference affected the proliferation, colony formation and invasion capacity of BCa cells, as well as EMT. Furthermore, knockdown of KRT17 enhanced cisplatin sensitivity in BCa cells. Mechanically, KRT17 ablation led to the inactivation of both AKT and ERK pathways.
Conclusions. Our results elucidate the vital role of KRT17 in the development of malignancy of BCa cells, probably by the activation of AKT and ERK pathways and suggest that it may represent a novel therapeutic target for BCa. *(Folia Histochemica et Cytobiologica 2021, Vol. 59, No. 1, 40–48)*

Key words: bladder cancer; SV-HUC-1 cells; 5637 cells; keratin 17; shRNA; EMT; proliferation; invasion; cisplatin sensitivity; AKT; ERK

Introduction

Bladder cancer (BCa) is one of the most common malignancies of the urinary tract with approximately 440,000 newly diagnosed and 150,000 deaths every year [1]. Approximately 25–30% patients are diagnosed as muscle-invasive BCa [2]; the rest are diagnosed as non-muscle-invasive BCa. Muscle-invasive BCa is more prone to infiltrate other tissues and metastasize. Patients with metastatic BCa have poor prognosis with less than 10% of 5-year survival rate [3]. Surgical techniques, radiation therapy and chemotherapy are widely applied in BCa treatment; however, the high rate of recurrence and mortality are not well controlled. For example, cisplatin is a front-line chemotherapeutic agent for BCa treatment since most patients show a good initial response to cisplatin, unfortunately they will ultimately develop

Correspondence address: Chen Li,
The First Affiliated Hospital of Hebei North University,
12 Changqing Road, Qiaoxi District,
Zhangjiakou City, Hebei Province, 075000, China
phone: 0313-8046907, e-mail: ChenLifgh12@163.com

the cisplatin-resistance [4]. The patients with cisplatin resistance usually suffer a recurrence what limits the therapeutic potential of chemotherapy [5]. Recent advances in morphological investigation have indicated some ultrastructural changes in cisplatin-resistant (Cis-R) bladder cancer cells, *e.g.*, more double membrane vesicles and pinocytic vesicles [6]. Moreover, the Cis-R cells develop some strategies to reduce cisplatin uptake and accelerate cisplatin efflux [7]. The development of malignancy and chemoresistance of BCa are not well understood; thus, there is a great need to increase our knowledge about progression of BCa. Keratins are members of the intermediate filament family of proteins, and are widely expressed in epithelial cells. Currently, there are 54 known distinct keratins in mammals, 28 type I keratins and 26 type II keratins [8], according to their substructure and sequence homology. The keratins provide structural support and maintain cellular integrity of epithelial cells. Besides, accumulating evidence suggests the regulatory roles of keratins in multiple cellular functions, including proliferation and motility. The role of keratins as markers in tumor progression has been widely documented. For instance, the loss of keratin 8 and 18 in epithelial cancer cells increases their migration and invasion capacity, as well as cisplatin sensitivity [9]. It was reported that keratin 19-positive hepatocellular carcinoma cells display such properties like self-renewal capacity, higher proliferation rate and 5-fluorouracil resistance [10]. Besides, the high level of keratin 14 was noticed to be closely associated with the nodal metastasis of lung cancer, and the further research revealed the relationship between keratin 14 and gastrokine 1 expression in metastasis [11]. The pro-tumor role of keratin 23 was also observed in human colorectal cancer by promoting stem cell properties, proliferation and migration [8]. Keratin 17 (KRT17) belongs to the type I intermediate filaments family. The aberrant expression of KRT17 has been investigated in various carcinomas, and could serve as a potential diagnostic and prognostic marker, including cervical carcinoma, breast cancer and oral carcinoma [12–14]. A recent study based on RNA-seq analysis of urinary extracellular vesicle mRNA from patients with urological diseases identified the overexpression of KRT17 in high stage BCa [15]. Moreover, KRT17 has been recognized as a sensitive and specific biomarker in diagnosis of urothelial neoplasia, and muscle-invasive urothelial carcinoma had a higher proportion of positive KRT17 detection than the non-muscle-invasive type [16]. These clinical findings may imply the potential role of KRT17 in bladder tumorigenesis; however, its specific effect remains to be elucidated.

In an attempt to certify the implication of KRT17 in BCa, we knockdowned KRT17 in two different BCa cell lines, T24 and 5637, and our results demonstrated that knockdown of KRT17 leads to a decrease of proliferation and invasion, as well as epithelial-mesenchymal transition (EMT); furthermore, KRT17-deficient BCa cells were more sensitive to cisplatin. Mechanistically, silencing of KRT17 deactivated AKT and ERK pathway by suppressing phosphorylation. These data may suggest the critical role of KRT17 in the tumorigenesis and cisplatin resistance of BCa implicating KRT17 as a possible target for BCa therapy.

Materials and methods

Cell culture and lentiviral transfection. The normal human urothelial cells SV-HUC-1 and human BCa cell lines 5637 were obtained from American Type Culture Collection (Manassas, VA, USA), and the human BCa cell lines (T24, J82 and TCCSUP) were obtained from the Chinese Academy of Sciences (Shanghai, China). All the cells were cultured in DMEM medium (Gibco, Carlsbad, CA, USA) supplemented with 10% fetal bovine serum (FBS). Lentiviral vectors expressing shRNA targeting KRT17 or negative control were generated from GenPharma (Shanghai, China). BCa cells were transfected with recombinant lentiviruses in the presence of 5 μg/mL polybrene according to the manufacturer's instruction. At 48 hours after infection, the efficiency of transfection was measured by western blot.

RNA isolation and quantitative RT-PCR (qRT-PCR). Total RNA was extracted using TRIzol (Invitrogen, Carlsbad, CA, USA) according to the manufacturer's instructions. Complementary DNA (cDNA) was synthesized using Takara First Strand cDNA Synthesis Kit following the manufacturer's instructions. Real-time (RT)-PCR amplifications were performed with SYBR Green (TaKaRa, Dalian, Liaoning, China). The GAPDH was used as reference to normalize the KRT17 expression. The genes primers and accession numbers employed in this study were listed in Table 1. The relative expression of the KRT17 was calculated using $2^{-\Delta\Delta CT}$ method [17].

Western blot assay. Total proteins were extracted from cells using pre-cooling mammalian protein extraction reagent RIPA (Beyotime Bio, Shanghai, China) containing cocktail (SigmaAldrich, St. Louis, MO, USA). BCA Protein Assay kit (Beyotime Bio) was applied for protein concentration determination. An equal amount of protein was separated with 10% SDS-PAGE and transferred onto polyvinylidene fluoride (PVDF) membranes (SigmaAldrich). After blocked by 5% non-fat milk for 2 h, the PVDF membranes were incubated overnight at 4°C with specific primary antibodies

Table 1. Genes, primers sequences and accession numbers

Gene	Accession number	Forward primer (5'-3')	Reverse primer (5'-3')
KRT17	NM_000422	CTCAGTACAAGAAAGAACCGGTGA	CACAATGGTACGCACCTGAC
GAPDH	NM_002046	AATCCCATCACCATCTTCCAG	CACGATACCAAAGTTGTCATGG

against keratin 17 (ab109725, 1:2000, Abcam, Cambridge, MA, USA), GAPDH (ab8245, 1:5000, Abcam), E-cadherin (ab238099, 1:2000, Abcam), N-cadherin (ab98952, 1:5000, Abcam), vimentin (ab92547, 1:1000, Abcam), p-AKT (SC-1619, 1:2000, Santa Cruz Biotechnology, Santa Cruz, CA, USA), AKT (SC-1619, 1:2000, Santa Cruz Biotechnology), p-ERK (ab76299, 1:2000, Abcam), ERK (ab184699, 1:3000, Abcam). Protein signals were visualized using Bio-Rad imaging system (Hercules, CA, USA) and analyzed using Image J Software (NIH, Bethesda, MD, USA).

Cell viability assay and colony formation assay. Cell viability was detected using the Cell Counting Kit-8 (CCK-8; Diojindo Laboratories, Kumamoto, Japan) following manufacturer's instructions. The transfected cells were seeded on 96-well plates at 2000 cells/well. CC-K8 solution was added at indicated time and cells were incubated for 1 h in dark. The absorbance at a wavelength of 450 nm was measured using a microplate reader.

For colony formation assay, cells were plated into 6-well plates at 500 cells/well and incubated at 37°C. After two weeks of cultivation, the plates were fixed with methanol and stained with crystal violet, and the colonies were counted and photographed.

Transwell assay. Approximately 2×10^4 cells suspended in serum-free medium were seeded to the upper chambers (8 μm pore size, Costar, Cambridge, MA, USA). The lower chamber was filled with medium containing10% FBS. After incubation at 37°C for 24 h, non-invasion cells on the upper chamber were removed and the invasion cells on the lower surface were fixed with 4% formaldehyde and stained with crystal violet. Images of stained cells were counted in 5 randomly selected microscopic fields.

Cisplatin sensitivity determination. The transfected cells were seeded into 96-well plates at a density of 5000 cells/well and incubated with increasing concentrations of cisplatin (SigmaAldrich) for 24 h or 48 h. After incubation, the cell viability was measured using the CCK-8 method according to the manufacturer's instructions.

Statistical analysis. All results are present as mean ± standard deviation (SD) from at least three independent determinations. Student *t*-test was performed to compare the difference between two groups. $P < 0.05$ was considered statistically significant.

Results

Expression of KRT17 was upregulated in BCa cells
Given the KRT17 as an oncoprotein, we first determined whether the expression KRT17 varies between normal and malignant cells. Firstly, one normal human urothelial cell line (SV-HUC-1) and four BCa cell lines (5637, T24, J82 and TCCSUP) were employed in our experiment to detect the expression of KRT17. As indicated in Figure 1A and 1B, KRT17 mRNA and protein levels were significantly higher in four BCa cell lines compared to normal urothelial cells, and T24 and 5637 cells showed the highest expression. These results may imply the involvement of KRT17 in malignance of bladder cancer cells.

Knockdown of KRT17 suppressed BCa cells proliferation
To study the biological role of KRT17 in the regulation of cell proliferation, the BCa cells with the highest level of KRT17 were selected for lentiviral knockdown assay. After 48 h past transfection, the knockdown efficiency was evaluated using western blot (Fig. 2A). As shown in Figure 2B, depletion of KRT17 led to a significant decline of cell viability in two BCa cell lines. Furthermore, KRT17 knockdown also impaired the colony-forming capacity in both types of cancer cells (Fig. 2C). Taken together, these findings suggested the proliferation inhibitory effects of KRT17 knockdown in BCa cells.

Knockdown of KRT17 suppressed BCa cells invasion and EMT
It is well established that invasion is the first step of metastasis, translocation of the cells of the primary tumor to the distant organs [18]. As previous reported, higher expression of KRT17 in muscle-invasive urothelial carcinoma [16], it is necessary to elucidate the role of KRT17 in BCa cell invasion. As shown in Figure 3A, the invasion capacity assessed by transwell assay was remarkably suppressed by KRT17 ablation in both BCa cell lines. Since cells which undergo EMT lose some epithelial features and gain features much like mesenchymal cells, including migratory capacity [19], we decided to determine whether the knockdown of KRT17 affect EMT process in BCa. In accordance with our hypothesis, silencing of KRT17 significantly
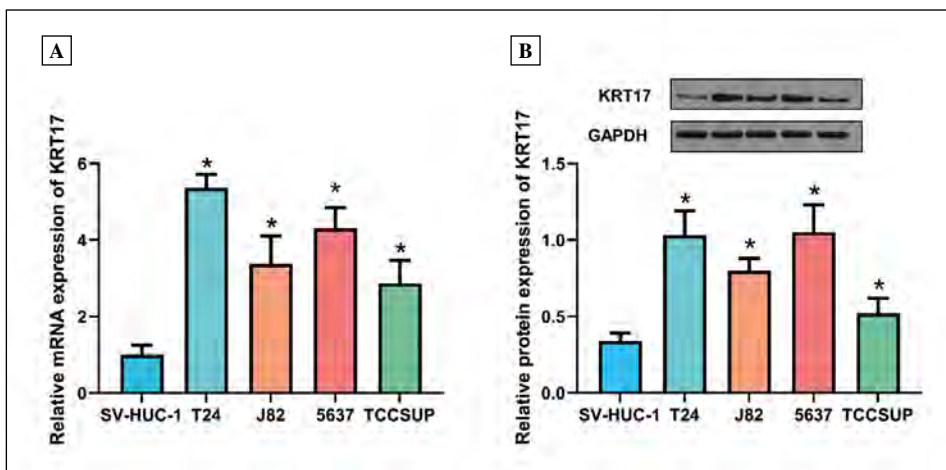
Figure 1. Expression of keratin 17 (KRT17) was increased in bladder cancer (BCa) cells. Relative KRT17 mRNA (**A**) and protein (**B**) expression in human BCa cells (T24, J82, 5637, TCCSUP cell lines) and normal human urothelial cells (SV-HUC-1), *p < 0.05, Student's *t*-test.
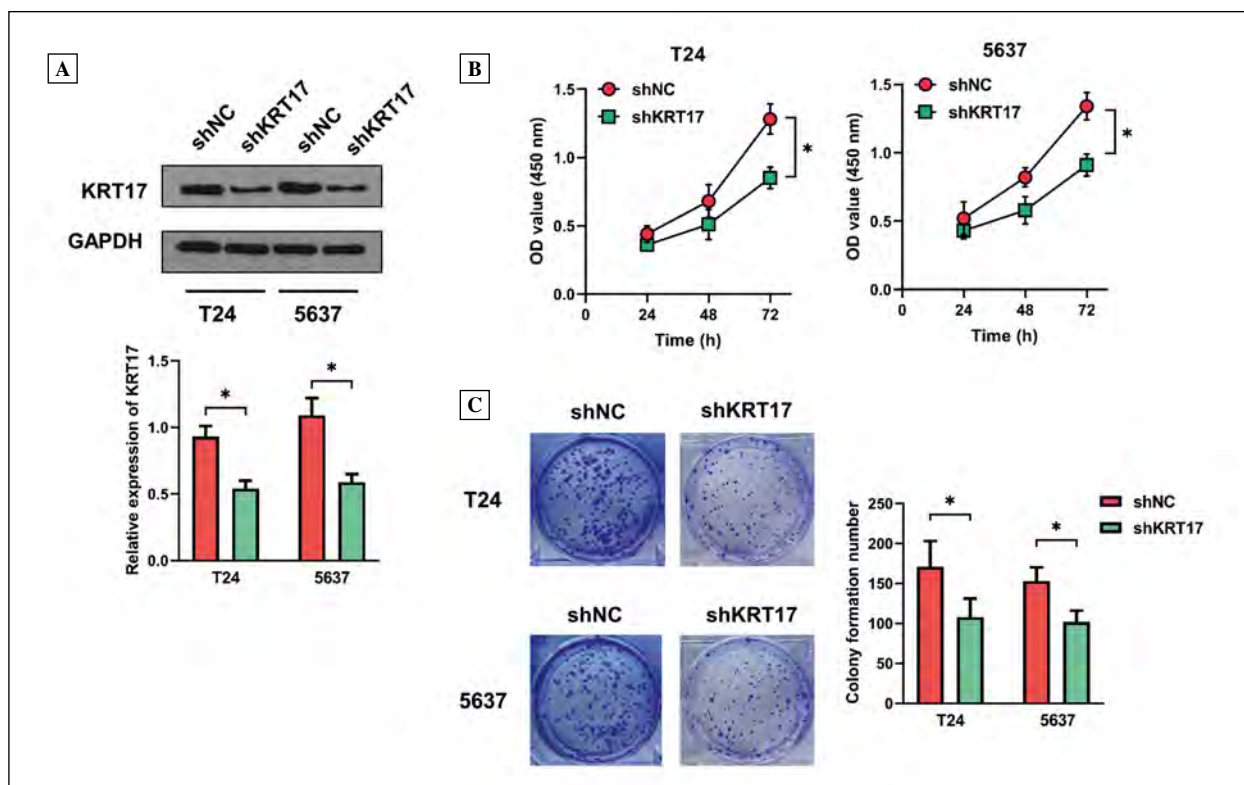

Figure 2. KRT17 depletion suppressed proliferation and colony formation of BCa cells. T24 and 5637 cells were transfected with KRT17 shRNA or scramble shRNA as described in Methods. **A.** The KRT17 knockdown efficiency in T24 BCa cells and normal urothelial 5637 cells was evaluated by western blot. **B.** and **C.** Viability and colony formation capacity of BCa cells was detected using CCK-8 (**B**) and colony formation assays (**C**), respectively (*p < 0.05, Student's *t*-test).

changed EMT-related markers, such as the increase of E-cadherin, and decrease of N-cadherin and vimentin expression (Fig. 3B). These data indicated that KRT17 may have an important role in BCa cells' invasion and EMT.

Knockdown of KRT17 enhanced the sensitivity to cisplatin of BCa cells

Previous studies have linked KRT17 expression with paclitaxel resistance in cervical cancer [20]. To determine whether depletion of KRT17 could influence the
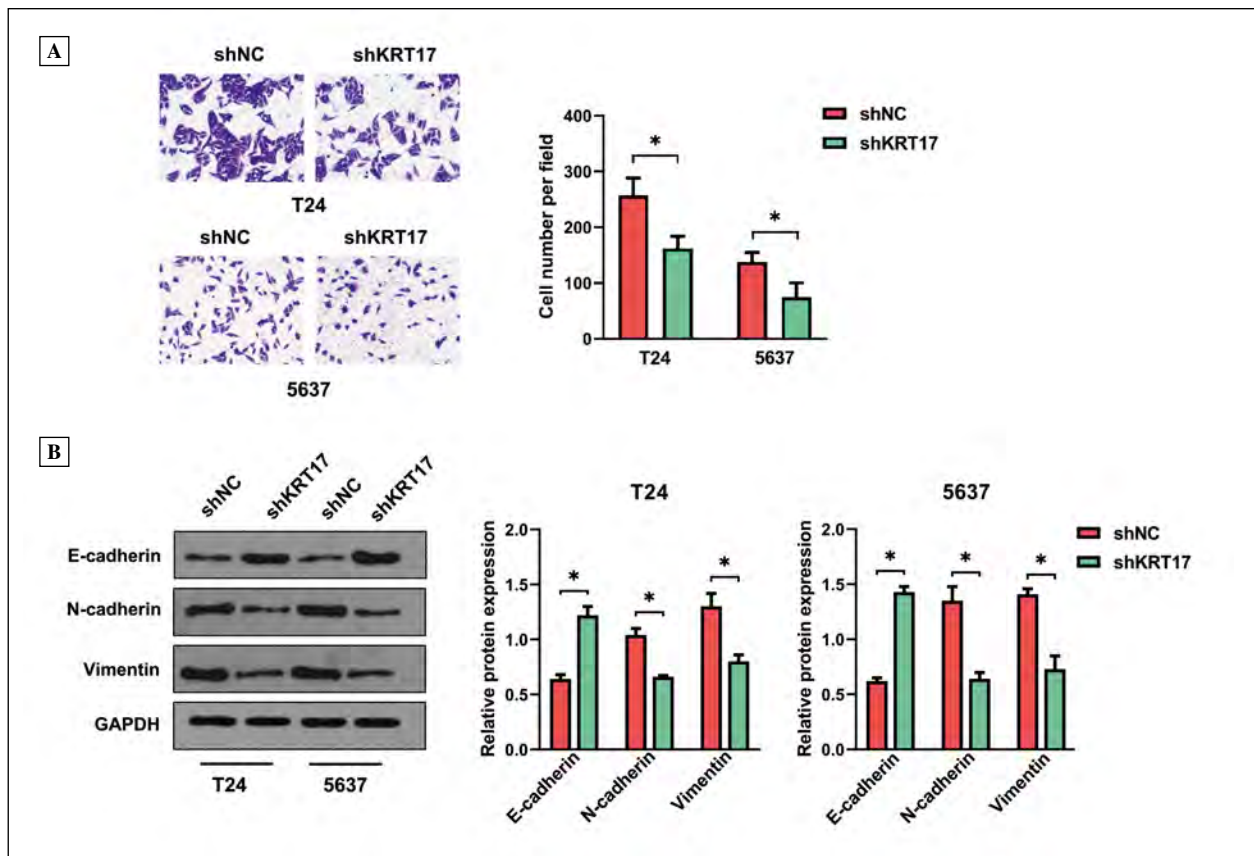
Figure 3. KRT17 depletion suppressed invasion capacity and epithelial-mesenchymal transition in BCa cells. **A.** Transwell assay was conducted to evaluate the invasion capacity of T24 BCa cells and normal urothelial 5637 cells after shKRT17 transfection. **B.** EMT-related expression of proteins (epithelial marker: E-cadherin; mesenchymal markers: N-cadherin and vimentin) was evaluated using western blot after transfection of T24 and 5637 cells with shKRT17 or its negative control (Y axis represent the relative protein abundance normalized to the GAPDH), $*p < 0.05$, Student's t-test.

cisplatin tolerance, BCa cell lines T24 and 5637, transfected with shKRT17 were incubated with indicated concentration of cisplatin for 24 h and 48 h. As shown in Figure 4A and 4B, survival T24 cells with KRT17 interference was dramatically reduced compared to the counterpart transfected with negative control, after incubation for 24 h and 48 h. A similar result was also investigated in 5637 cells (Fig. 4C and 4D), suggesting the implication of KRT17 in the cisplatin tolerance of BCa.

KRT17 regulated AKT and ERK pathway

It has been reported previously that KRT17 silencing inactivates ERK1/2 but not AKT pathway in pancreatic cancer cells [21]. Therefore, we tested whether the same mechanism of KRT17 action is involved in BCa. The activation of ERK and AKT pathway was evaluated by western blot as shown in Figure 5. Our results suggest that phosphorylated-ERK1/2 was decreased in KRT17-knockdown cells while the content of the total ERK1/2 remained unchanged. Besides, the

activation of AKT was also reduced after KRT17 ablation in both cell types when compared to the control, as assessed by the reduction of phosphorylated-AKT. Thereby, these results indicate that targeting KRT17 may exert antitumor function through inactivation of both ERK and AKT pathways.

Discussion

BCa is still a major cause of mortality of human urinary tract malignancies due to the distant metastasis and high recurrence rates. Metastasis is an important feature of malignancy and EMT is a critical process for metastasis of cancer cells. Cells which undergo EMT lose some epithelial features and gain features much like mesenchymal cells, with more migratory capacity, escaping from the primary tumor and disseminating to other organs *via* continuity or by the blood or lymphatic vessels [22]. Since the gain of invasive capacity increases aggressiveness and mortality of BCa, a better understanding of the pathogenesis
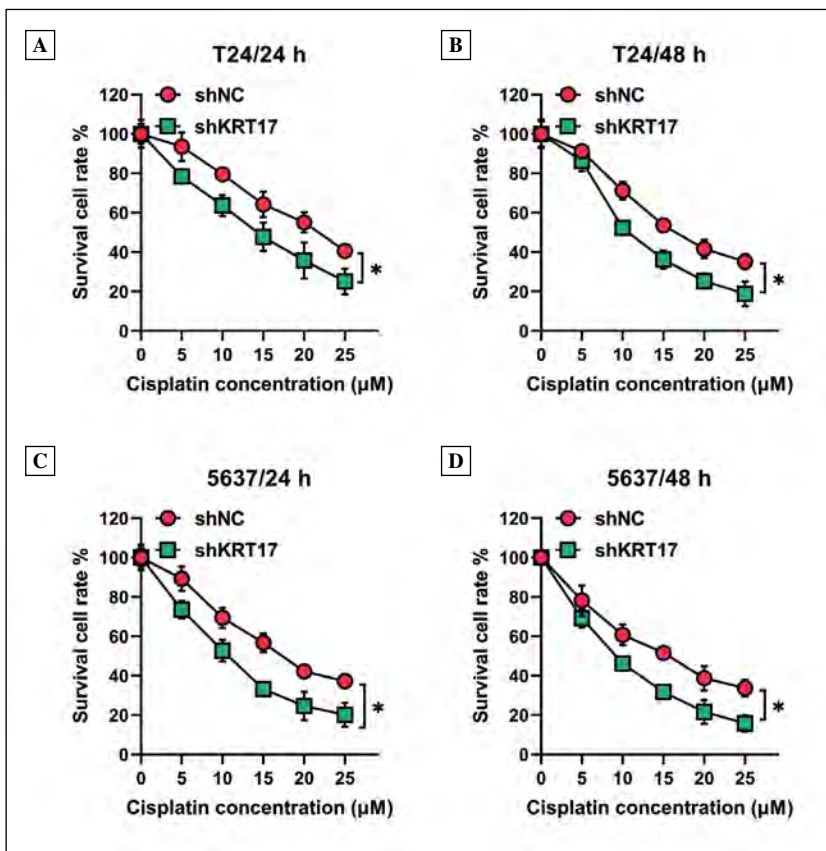
Figure 4. KRT17 depletion increased the cisplatin sensitivity of BCa cells. Cisplatin tolerance of T24 (A &B) and 5637 (C & D) cells was assessed after shNC or shKRT17 transfection after 24 h and 48 h of incubation with the indicated concentration of cisplatin, respectively. *p <0.05, Student's *t*-test.
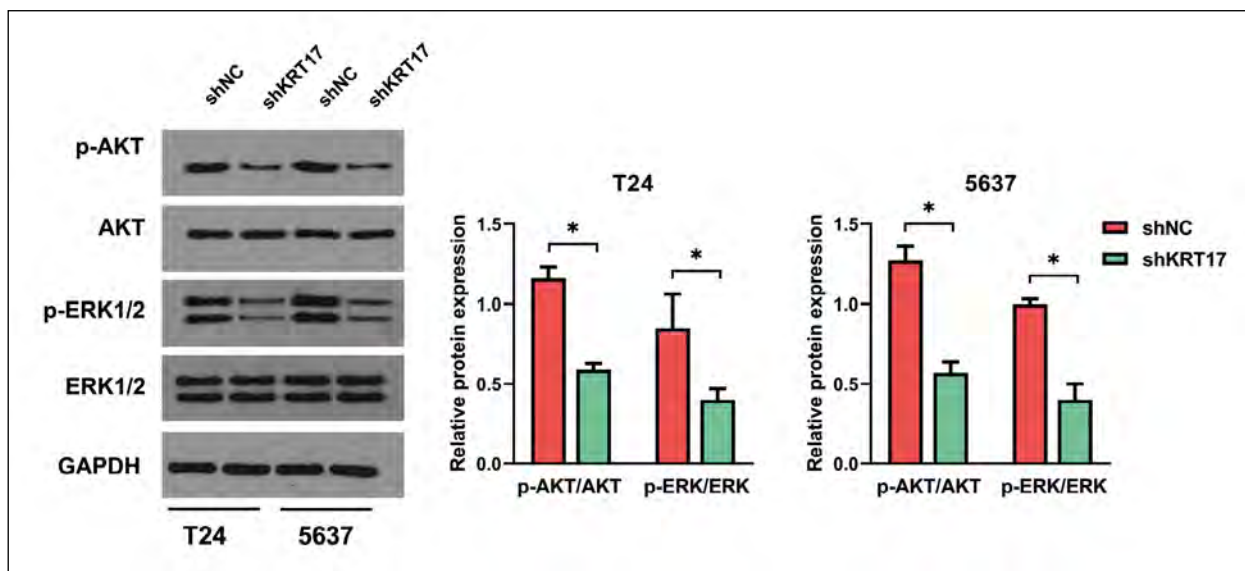

Figure 5. KRT17 depletion led to the inactivation of AKT and ERK pathways. Western blot was conducted to detect The effects of KRT17 knockdown on AKT and ERK pathways activation were assessed by western blot, p-AKT and p-ERK1/2 represent phospho-AKT and phospho-ERK1/2, AKT and ERK1/2 represent total AKT and phospho-ERK1/2. Y axis represents the relative protein abundance normalized to the GAPDH. *p < 0.05, Student's *t*-test.

of BCa is of great importance for anticancer therapy. In this study, we reported that KRT17 expression was associated with BCa malignant characteristics, such as proliferation, invasion, EMT and chemotherapy resistance. In addition, we also revealed that the silencing of KRT17 leads to the inactivation of both AKT and ERK pathway.

Recent studies have established that the aberrant expression of KRT17 has been observed in various types of malignancies. For instance, a study on pancreatic cancer suggests that high expression of KRT17 is closely related with short survival and implies aggressive form of pancreatic ductal adenocarcinoma [23]. Moreover, KRT17 expression is correlated with triple-negative breast cancer and predicts poor prognosis [14]. In our present study, higher KRT17 expression was found in BCa cells than normal human urothelial cell, similarly as shown by Murakami *et al.* [15] and Babu *et al.* [16]. Together, these findings may imply the potential role of KRT17 in the bladder tumorigenesis.

The relationship between KRT17 and cancer growth and metastasis has been documented in several solid tumors. For instance, KRT17 ablation suppresses the proliferation of oral squamous cell carcinoma *in vitro* and *in vivo* in nude mice [24]. Similarly, the pro-proliferation function of KRT17 was also observed in pancreatic cancer cell line [21]. It was demonstrated that pancreatic cancer cells transfected with KRT17 siRNA showed lower Reactive-Oxygen-Species and mTOR/S6K1 phosphorylation levels, as well as reduced proliferation, migration and invasion [25]. In lung adenocarcinoma, overexpression of KRT17 is closely associated with advanced TNM stage and poor overall survival, and KRT17 depletion remarkably suppresses cancer cell proliferation and invasion *in vitro* [26]. Besides, the high expression of KRT17 also predicts the poor prognosis in cervical cancer, and further investigations revealed that KRT17 functions as a negative regulator of $p27^{KIP1}$, which prevents cell G_0-G_1 to S-phase transitions [27]. KRT17 loss-of-function inhibits cervical cancer cells proliferation by modulating $p27^{KIP1}$ subcellular localization and degradation [27]. In the present study, we noticed that BCa cells with KRT17 depletion showed decreased viability, colony formation capacity and invasion, consistent with the previous observations in other cancer cell lines.

It is widely accepted that EMT plays critical roles in cancer progressions, including initiation, proliferation, dissemination, metastasis and chemotherapy resistance [28]. During the process of EMT, tumor cells lose their epithelial characteristics and acquire a mesenchymal phenotype, supporting cell survival and metastasis [29]. The involvement of KRT17 in EMT progression is also reported by some recent studies. Chiang and colleagues demonstrates the potential role of KRT17 in EMT process in areca nut-induced cancer [30]. Recent studies conducted on cervical cancer cells [20] and non-small cell lung cancer cells [31] also confirm the contribution of KRT17 in the EMT process. We noticed that KRT17 knockdown impaired EMT in BCa cell lines, in accordance with these previous reports.

It is well established that cancer cells would acquire some features similar to cancer stem cells, which confers the capacity to drug efflux or other mechanisms to resist chemotherapy cytotoxicity [31]. Data from studies of cervical cancer has proven that KRT17 depletion leads to drug sensitivity [20, 27]. In our study, the interference of KRT17 indeed increased cisplatin sensitivity, and this sensitivity to cisplatin may result from the EMT process reversal.

Intriguingly, when we analyzed the downstream pathways of KRT17, we noticed that the ablation of KRT17 also leads to the deactivation of both AKT and ERK pathway. It was reported that KRT17 deficiency impairs the activation of ERK, while makes little difference on AKT activation in pancreatic cancer cells [21], which disagrees with our present results. However, a recent *in vitro* and *in vivo* study on osteosarcoma cells have shown that KRT17 participates in the regulation of the AKT/mTOR/HIFα pathway [32]. Besides, the pro-tumor effect of KRT17 was found to be AKT-dependent in gastric cancer [33], as well as in esophageal squamous cell carcinoma [34]. The inconsistences between the reported studies may be caused by the underlying cell type specificity in various types of tumor.

In the present work, we confirmed for the first time that KRT17 may promote BCa progression by means of various processes including proliferation, migration, invasion, EMT and drug resistance. The silencing of KRT17 impairs both ERK and AKT phosphorylation activation in BCa cells, suggesting ERK and AKT as downstream effectors of KRT17.

We are aware that our study has some weak points. The main drawback of this study is that although we revealed the role of KRT17 in BCa malignancy and identified ERK and AKT pathways as the downstream of KRT17, the correlation between BCa malignancy and pathways are not well illuminated. In other words, whether KRT17 affects BCa malignancy *via* modulation of ERK and AKT pathways is still elusive. In conclusion, our study is the first to suggest the vital role of KRT17 in the progression of bladder cancer, and may imply the potential therapeutic value of KRT17 targeting in BCa treatment.

Conflict of interests

All authors declare no conflicts of interest in this work.

Acknowledgement

Not applicable.

Funding

Not applicable.

Availability of data and materials

All data generated or analyzed during this study are included in this published article.

Authors' contributions

CL designed the study, supervised the data collection, analyzed the data, HWS and CGR interpreted the data and prepare the manuscript for publication, XDL supervised the data collection, analyzed the data and reviewed the draft of the manuscript.

Ethics approval and consent to participate

Not applicable.

References

1. Lv M, Zhong Z, Huang M, et al. lncRNA H19 regulates epithelial-mesenchymal transition and metastasis of bladder cancer by miR-29b-3p as competing endogenous RNA. Biochim Biophys Acta Mol Cell Res. 2017; 1864(10): 1887–1899, doi: 10.1016/j.bbamcr.2017.08.001, indexed in Pubmed: 28779971.
2. Mao W, Huang X, Wang L, et al. Circular RNA hsa_circ_0068871 regulates FGFR3 expression and activates STAT3 by targeting miR-181a-5p to promote bladder cancer progression. J Exp Clin Cancer Res. 2019; 38(1): 169, doi: 10.1186/s13046-019-1136-9, indexed in Pubmed: 30999937.
3. Kamat A, Hahn N, Efstathiou J, et al. Bladder cancer. The Lancet. 2016; 388(10061): 2796–2810, doi: 10.1016/s0140-6736(16)30512-8, indexed in Pubmed: PMID: 27345655.
4. Drayton RM, Dudziec E, Peter S, et al. Reduced expression of miRNA-27a modulates cisplatin resistance in bladder cancer by targeting the cystine/glutamate exchanger SLC7A11. Clin Cancer Res. 2014; 20(7): 1990–2000, doi: 10.1158/1078-0432.CCR-13-2805, indexed in Pubmed: 24516043.
5. Choi W, Porten S, Kim S, et al. Identification of distinct basal and luminal subtypes of muscle-invasive bladder cancer with different sensitivities to frontline chemotherapy. Cancer Cell. 2014; 25(2): 152–165, doi: 10.1016/j.ccr.2014.01.009, indexed in Pubmed: 24525232.
6. Yoon SJ, Park I, Kwak C, et al. Ultrastructural change due to acquired cisplatin resistance in human bladder cancer cells. Oncol Rep. 2003; 10(5): 1363–1367, doi: doi: 10.3892/or.10.5.1363, indexed in Pubmed: 12883708.
7. Drayton RM, Catto JWF. Molecular mechanisms of cisplatin resistance in bladder cancer. Expert Rev Anticancer Ther.

8. 2012; 12(2): 271–281, doi: 10.1586/era.11.201, indexed in Pubmed: 22316374.
8. Zhang N, Zhang R, Zou K, et al. Keratin 23 promotes telomerase reverse transcriptase expression and human colorectal cancer growth. Cell Death Dis. 2017; 8(7): e2961, doi: 10.1038/cddis.2017.339, indexed in Pubmed: 28749462.
9. Fortier AM, Asselin E, Cadrin M. Keratin 8 and 18 loss in epithelial cancer cells increases collective cell migration and cisplatin sensitivity through claudin1 up-regulation. J Biol Chem. 2013; 288(16): 11555–11571, doi: 10.1074/jbc.M112.428920, indexed in Pubmed: 23449973.
10. Kawai T, Yasuchika K, Ishii T, et al. Keratin 19, a cancer stem cell marker in human hepatocellular carcinoma. Clin Cancer Res. 2015; 21(13): 3081–3091, doi: 10.1158/1078-0432.CCR-14-1936, indexed in Pubmed: 25820415.
11. Yao S, Huang HY, Han X, et al. Keratin 14-high subpopulation mediates lung cancer metastasis potentially through Gkn1 upregulation. Oncogene. 2019; 38(36): 6354–6369, doi: 10.1038/s41388-019-0889-0, indexed in Pubmed: 31320708.
12. Hobbs RP, Batazzi AS, Han MC, et al. Loss of Keratin 17 induces tissue-specific cytokine polarization and cellular differentiation in HPV16-driven cervical tumorigenesis in vivo. Oncogene. 2016; 35(43): 5653–5662, doi: 10.1038/onc.2016.102, indexed in Pubmed: 27065324.
13. Toyoshima T, Vairaktaris E, Nkenke E, et al. Cytokeratin 17 mRNA expression has potential for diagnostic marker of oral squamous cell carcinoma. J Cancer Res Clin Oncol. 2008; 134(4): 515–521, doi: 10.1007/s00432-007-0308-8, indexed in Pubmed: 17786476.
14. Merkin RD, Vanner EA, Romeiser JL, et al. Keratin 17 is overexpressed and predicts poor survival in estrogen receptor-negative/human epidermal growth factor receptor-2-negative breast cancer. Hum Pathol. 2017; 62: 23–32, doi: 10.1016/j.humpath.2016.10.006, indexed in Pubmed: 27816721.
15. Murakami T, Yamamoto CM, Akino T, et al. Bladder cancer detection by urinary extracellular vesicle mRNA analysis. Oncotarget. 2018; 9(67): 32810–32821, doi: 10.18632/oncotarget.25998, indexed in Pubmed: 30214686.
16. Babu S, Mockler DC, Roa-Peña L, et al. Keratin 17 is a sensitive and specific biomarker of urothelial neoplasia. Mod Pathol. 2019; 32(5): 717–724, doi: 10.1038/s41379-018-0177-5, indexed in Pubmed: 30443013.
17. VanGuilder HD, Vrana KE, Freeman WM. Twenty-five years of quantitative PCR for gene expression analysis. Biotechniques. 2008; 44(5): 619–626, doi: 10.2144/000112776, indexed in Pubmed: 18474036.
18. Clark AG, Vignjevic DM. Modes of cancer cell invasion and the role of the microenvironment. Curr Opin Cell Biol. 2015; 36: 13–22, doi: 10.1016/j.ceb.2015.06.004, indexed in Pubmed: 26183445.
19. Kalluri R, Weinberg RA. The basics of epithelial-mesenchymal transition. J Clin Invest. 2009; 119(6): 1420–1428, doi: 10.1172/JCI39104, indexed in Pubmed: 19487818.
20. Li J, Chen Q, Deng Z, et al. KRT17 confers paclitaxel-induced resistance and migration to cervical cancer cells. Life Sci. 2019; 224: 255–262, doi: 10.1016/j.lfs.2019.03.065, indexed in Pubmed: 30928404.
21. Chen P, Shen Z, Fang X, et al. Silencing of keratin 17 by lentivirus-mediated short hairpin RNA inhibits the proliferation of PANC-1 human pancreatic cancer cells. Oncol Lett. 2020; 19(5): 3531–3541, doi: 10.3892/ol.2020.11469, indexed in Pubmed: 32269627.
22. Yamashita N, Tokunaga E, Iimori M, et al. Epithelial paradox: clinical significance of coexpression of E-cadherin and vimentin with regard to invasion and metastasis of breast

cancer. Clin Breast Cancer. 2018; 18(5): e1003–e1009, doi: 10.1016/j.clbc.2018.02.002, indexed in Pubmed: 29526677.

23. Roa-Peña L, Leiton CV, Babu S, et al. Keratin 17 identifies the most lethal molecular subtype of pancreatic cancer. Sci Rep. 2019; 9(1): 11239, doi: 10.1038/s41598-019-47519-4, indexed in Pubmed: 31375762.

24. Khanom R, Nguyen CT, Kayamori K, et al. Keratin 17 Is Induced in Oral Cancer and Facilitates Tumor Growth. PLoS One. 2016; 11(8): e0161163, doi: 10.1371/journal.pone.0161163, indexed in Pubmed: 27512993.

25. Li D, Ni XF, Tang H, et al. KRT17 functions as a tumor promoter and regulates proliferation, migration and invasion in pancreatic cancer via mTOR/S6k1 pathway. Cancer Manag Res. 2020; 12: 2087–2095, doi: 10.2147/CMAR.S243129, indexed in Pubmed: 32256116.

26. Liu J, Liu L, Cao L, et al. Keratin 17 promotes lung adenocarcinoma progression by enhancing cell proliferation and invasion. Med Sci Monit. 2018; 24: 4782–4790, doi: 10.12659/MSM.909350, indexed in Pubmed: 29991674.

27. Escobar-Hoyos LF, Shah R, Roa-Peña L, et al. Keratin-17 promotes p27KIP1 nuclear export and degradation and offers potential prognostic utility. Cancer Res. 2015; 75(17): 3650–3662, doi: 10.1158/0008-5472.CAN-15-0293, indexed in Pubmed: 26109559.

28. Brabletz T, Kalluri R, Nieto MA, et al. EMT in cancer. Nat Rev Cancer. 2018; 18(2): 128–134, doi: 10.1038/nrc.2017.118, indexed in Pubmed: 29326430.

29. Bill R, Christofori G. The relevance of EMT in breast cancer metastasis: Correlation or causality? FEBS Lett. 2015; 589(14): 1577–1587, doi: 10.1016/j.febslet.2015.05.002, indexed in Pubmed: 25979173.

30. Chiang CH, Wu CC, Lee LY, et al. Proteomics analysis reveals involvement of Krt17 in areca nut-induced oral carcinogenesis. J Proteome Res. 2016; 15(9): 2981–2997, doi: 10.1021/acs.jproteome.6b00138, indexed in Pubmed: 27432155.

31. Du B, Shim JS. Targeting epithelial-mesenchymal transition (EMT) to overcome drug resistance in cancer. Molecules. 2016; 21(7), doi: 10.3390/molecules21070965, indexed in Pubmed: 27455225.

32. Yan X, Yang C, Hu W, et al. Knockdown of KRT17 decreases osteosarcoma cell proliferation and the Warburg effect via the AKT/mTOR/HIF1α pathway. Oncol Rep. 2020; 44(1): 103–114, doi: 10.3892/or.2020.7611, indexed in Pubmed: 32627037.

33. Chivu-Economescu M, Dragu DL, Necula LG, et al. Knockdown of KRT17 by siRNA induces antitumoral effects on gastric cancer cells. Gastric Cancer. 2017; 20(6): 948–959, doi: 10.1007/s10120-017-0712-y, indexed in Pubmed: 28299464.

34. Liu Z, Yu S, Ye S, et al. Keratin 17 activates AKT signalling and induces epithelial-mesenchymal transition in oesophageal squamous cell carcinoma. J Proteomics. 2020; 211: 103557, doi: 10.1016/j.jprot.2019.103557, indexed in Pubmed: 31669361.

ORIGINAL PAPER

Genistein exerts a cell-protective effect via Nrf2/HO-1/ /PI3K signaling in A$\beta_{25\text{-}35}$-induced Alzheimer's disease models *in vitro*

Shanqing Yi[1, #], Shuangxi Chen[1, #], Jian Xiang[2, #], Jian Tan[1], Kailiang Huang[1], Hao Zhang[3], Yilin Wang[1, 3], Heng Wu[1, *]

[1]The First Affiliated Hospital, University of South China, Hengyang, Hunan 421001, PR China
[2]Second People's Hospital of Shaoyang City, Shaoyang, Hunan 422001, PR China
[3]The Affiliated Nanhua Hospital, University of South China, Hengyang, Hunan 421001, PR China
[#]These authors contributed equally to this study.

Abstract

Introduction. Alzheimer's disease (AD), a very common neurodegenerative disorder, is mainly characterized by the deposition of β-amyloid protein (Aβ) and extensive neuronal cell death. Currently, there are no satisfactory therapeutic approaches for AD. Although neuroprotective effects of genistein against Aβ-induced toxicity have been reported, the underlying molecular mechanisms remain unclear. Furthermore, the PI3K/Akt/Nrf2 signaling pathway is associated with AD. The aim of the study was to investigate whether genistein can modulate Nrf2/HO-1/PI3K signaling to treat AD.
Materials and methods. Cell viability assay, the measurement of heme oxygenase-1 (HO-1) expression by reverse transcription-polymerase chain reaction (RT-qPCR), and western blot were performed on the SH-SY5Y cells induced by Aβ_{25-35} in response to the treatment with genistein. Moreover, PI3K p85 phosphorylation was measured.
Results. Genistein enhanced the HO-1expression at both the mRNA and protein levels, as well as the PI3K p85 phosphorylation level. In addition, genistein increased the survival of SH-SY5Y cells treated with Aβ_{25-35}*via* HO-1 signaling. However, following transfection with Nrf2 small interfering RNA (siRNA) and treatment with LY294002, an inhibitor of PI3K p85, genistein could not upregulate HO-1 to exert neuroprotective effects on SH-SY5Y cells treated with Aβ_{25-35}.
Conclusions. These results suggest that genistein exerts a neuroprotective effect on SH-SY5Y cells *in vitro via* Nrf2/ /HO-1/PI3K signaling, providing a foundation for the application of genistein in the treatment of neurodegenerative diseases related to Nrf2/HO-1/PI3K signaling. *(Folia Histochemica et Cytobiologica 2021, Vol. 59, No. 1, 49–56)*

Key words: Alzheimer's disease; amyloid β_{25-35}; *in vitro*; SH-SY5Y cells; genistein; heme oxygenase-1; Nrf2; siRNA; Nrf2/HO-1/PI3K pathway

Introduction

Alzheimer's disease (AD), a progressive neurodegenerative disease, affects the aging population around the world [1] and accounts for approximately 60–80% of dementia cases [2]. AD is characterized by the accumulation of β-amyloid peptide (Aβ), neurofibrillary tangles (NFTs) and neuronal loss [3, 4]. The deposition of Aβ may serve as the key step in the initiation of the AD pathological process, and other downstream events, including neuroinflammation, oxidative stress and tau protein accumulation, may be the main causes of neurodegeneration [5]. Currently, despite large improvements in understanding the pathogenesis of AD, existing drugs can only alleviate the symptoms and slow the progression of cognitive declines; there

Correspondence address: Heng Wu
The First Affiliated Hospital,
University of South China, Hengyang,
Hunan 421001, PR China
e-mail: 2915176817@qq.com

are no effective strategies for the treatment of AD [6–8]. As a consequence, identifying the pathological molecular mechanisms is a very important research target related to the treatment of AD.

The present study aimed to focus on the natural products with cost-effective and fewer toxic properties. It has been widely acknowledged that phytochemicals, including genistein, curcumin, resveratrol, quercetin and catechins, are promising therapeutics for the treatment of AD due to their functions in inhibiting oxidative stress, neuroinflammation and mitochondrial dysfunction [9]. Genistein, a natural isoflavone constituent found in soybean extract, can cross the blood-brain barrier in mice [10] and it possesses a variety of pharmacological activities, including anticancer, anti-fibrotic, anti-inflammatory and anti-oxidative activities [11, 12]. Additionally, genistein is a cell-permeable, reversible, substrate competitive inhibitor of protein tyrosine kinases, including autophosphorylation of epidermal growth factor receptor kinase, and regulates diverse intracellular signal transductions [13]. Genistein downregulates the production of TNF-α and the activation of NF-κB in endothelial cells [14, 15], and reduces the production of TLR4 in lipopolysaccharide (LPS)-induced BV2 microglia cell line [16]. Genistein has also been reported to improve learning and memory in numerous diseases [17–19], as well as ameliorate astrogliosis in AD [20, 21].

Since multiple and interdependent mechanisms are involved in the pathological process of AD, the present study searched for other targets relating to genistein that could ameliorate AD. Therefore, nuclear factor erythroid 2-related factor 2(Nrf2)/ /heme oxygenase-1 (HO-1) signaling was selected as a target of the present study. In the physiological state, induction of HO-1 may serve as a beneficial or adaptive response to a number of stimuli, indicating a protective role in numerous disorders [22]. It has been reported that the agents can exert essential protective roles against oxidative stress and inflammation *via* modulating Nrf2/HO-1 [23]. HO-1 has been found to exhibit anti-inflammatory, immunomodulatory and cytoprotective properties, the therapeutic potential of HO-1 can be harnessed by the use of phytochemicals and novel HO-1 inducers [24]. In addition, genistein can upregulate HO-1 expression in mice with doxorubicin-induced cardiotoxicity [25] and in PC12 neuronal cells incubated with amyloid β_{25-35} [26].

Taken together, the aim of the present study was to evaluate the effects and underlying mechanisms of genistein in SH-SY5Y cells treated with $A\beta_{25-35}$, a peptide applied to mimic the neuropathological conditions of AD. It was revealed that genistein may exert a cell-protective effect against $A\beta_{25-35}$-induced neurotoxicity in SH-SY5Y cells *via* Nrf2/HO-1/phosphatidylinositol-3 kinase (PI3K) signaling.

Materials and methods

Genistein. Genistein (cat.345834, SigmaAldrich, St. Louis, MO, USA), dissolved in 0.1% DMSO as a stock solution of 3 mM, was further diluted in culture medium and added to SH-SY5Ycells at the indicated final concentration.

Preparation of Aβ peptide. $A\beta_{25-35}$was purchased from Shanghai Strong Biotechnology Co., Ltd. (Shanghai, China) and prepared as described by Kreutz *et al.* [27]. Before the treatment of SH-SY5Y cells, aliquots dissolved in sterilized ddH$_2$O (1 mg/ml) and stored at −20°C. Then aliquots of $A\beta_{25-35}$ were incubated for 96 h at 37°C to obtain the aggregated $A\beta$.

Nrf2 small interfering RNA (siRNA). The Nrf2 siRNA was purchased from Shanghai Sangon Co., Ltd. (Shanghai, China). The Nrf2 siRNA sequences were sense, 5'-GGUUGA GAC UAC CAU GGU UTT-3' and anti-sense, 5'-AAC CAU GGU AGU CUC AAC CTT-3'. The control siRNA sequences were sense 5'-UUC UCC GAA CGU GUC ACG UTT-3' and anti-sense, 5'-ACG UGA CAC GUU CGG AGA ATT-3'. After cells were washed in PBS, Lipofectamine®2000 reagent (Solarbio Science & Technology Co.) was used for siRNA transfection. The transfection was performed for 4 h.

Cell culture and treatments. SH-SY5Y cells were cultured as described by He *et al.* [28]. A total of 1 × 10⁴ SH-SY5Y cells were seeded into 96-well cell culture plates (for the cell viability assay) or 24-well cell culture plates (for reverse transcription-quantitative PCR (RT-qPCR), and western blot analysis) and treated as follows: (i) Cells were pretreated with genistein (10, 30 or 50 μM) for 90 min prior to co-culture with $A\beta_{25-35}$ at 20 mM for 24 h; (ii) cells were pretreated with ZnPP (Zinc Protoporphyrin, an inhibitor of the HO-1, 10 μM) and genistein (10, 30 or 50 μM) for 90 min prior to a 24-h co-culture with $A\beta_{25-35}$ at 20 μM; (iii) cells were pretreated with Nrf2 siRNA (100 nM) and genistein (10, 30 or 50 μM) for 90 min prior to a 24-h co-culture with $A\beta_{25-35}$ at 20 μM; and (iv) cells were pretreated with LY294002 (10 or 20 μM) and genistein (10, 30 or 50 μM) for 90 min prior to a 24-h co-culture with $A\beta_{25-35}$ at 20 μM. Subsequently, a cell viability assay, RT-qPCR and western blot were performed.

Cell viability assay. The cell viability assay was performed as described previously [29]. At the indicated time-points, SH-SY5Y cells were incubated with the culture medium supplemented with 10 μL of 3-(4,5-dimethyl-2-thiazolyl)-2, 5-diphenyl-2-H-tetrazolium bromide (MTT, at a concentration of 500 μg/ml) (M1020, Solarbio, Beijing, China) for 4 h. After aspirating the culture medium, 100 μL DMSO was then added. Following incubation at 37°C for 30 min,

the optical density was measured spectrophotometrically at 410 nm.

Reverse transcription-polymerase chain reaction (RT-qPCR). RT-qPCR was performed according to the standard protocols and as described previously [30]. Quantitative real-time PCR was performed using SYBR Green Kit (Takara) in an iCycler iQTM (Bio-Rad, Hercules, CA, USA). The primer sequences used for qPCR were as follows: HO-1, 5'-CAT CCT GCG TCT GGA CCT GG' (sense) and 5'-TAA TGT CAC GCA GAT TTC C-3' (antisense); and GAPDH, 5'-ATG GCC TCC CTG TAC CAC ATC-3' (sense) and 5'-TGT TGC GCT CAA TCT CCT CCT-3' (antisense).

Western blot. Western blot was performed as described previously [31]. Protein samples heated at 95°C were separated via 10% sodium dodecyl sulfate-polyacrylamide gel electrophoresis (SDS-PAGE) and electroblotted onto polyvinylidene difluoride (PVDF) membranes (EMD Millipore) at 300 mA for 3 h. The membranes were blocked with 5% non-fat dry milk or BSA dissolved in Tris-HCl saline buffer containing 0.1% Tween-20 (TBST, PH 7.4). Subsequently, the blots were incubated overnight at 4°C with one of the following antibodies: Rabbit anti-HO-1 (1:1000; ab13248, Abcam, Cambridge, UK), rabbit anti-Nrf2 (1:1000; ab137550, Abcam), rabbit anti-PI3K p85 (1:1000; ab191606, Abcam) and rabbit anti-β-actin (1:500; ab8227, Abcam). After washing three times for 5 min each in TBST, the membranes were incubated with HRP-coupled goat anti-rabbit secondary antibodies (1:1000; Boster,

Wuhan, China) diluted in TBST for 1 h. Membranes were washed three times in TBST for 5 min each at room temperature. The immunoreactive signals were then visualized with enhanced chemiluminescence solution (Bio-Rad). The signal intensity was quantified by densitometry using ImageJ 5.0 software (Dental Diagnosis Science, San Antonio, TX, USA).

Statistical analysis. Data are presented as the mean $\pm$ SD. Comparisons between groups were performed using ANOVA followed by Bonferroni's *post hoc* test using GraphPad Prism 6 software. Statistical significance was considered at $P < 0.05$.

Results

Genistein increased the HO-1 expression in SH-SY5Y cells treated with $A\beta_{25-35}$

To investigate the effects of genistein on the SH-SY5Y cells induced by $A\beta_{25-35}$, RT-qPCR and western blot analyses were performed after the cells were pretreated with genistein and co-cultured with $A\beta_{25-35}$. It was observed that, in comparison with the vehicle control, the HO-1 mRNA level was increased in response to $A\beta_{25-35}$ treatment. Compared with the $A\beta_{25-35}$-treated group, genistein (10, 30 and 50 μM) significantly increased the HO-1 mRNA level of $A\beta_{25-35}$-treated SH-SY5Y cells (Fig. 1A).

Similar pattern of HO-1 response to $A\beta_{25-35}$ and genistein treatment was observed at the protein levels (Fig. 1B–C).
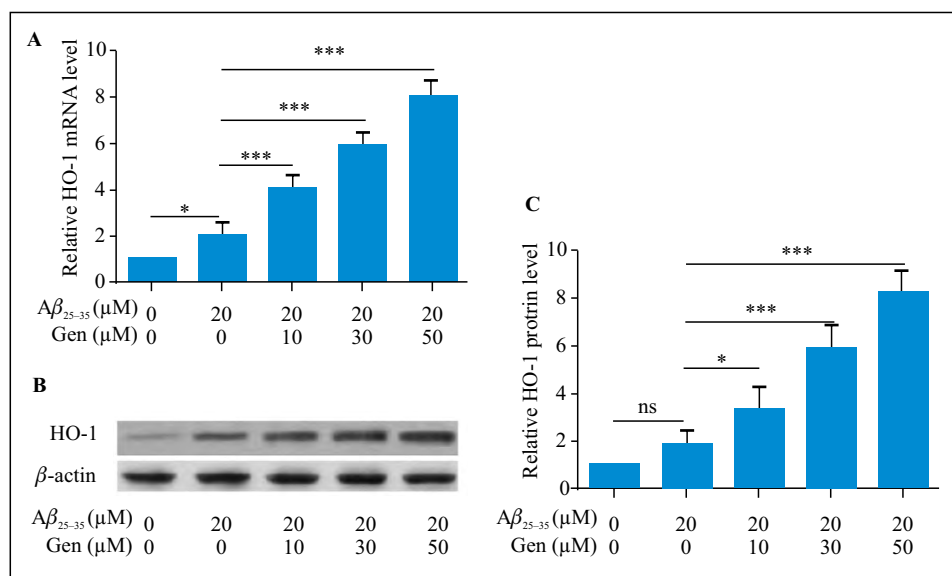

Figure 1. Determination of the effects of genistein on HO-1 level in SH-SY5Y cells induced by $A\beta_{25-35}$. A total of 1×10^4 SH-SY5Y cells were pretreated with genistein at the concentrations of 10, 30 and 50 μM for 90 min prior to a 24-h co-culture with $A\beta_{25-35}$ (20 mM). Subsequently, RT-qPCR and western blot were performed as described in methods. **A.** HO-1 mRNA level. **B** and **C.** Relative HO-1 protein content was assessed with western blot in cells treated with $A\beta_{25-35}$ and without or with various concentrations of genistein (Gen). *$p < 0.05$, ***$p < 0.001$ from five independent experiments.

Genistein reduced the death of SH-SY5Y cells treated with $A\beta_{25-35}$ via upregulating HO-1

To investigate the effect of genistein on $A\beta_{25-35}$-induced apoptosis of SH-SY5Y cells, a MTT assay was performed.

A cell viability assay revealed that, in comparison with the vehicle control, the cell survival rate was decreased in response to $A\beta_{25-35}$ treatment. Genistein (10, 30 and 50 μM) significantly increased the survival rate of $A\beta_{25-35}$-treated SH-SY5Y cells. Additionally,

inhibition of HO-1 by ZnPP (Zinc Protoporphyrin, an inhibitor of the HO-1) reduced the effects of genistein on the cell survival rate of SH-SY5Y cells treated with $A\beta_{25-35}$ (Fig. 2).

Inhibiting Nrf2 signaling reverses the neuroprotective effect of genistein on upregulating HO-1 in $A\beta_{25-35}$-treated SH-SY5Y cells

To investigate the effects of the Nrf2 signaling pathway on the neuroprotective role of genistein on upregulating HO-1 in SH-SY5Y cells induced by $A\beta_{25-35}$, HO-1 protein level was evaluated by western blot after the cells were pretreated with Nrf2 siRNA and genistein.

It was observed that, following inhibition of Nrf2 signaling by Nrf2 siRNA, the effect of genistein on the upregulation of HO-1 protein level in $A\beta_{25-35}$-treated SH-SY5Y cells was partially abolished (Fig. 3A, B).

Inhibiting PI3K signaling reverses the effect of genistein on upregulating HO-1 in $A\beta_{25-35}$-treated SH-SY5Y cells

To investigate the effects of the PI3K signaling pathway on the neuroprotective role of genistein on upregulating HO-1 in SH-SY5Y cells induced by $A\beta_{25-35}$, PI3K p85 phosphorylation level and HO-1 protein level were evaluated by western blot after the cells were pretreated with LY294002 (an inhibitor of PI3K p85) and genistein, and co-cultured with $A\beta_{25-35}$. It was observed that in comparison with the vehicle control, the P85 phosphorylation level was decreased in response to $A\beta_{25-35}$ treatment. Compared with the
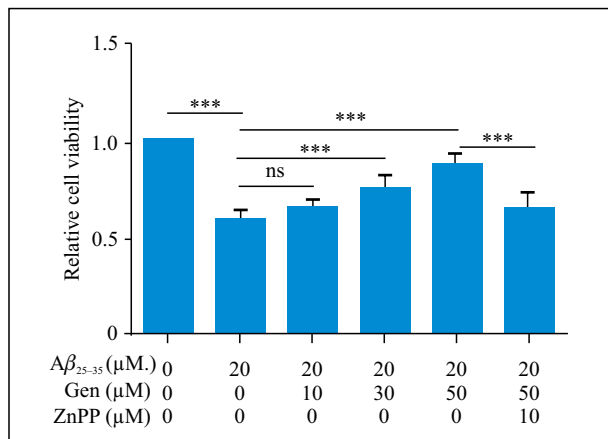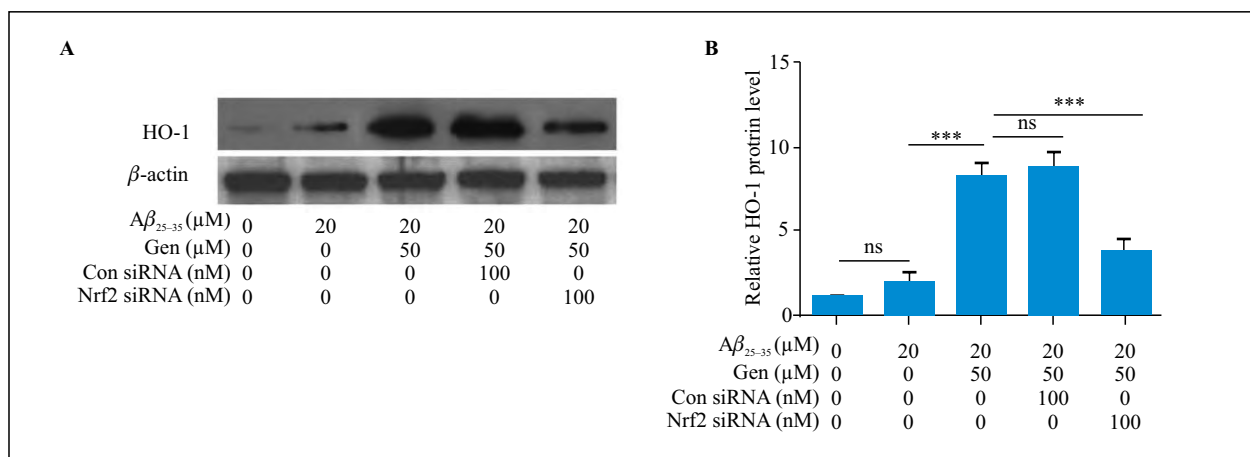

Figure 2. Determination of the effects of genistein on the survival of SH-SY5Y cells induced by $A\beta_{25-35}$ after inhibiting the HO-1. A total of 1×10^4 SH-SY5Y cells were co-pretreated with ZnPP (Zinc Protoporphyrin, an inhibitor of the HO-1) and genistein at the concentrations of 10, 30 and 50 μM for 90 min prior to a 24-h co-culture with $A\beta_{25-35}$ (20 mM). A cell viability assay was then performed. ***$p < 0.01$ from five independent experiments.

Figure 3. Determination of the effects of genistein on the HO-1 in SH-SY5Y cells induced by $A\beta_{25-35}$ after inhibiting Nrf2. 1×10^4 SH-SY5Y cells were co-pretreated with Nrf2 siRNA and 50 μM genistein for 90 min prior to a 24-h co-culture with $A\beta_{25-35}$, followed by western blot. **A–B.** HO-1 protein level was upregulated after the treatment with genistein. Abbreviations: con siRNA — control siRNA; ***$p < 0.001$ from five independent experiments.
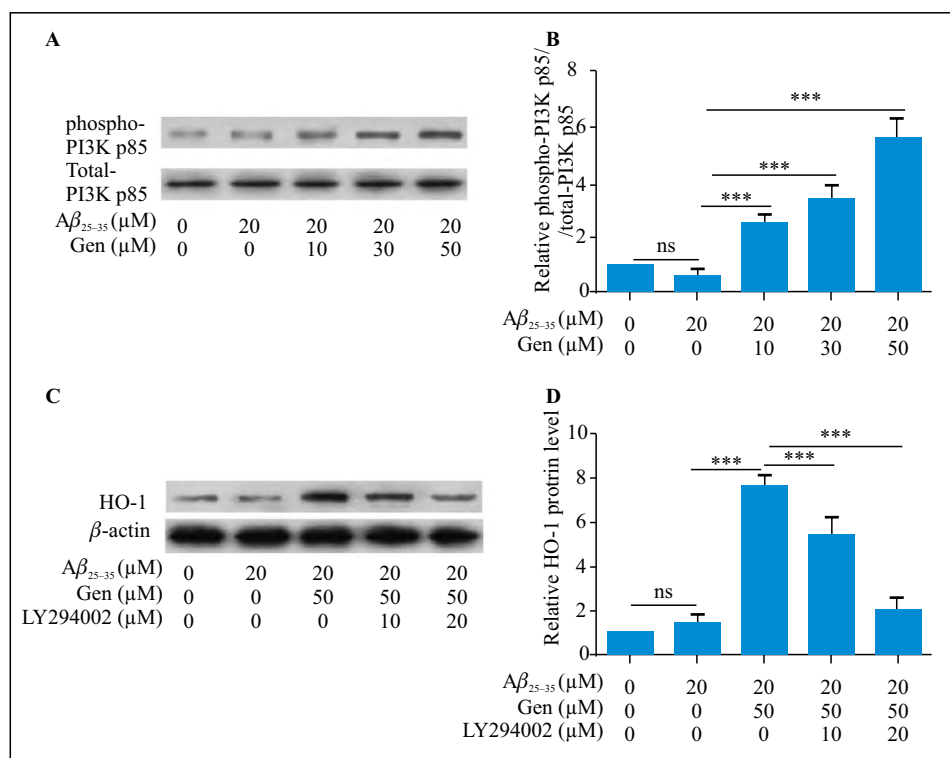
Figure 4. Determination of the effects of genistein on the HO-1 levels in SH-SY5Y cells induced by $A\beta_{25-35}$ after inhibiting the PI3K. A total of 1×10^4 SH-SY5Y cells were co-pretreated with LY294002 and genistein at a concentration of 10, 30 or 50 μM for 90 min prior to a 24-h co-culture with $A\beta_{25-35}$, followed by western blot. **A–B.** The PI3K p85 phosphorylation level in the nucleus was upregulated in SH-SY5Y cells in a dose-dependent manner. **C–D.** The HO-1 protein level in the nucleus was downregulated. ***$p < 0.001$ from five independent experiments.

$A\beta_{25-35}$-treated group, genistein (10, 30 and 50 μM) significantly increased the PI3K p85 phosphorylation level of $A\beta_{25-35}$-treated SH-SY5Y cells (Fig. 4A, B). It was also observed that, after inhibiting PI3K signaling, genistein did not upregulate HO-1 protein level in $A\beta_{25-35}$-treated SH-SY5Y cells (Fig. 4C, D).

Discussion

Previous studies have examined the potential use of genistein as a treatment for AD [32]; genistein has been shown to exert a protective effect in AD *in vitro via* the Nrf2 signaling pathway [33–35]. In the present study, genistein treatment increased cell survival in SH-SY5Y cells treated with $A\beta_{25-35}$. Furthermore, following inhibition of the Nrf2 and PI3K p85 signaling pathways, genistein was unable to exert these cell-protective roles. These findings suggested that genistein treatment may protect SH-SY5Y cells from the neurotoxicity induced by $A\beta_{25-35}$ treatment *via* the Nrf2/HO-1/PI3K signaling pathway.

$A\beta$ peptide fragments can induce neuronal cell death directly or indirectly [36], and oligomeric $A\beta$ peptides have been identified as a key factor in the multiple pathogenic changes in AD and, more generally, in dementia [37]. Deposition of $A\beta_{25-35}$ in the brain triggers tau protein phosphorylation and formation of intracellular NFTs, subsequently leading to mitochondrial dysfunction and membrane rupture, which then proceeds to necrosis or apoptosis [38]. It has been reported in previous *in vitro* studies that genistein protects against cell death [39, 40]. Genistein protects against $A\beta$-induced toxicity in SH-SY5Y cells by regulation of Akt and Tau phosphorylation [41]. Genistein and galantamine combinations decrease $A\beta_{(1-42)}$-induced genotoxicity and cell death in SH-SY5Y Cell Line [42]. The present study used SH-SY5Y cells to generate an *in vitro* model to investigate the effect of genistein on the neurotoxicity induced by $A\beta_{25-35}$.

Increased oxidative stress occurs in response to increased $A\beta$ levels [43]. Oxidative stress has generally been implicated in neurodegenerative disorders and, more specifically, in the onset and development of AD [44]. HO-1 induction may indicate a pro-oxidative status since HO-1 is activated under oxidative stress. Zhai *et al.* demonstrated that genistein upregulated HO-1 and GCLC expression via the EKR1/2 and PKC/Nrf2 pathways during oxidative stress using

a H_2O_2-induced cell model [45]. Genistein can exert neuroprotective effects against Aβ-induced oxidative stress *via* activating α7nAChR and its downstream phosphatidylinositol 3-kinase (PI3K)/Akt/Nrf2 signaling cascades [46]. The present study observed that genistein could promote the survival of SH-SY5Y cells treated with Aβ_{25-35} *via* HO-1 signaling.

Nrf2 is considered a "master regulator" of the antioxidant response, and it is also a regulator of maintaining the body's redox homeostasis [47]. Under an oxidative stimulus, Nrf2 is translocated to the nucleus where it interacts with small proteins and binds to ARE to activate the transcription of antioxidant genes, such as the nicotinamide adenine dinucleotide phosphate oxidase complex: quinone oxidoreductase 1, glutathione S-transferases, γ-glutamylcysteine ligase and heme oxygenase 1 [48]. It has been reported that genistein treatment can activate the Nrf2 pathway to augment the antioxidative system *in vitro* and *in vivo* [49]. The present study revealed that genistein could upregulate Nrf2 to increase HO-1 in SH-SY5Y cells treated with Aβ_{25-35}.

Akt is a serine/threonine kinase that regulates a wide range of processes, including cell survival, cell growth and apoptosis [50]. Previous studies have reported that Aβ peptide may decrease Akt phosphorylation, thus inhibiting its activation [51]. Reduced activation of Akt is known to induce tau protein hyperphosphorylation and cell death [50]. Genistein can stimulate the PI3K/Akt pathway and thereby the release of NO [52]. The present study revealed that genistein could upregulate PI3K phosphorylation to increase HO-1 in SH-SY5Y cells treated with Aβ_{25-35}.

In conclusion, the present study demonstrated that genistein could alleviate the neurotoxicity of Aβ_{25-35} in SH-SY5Y cells by improving the cell survival and anti-oxidative response. These effects may be reversed by inhibiting the Nrf2 and PI3K signaling pathways. These findings suggest that a novel strategy for the treatment of AD may involve genistein.

Acknowledgements

Declaration of competing interest

All authors declare no competing interests.

References

1. Hickman RA, Faustin A, Wisniewski T. Alzheimer Disease and Its Growing Epidemic: Risk Factors, Biomarkers, and the Urgent Need for Therapeutics. Neurol Clin. 2016; 34(4): 941–953, doi: 10.1016/j.ncl.2016.06.009, indexed in Pubmed: 27720002.
2. Alzheimer's Association. 2013 Alzheimer's disease facts and figures. Alzheimers Dement. 2013; 9(2): 208–245, doi: 10.1016/j.jalz.2013.02.003, indexed in Pubmed: 23507120.
3. Menendez-Gonzalez M, Padilla-Zambrano HS, Alvarez G, et al. Targeting Beta-Amyloid at the CSF: A New Therapeutic Strategy in Alzheimer's Disease. Front Aging Neurosci. 2018; 10: 100, doi: 10.3389/fnagi.2018.00100, indexed in Pubmed: 29713273.
4. Nalivaeva NN, Turner AJ. Targeting amyloid clearance in Alzheimer's disease as a therapeutic strategy. Br J Pharmacol. 2019; 176(18): 3447–3463, doi: 10.1111/bph.14593, indexed in Pubmed: 30710367.
5. Long JM, Holtzman DM. Alzheimer Disease: An Update on Pathobiology and Treatment Strategies. Cell. 2019; 179(2): 312–339, doi: 10.1016/j.cell.2019.09.001, indexed in Pubmed: 31564456.
6. Babaei P, Soltani Tehrani B, Alizadeh A. Transplanted bone marrow mesenchymal stem cells improve memory in rat models of Alzheimer's disease. Stem Cells Int. 2012; 2012: 369417, doi: 10.1155/2012/369417, indexed in Pubmed: 22754576.
7. Eftekharzadeh M, Nobakht M, Alizadeh A, et al. The effect of intrathecal delivery of bone marrow stromal cells on hippocampal neurons in rat model of Alzheimer's disease. Iran J Basic Med Sci. 2015; 18(5): 520–525, indexed in Pubmed: 26124940.
8. Nasiri E, Alizadeh A, Roushandeh AM, et al. Melatonin-pretreated adipose-derived mesenchymal stem cells efficeintly improved learning, memory, and cognition in an animal model of Alzheimer's disease. Metab Brain Dis. 2019; 34(4): 1131–1143, doi: 10.1007/s11011-019-00421-4, indexed in Pubmed: 31129766.
9. Vaiserman A, Koliada A, Lushchak O. Neuroinflammation in pathogenesis of Alzheimer's disease: Phytochemicals as potential therapeutics. Mech Ageing Dev. 2020; 189: 111259, doi: 10.1016/j.mad.2020.111259, indexed in Pubmed: 32450086.
10. Liu LX, Chen WF, Xie JX, et al. Neuroprotective effects of genistein on dopaminergic neurons in the mice model of Parkinson's disease. Neurosci Res. 2008; 60(2): 156–161, doi: 10.1016/j.neures.2007.10.005, indexed in Pubmed: 18054104.
11. Li WF, Yang K, Zhu P, et al. Genistein Ameliorates Ischemia/Reperfusion-Induced Renal Injury in a SIRT1-Dependent Manner. Nutrients. 2017; 9(4), doi: 10.3390/nu9040403, indexed in Pubmed: 28425936.
12. Ganai AA, Farooqi H. Bioactivity of genistein: A review of in vitro and in vivo studies. Biomed Pharmacother. 2015; 76: 30–38, doi: 10.1016/j.biopha.2015.10.026, indexed in Pubmed: 26653547.
13. Polkowski K, Mazurek AP. Biological properties of genistein. A review of in vitro and in vivo data. Acta Pol Pharm. 2000; 57(2): 135–155, indexed in Pubmed: 10934794.
14. Gao X, Liu K, Huang F, et al. Positive and negative regulation of insulin action by genistein in the endothelium. J Nutr Biochem. 2013; 24(1): 222–230, doi: 10.1016/j.jnutbio.2012.05.008, indexed in Pubmed: 22901685.
15. Jia Z, Babu PV, Si H, et al. Genistein inhibits TNF-α-induced endothelial inflammation through the protein kinase pathway A and improves vascular inflammation in C57BL/6 mice. Int J Cardiol. 2013; 168(3): 2637–2645, doi: 10.1016/j.ijcard.2013.03.035, indexed in Pubmed: 23587398.
16. Jeong JW, Lee HH, Han MHo, et al. Anti-inflammatory effects of genistein via suppression of the toll-like receptor 4-mediated signaling pathway in lipopolysaccharide-stimulated BV2 microglia. Chem Biol Interact. 2014; 212: 30–39, doi: 10.1016/j.cbi.2014.01.012, indexed in Pubmed: 24491678.

17. Bagheri M, Joghataei MT, Mohseni S, et al. Genistein ameliorates learning and memory deficits in amyloid β(1-40) rat model of Alzheimer's disease. Neurobiol Learn Mem. 2011; 95(3): 270–276, doi: 10.1016/j.nlm.2010.12.001, indexed in Pubmed: 21144907.

18. Kohara Y, Kawaguchi S, Kuwahara R, et al. Genistein improves spatial learning and memory in male rats with elevated glucose level during memory consolidation. Physiol Behav. 2015; 140: 15–22, doi: 10.1016/j.physbeh.2014.12.005, indexed in Pubmed: 25481356.

19. Wang R, Tu J, Zhang Q, et al. Genistein attenuates ischemic oxidative damage and behavioral deficits via eNOS/Nrf2/HO-1 signaling. Hippocampus. 2013; 23(7): 634–647, doi: 10.1002/hipo.22126, indexed in Pubmed: 23536494.

20. Bagheri M, Rezakhani A, Nyström S, et al. Amyloid beta(1-40)-induced astrogliosis and the effect of genistein treatment in rat: a three-dimensional confocal morphometric and proteomic study. PLoS One. 2013; 8(10): e76526, doi: 10.1371/journal.pone.0076526, indexed in Pubmed: 24130779.

21. Bagheri M, Roghani M, Joghataei MT, et al. Genistein inhibits aggregation of exogenous amyloid-beta₁–₄₀ and alleviates astrogliosis in the hippocampus of rats. Brain Res. 2012; 1429: 145–154, doi: 10.1016/j.brainres.2011.10.020, indexed in Pubmed: 22079317.

22. Chung HT, Pae HO, Cha YN. Role of heme oxygenase-1 in vascular disease. Curr Pharm Des. 2008; 14(5): 422–428, doi: 10.2174/138161208783597335, indexed in Pubmed: 18289069.

23. Ma Z, Lu Y, Yang F, et al. Rosmarinic acid exerts a neuroprotective effect on spinal cord injury by suppressing oxidative stress and inflammation via modulating the Nrf2/HO-1 and TLR4/NF-κB pathways. Toxicol Appl Pharmacol. 2020 [Epub ahead of print]; 397: 115014, doi: 10.1016/j.taap.2020.115014, indexed in Pubmed: 32320792.

24. Campbell NK, Fitzgerald HK, Dunne A. Regulation of inflammation by the antioxidant haem oxygenase 1. Nat Rev Immunol. 2021 [Epub ahead of print], doi: 10.1038/s41577-020-00491-x, indexed in Pubmed: 33514947.

25. Bai Z, Wang Z. Genistein protects against doxorubicin-induced cardiotoxicity through Nrf-2/HO-1 signaling in mice model. Environ Toxicol. 2019; 34(5): 645–651, doi: 10.1002/tox.22730, indexed in Pubmed: 30734460.

26. Ma W, Yuan L, Yu H, et al. Genistein as a neuroprotective antioxidant attenuates redox imbalance induced by beta-amyloid peptides 25-35 in PC12 cells. Int J Dev Neurosci. 2010; 28(4): 289–295, doi: 10.1016/j.ijdevneu.2010.03.003, indexed in Pubmed: 20362658.

27. Kreutz F, Frozza RL, Breier AC, et al. Amyloid-β induced toxicity involves ganglioside expression and is sensitive to GM1 neuroprotective action. Neurochem Int. 2011; 59(5): 648–655, doi: 10.1016/j.neuint.2011.06.007, indexed in Pubmed: 21723896.

28. He D, Chen S, Xiao Z, et al. Bisdemethoxycurcumin exerts a cell-protective effect via JAK2/STAT3 signaling in a rotenone-induced Parkinson's disease model in vitro. Folia Histochem Cytobiol. 2020; 58(2): 127–134, doi: 10.5603/FHC.a2020.0011, indexed in Pubmed: 32557525.

29. Chen SX, He JH, Mi YJ, et al. A mimetic peptide of α2,6-sialyllactose promotes neuritogenesis. Neural Regen Res. 2020; 15(6): 1058–1065, doi: 10.4103/1673-5374.270313, indexed in Pubmed: 31823885.

30. Chen S, He B, Zhou G, et al. Berberine enhances L1 expression and axonal remyelination in rats after brachial plexus root avulsion. Brain Behav. 2020; 10(10): e01792, doi: 10.1002/brb3.1792, indexed in Pubmed: 32770668.

31. Chen S, Jiang Q, Huang P, et al. The L1 cell adhesion molecule affects protein kinase D1 activity in the cerebral cortex in a mouse model of Alzheimer's disease. Brain Res Bull. 2020; 162: 141–150, doi: 10.1016/j.brainresbull.2020.06.004, indexed in Pubmed: 32540419.

32. Vi a J, Gambini J, García-García FJ, et al. Role of oestrogens on oxidative stress and inflammation in ageing. Horm Mol Biol Clin Investig. 2013; 16(2): 65–72, doi: 10.1515/hmbci-2013-0039, indexed in Pubmed: 25436748.

33. Park YJ, Jang Y, Kwon YH. Protective effect of isoflavones against homocysteine-mediated neuronal degeneration in SH-SY5Y cells. Amino Acids. 2010; 39(3): 785–794, doi: 10.1007/s00726-010-0523-5, indexed in Pubmed: 20204436.

34. Park YJ, Jang Ym, Kwon YH. Isoflavones prevent endoplasmic reticulum stress-mediated neuronal degeneration by inhibiting tau hyperphosphorylation in SH-SY5Y cells. J Med Food. 2009; 12(3): 528–535, doi: 10.1089/jmf.2008.1069, indexed in Pubmed: 19627200.

35. Ding J, Yu HL, Ma WW, et al. Soy isoflavone attenuates brain mitochondrial oxidative stress induced by β-amyloid peptides 1-42 injection in lateral cerebral ventricle. J Neurosci Res. 2013; 91(4): 562–567, doi: 10.1002/jnr.23163, indexed in Pubmed: 23239252.

36. Wang DM, Li SQ, Zhu XY, et al. Protective effects of hesperidin against amyloid-β (Aβ) induced neurotoxicity through the voltage dependent anion channel 1 (VDAC1)-mediated mitochondrial apoptotic pathway in PC12 cells. Neurochem Res. 2013; 38(5): 1034–1044, doi: 10.1007/s11064-013-1013-4, indexed in Pubmed: 23475456.

37. Karran E, Mercken M, De Strooper B. The amyloid cascade hypothesis for Alzheimer's disease: an appraisal for the development of therapeutics. Nat Rev Drug Discov. 2011; 10(9): 698–712, doi: 10.1038/nrd3505, indexed in Pubmed: 21852788.

38. Tabaton M, Piccini A. Role of water-soluble amyloid-beta in the pathogenesis of Alzheimer's disease. Int J Exp Pathol. 2005; 86(3): 139–145, doi: 10.1111/j.0959-9673.2005.00428.x, indexed in Pubmed: 15910548.

39. Xu HN, Li LX, Wang YX, et al. Genistein inhibits Aβ -induced SH-SY5Y cell damage by modulating the expression of apoptosis-related proteins and Ca influx through ionotropic glutamate receptors. Phytother Res. 2019; 33(2): 431–441, doi: 10.1002/ptr.6239, indexed in Pubmed: 30450837.

40. You F, Li Q, Jin G, et al. Genistein protects against Aβ induced apoptosis of PC12 cells through JNK signaling and modulation of Bcl-2 family messengers. BMC Neurosci. 2017; 18(1): 12, doi: 10.1186/s12868-016-0329-9, indexed in Pubmed: 28081713.

41. Petry FD, Coelho BP, Gaelzer MM, et al. Genistein protects against amyloid-beta-induced toxicity in SH-SY5Y cells by regulation of Akt and Tau phosphorylation. Phytother Res. 2020; 34(4): 796–807, doi: 10.1002/ptr.6560, indexed in Pubmed: 31795012.

42. Castillo WO, Palomino NV, Takahashi CS, et al. Genistein and Galantamine Combinations Decrease β-Amyloid Peptide -Induced Genotoxicity and Cell Death in SH-SY5Y Cell Line: an In Vitro and In Silico Approach for Mimic of Alzheimer's Disease. Neurotox Res. 2020; 38(3): 691–706, doi: 10.1007/s12640-020-00243-8, indexed in Pubmed: 32613603.

43. Yu W, Bonnet M, Farso M, et al. The expression of apoptosis inducing factor (AIF) is associated with aging-related cell death in the cortex but not in the hippocampus in the TgCRND8 mouse model of Alzheimer's disease. BMC Neurosci. 2014; 15: 73, doi: 10.1186/1471-2202-15-73, indexed in Pubmed: 24915960.

44. Merelli A, Repetto M, Lazarowski A, et al. Hypoxia, Oxidative Stress, and Inflammation: Three Faces of Neurodegenerative Diseases. J Alzheimers Dis. 2020 [Epub ahead of print], doi: 10.3233/JAD-201074, indexed in Pubmed: 33325385.

45. Zhai X, Lin M, Zhang F, et al. Dietary flavonoid genistein induces Nrf2 and phase II detoxification gene expression via ERKs and PKC pathways and protects against oxidative stress in Caco-2 cells. Mol Nutr Food Res. 2013; 57(2): 249–259, doi: 10.1002/mnfr.201200536, indexed in Pubmed: 23255485.

46. Guo J, Yang G, He Y, et al. Involvement of α7nAChR in the Protective Effects of Genistein Against β-Amyloid-Induced Oxidative Stress in Neurons via a PI3K/Akt/Nrf2 Pathway-Related Mechanism. Cell Mol Neurobiol. 2021; 41(2): 377–393, doi: 10.1007/s10571-020-01009-8, indexed in Pubmed: 33215356.

47. Chen QM, Maltagliati AJ. Nrf2 at the heart of oxidative stress and cardiac protection. Physiol Genomics. 2018; 50(2): 77–97, doi: 10.1152/physiolgenomics.00041.2017, indexed in Pubmed: 29187515.

48. Batliwala S, Xavier C, Liu Y, et al. Involvement of Nrf2 in Ocular Diseases. Oxid Med Cell Longev. 2017; 2017: 1703810, doi: 10.1155/2017/1703810, indexed in Pubmed: 28473877.

49. Wang L, Li A, Liu Y, et al. Genistein protects against acetaminophen-induced liver toxicity through augmentation of SIRT1 with induction of Nrf2 signalling. Biochem Biophys Res Commun. 2020; 527(1): 90–97, doi: 10.1016/j.bbrc.2020.04.100, indexed in Pubmed: 32446397.

50. Hemmings BA, Restuccia DF. The PI3K-PKB/Akt pathway. Cold Spring Harb Perspect Biol. 2015; 7(4), doi: 10.1101/cshperspect.a026609, indexed in Pubmed: 25833846.

51. Hoppe JB, Frozza RL, Pires EN, et al. The curry spice curcumin attenuates beta-amyloid-induced toxicity through beta-catenin and PI3K signaling in rat organotypic hippocampal slice culture. Neurol Res. 2013; 35(8): 857–866, doi: 10.1179/1743132813Y.0000000225, indexed in Pubmed: 23816368.

52. Yang Y, Nie W, Yuan J, et al. Genistein activates endothelial nitric oxide synthase in broiler pulmonary arterial endothelial cells by an Akt-dependent mechanism. Exp Mol Med. 2010; 42(11): 768–776, doi: 10.3858/emm.2010.42.11.078, indexed in Pubmed: 20926919.

ORIGINAL PAPER

VM
VIA MEDICA

miR-378a-5p regulates CAMKK2/AMPK pathway to contribute to cerebral ischemia/reperfusion injury-induced neuronal apoptosis

Yun Zhang[1, 2], Peilan Zhang[1], Chunying Deng[1, 3]

[1]Clinical College of Neurology, Neurosurgery and Neurorehabilitation, Tianjin Medical University, 300350, China

[2]Department of Geriatrics, Tangshan Gongren Hospital, Tangshan City, Hebei Province, 063000, China

[3]Department of Neurology, North China University of Science and Technology Affiliated Hospital, Tangshan City, Hebei Province, 063000, China

Abstract

Introduction. The pathological mechanism of cerebral ischemia/reperfusion (CIR) injury is complicated and unclear. Apart from the involvement of many low-molecular factors it was found that several miRNAs were dysregulated during and after CIR injury in cell models. This study aimed to explore the effects of miR-378a-5p on *in vitro* model of (CIR) injury-induced neuronal apoptosis and provide a new mechanism of CIR injury.
Material and methods. Primary hippocampal neurons were isolated from newborn Sprague-Dawley rats. Oxygen-glucose deprivation/reoxygenation (OGDR) for 24 h and 48 h was used as an *in vitro* model of CIR. Cell viability was measured using MTT assay and apoptosis was determined by flow cytometry. Quantitative real time PCR (qRT-PCR) assay and Western blotting were used to examine mRNA and protein expressions, respectively. TargetScan was used to predict the direct target of miR-378a-5p and luciferase assay was used to validate that calmodulin-dependent protein kinase kinase-2 (CAMKK2) was the direct target of miR-378a-5p.
Results. miR-378a-5p expression was significantly increased after OGDR at 24 h and 48 h. After OGDR, cell viability was reduced, which was reversed by miR-378a-5p and enhanced by shCAMKK2 plasmid. Cell apoptosis was increased after OGDR, which was prevented by miR-378a-5p and enhanced by shCAMKK2 plasmid. Results of TargetScan and luciferase assay demonstrated that miR-378a-5p could directly bind to 3'-untranslated region (3'-UTR) of CAMKK2. Both mRNA and protein expression of CAMKK2 were downregulated by miR-378a-5p mimics and upregulated by miR-378a-5p inhibitors. Phosphorylation of adenosine monophosphate-activated protein kinase (AMPK) was positively associated with expression of CAMKK2.
Conclusions. Data of this study indicated that miR-378a-5p was significantly overexpressed after OGDR. miR-378a-5p could bind to 3'-UTR of CAMKK2 to inhibit cell proliferation through regulation of CAMKK2/AMPK pathway providing a new mechanism and biomarker for the diagnosis and potential treatment of CIR injury. (*Folia Histochemica et Cytobiologica 2021, Vol. 59, No. 1, 57–65*)

Key words: miR-378a-5p; primary hippocampal neurons; rat; oxygen-glucose deprivation/reoxygenation; CAMKK2/AMPK pathway; apoptosis

Correspondence address: Peilan Zhang
Department of Neurology, Tianjin Huanhu Hospital,
No. 6 Jizhao Road, Jinnan District, Tianjin, China
phone: 86+022-59065241
e-mail: zhangpeilan666@163.com

Introduction

The brain is an organ highly sensitive to hypoxia [1]. Cerebral ischemia/reperfusion (CIR) injury occurs when blood supply to the brain is suspended and

subsequently restored [2]. Cerebral IR injury can induce brain dysfunction, which contributes to high mortality and disability [3]. The pathological mechanism of CIR injury is complicated and unclear. Many biological processes are involved in it, including the generation of reactive oxygen species (ROS), reduction of adenosine triphosphate (ATP) and antioxidative factors, including activation of adenosine monophosphate-activated protein kinase (AMPK) signaling pathway [4, 5].

The major function of AMPK is to monitor the changes of cellular energy and control the ATP level, thus AMPK activity is regulated by the ratio of AMP/ADP to ATP [6]. Phosphorylation of Thr172 is required for the activation of AMPK, which is directly mediated by serine/threonine kinase LKB1, a tumor suppressor protein [7]. In addition, phosphorylation of AMPK on Thr172 can also be mediated *via* calmodulin-dependent protein kinase kinase-2 (CAMKK2) in response to calcium flux [8]. Activation of AMPK can promote glucose uptake *via* activation of Akt-mTOR pathway, inhibit protein and lipid synthesis, and suppress cell growth [9]. AMPK is also involved in CIR injury through multiple signaling pathways, including NF-κB signaling pathway and NLRP3 inflammasome activation pathway [10, 11]. As a class of small non-coding RNAs (28-25 nucleotides), microRNAs (miRNAs) can directly target the 3'-untranslated region (3'-UTR) of mRNAs, thereby downregulating protein expression [12]. Several miRNAs were dysregulated during and after CIR injury in cell models [13]. In vascular smooth muscle cells, miR-378a-5p has been reported to promote cell proliferation and migration through targeting cyclin-dependent kinase 1 (CDK1), a protein that promotes cell cycle entering M phase from G2 phase [14]. Overexpression of miR-378a-5p can directly target 3'-UTR of E2F transcription factor 3 (E2F3), leading to lens epithelial cell apoptosis in cataract [15]. However, no studies have reported the effects of miR-378a-5p on CIR injury. This study aims to investigate the effects of miR-378a-5p on *in vitro* model of CIR-induced neuronal cell apoptosis and provide a new mechanism of diagnosis and treatment for CIR injury.

Material and methods

Cell culture, treatment and transfection. Human embryonic kidney 293 (HEK293) cells were obtained from Beijing Smart Treasure Biological Technology Co., Ltd. (Genobio, China) and cultured in DMEM (Procell, Wuhan, China) supplemented with fetal bovine serum (FBS, 10%, Thermo Fisher, Carlsbad, CA, USA) and 1%, penicillin-streptomycin solution (Solarbio, Beijing, China) with 5% CO_2 at 37°C.

Primary hippocampal neurons were isolated from newborn Sprague-Dawley rats [16]. Briefly, the hippocampal tissues were cut into small pieces and digested with trypsin-EDTA (0.25%, STEMCELL, Seattle, WA, USA). The isolated primary hippocampal neurons were seeded in 6-well plates which were precoated with 0.01% poly-L-lysine and cultured in DMEM containing 10% FBS and 1% penicillin-streptomycin solution (Solarbio) in an atmosphere of 5% CO_2 and 95% air at 37°C. All experiment procedures were carried following the ethical standards under a protocol approved by the Animal Experiment Ethics Committee of North China University of Science and Technology, and were executed conforming to the Guide for the Care and Use of Laboratory Animals published by the US National Institutes of Health (No. 85-23, 1996) [17].

The *in vitro* IR model was achieved by oxygen-glucose deprivation/reoxygenation (OGDR). Briefly, the primary hippocampal neurons were seeded in the 6-well plate at the density of 1×10^6 cells/well and the medium was changed to glucose-free DMEM in an atmosphere of 1% O_2, 94% N_2 and 5% CO_2 (hypoxic condition) at 37°C for 3 h. Thereafter, the neurons were cultured in normal DMEM in an atmosphere of 95% air and 5% CO_2 (normoxic condition) up to 48 h. Neurons cultured in normal medium under normoxic condition were used as control group.

Transfection was performed by mixing miR-378a-5p mimics, miR-378a-5p inhibitors and their negative controls (Ribobio, Guangzhou, China), and shCAMKK2 and its negative control (BersinBio, Guangzhou, China) with lipofectamine 2000 (Invitrogen, Carlsbad, WA, USA) according to manufacturer's protocols. The primary hippocampal neurons were cultured in the 6-well plate at the density of 1×10^6 cells/well with FBS-free medium. The transfection complex was added into neurons and incubated for 6–8 h. The medium was then replaced by normal culture medium. Neurons were cultured for 24 h at 37°C and collected for further analysis.

Determination of cell viability and cell survival. *MTT assay*. The neurons were cultured in 96-well plates. After transfection, MTT (5 mg/ml in phosphate-buffered saline (PBS, Abcam, Cambridge, UK) was added into each well and incubated for 4 h following the manufacturer's instruction. The formazan was dissolved by dimethyl sulfoxide. The absorbance value at 490 nm was measured and recorded by a spectrophotometer (BioTek, Winooski, VT, USA).

Trypan blue assay. Cell survival was determined using Trypan blue assay. The neurons were cultured in 6-well plate. After transfection, the medium was removed and cells were washed using PBS. 0.4% of trypan blue solution (SigmaAldrich, St. Louis, MO, USA) was added into each well at a ratio of 1:9 *vs.* PBS. The results were observed

and photographs were acquired under a microscope within 3 min. All the cells visible in the view field were counted in tree view fields in each experimental group.

Apoptosis measurement by flow cytometry. The neurons were cultured in 6-well plates. After transfection, cells were suspended in 1.5 ml of tubes and washed with PBS. The suspended cells were stained by the commercial FITC/PI apoptosis detection kit (Beyotime) according to the manufacturer's protocol. Cell apoptosis was analyzed with a flow cytometer (Becton Dickinson, Mountain View, CA, USA) by two parameter dot-plots. A total of 20,000 cells were recorded in each run.

Luciferase reporter assay. HEK293 cells were cultured in 6-well plates at the density of 1×10^6 cells/well. 3'-UTR of CAMKK2 with wild type sequence (CAMKK2-WT) and mutant sequence (CAMKK2-MUT) of miR-378a-5p complementary sites were cloned into pGL3 luciferase reporter vectors (Promega, Madison, WI, USA) respectively. pGL3-CAMKK2-WT or pGL3-CAMKK2-MUT was co-transfected with miR-378a-5p mimics and its negative control. Luciferase activity was detected using Luciferase Reporter Assay Kit (BioVision, Milpitas, CA, USA).

Extraction of RNA and quantitative real time PCR (qRT-PCR) assay. Total RNA extraction was performed using TRIzol reagent (Thermo Fisher). Reverse transcription was performed with 1 μg of RNA using QuantiTect Reverse Transcription Kit (QIAGEN, Dusseldorf, Germany). RNA expression was examined using QuantiTect SYBR Green RT-PCR Kit (QIAGEN) with the StepOnePlus system (Applied Biosystems, USA). Relative RNA expression was quantified by $2^{-\Delta\Delta Ct}$ method. The primer sequences (SigmaAldrich) used in this study were: β-actin forward, 5'-AGCCTCGCCTTTGCCGA-3' and reverse, 5'-CTGGTGCCTGGGGCG-3'; CAMKK2 forward, 5'-CGGTCGCAAGCTGTCTCTG-3' and reverse, 5'-GCGTCCGTTCATGTCCAGG-3'; U6 forward, 5'-AGTAAGCCCTTGCTGTCAGTG-3' and reverse, 5'-CCTGGGTCTGATAATGCTGGG-3'. Relative expression of miR-378a-5p was determined using miScript Primer Assays (QIAGEN) and normalized by U6 small RNA.

Western blotting. Cell lysates was extracted by RIPA cell lysis buffer (Beyotime). Total proteins (5 μg) were loaded in SDS-PAGE and separated via electrophoresis. The separated proteins then transferred to PVDF membrane followed by blockade of membranes with 5% of milk. The blocked membranes were probed with the proper primary antibodies at 4°C overnight and then incubated with secondary antibodies for 2 h at room temperature. The signal of protein bands was detected using ECL Detection

reagents (SigmaAldrich, USA). The primary antibodies (Cell Signaling, Danvers, MA, USA) used in this study were: Bax (CST#2774S, 1:500 dilution), cleaved caspase-3 (CST#9664, 1:1000 dilution), caspase-3 (CST#9662S, 1:1000 dilution), CAMKK2 (ab96531, 1:500 dilution, Abcam), p-AMPK (CST#2535, 1:2000 dilution), AMPK (CST#2532, 1:2000 dilution), β-actin (CST#4970, 1:5000 dilution).

Statistical analysis. GraphPad Prism 8.0 software (Grapgpad Inc., San Diego, CA, USA) was used to carry out all the data analysis. Student t-test was used to compare the difference between two groups. One-way ANOVA was used to compare between multiple groups. All data were expressed as mean $\pm$ SD. $p < 0.05$ indicated statistically significant difference.

Results

miR-378a-5p was overexpressed after OGDR in primary hippocampal neurons

After OGDR, overexpression of miR-378a-5p was detected at 24 h and 48 h compared with control group (Fig. 1). No change of miR-378a-5p was observed in the control group. The expression of miR-378a-5p was upregulated by OGDR in a time-dependent manner (Fig. 1).
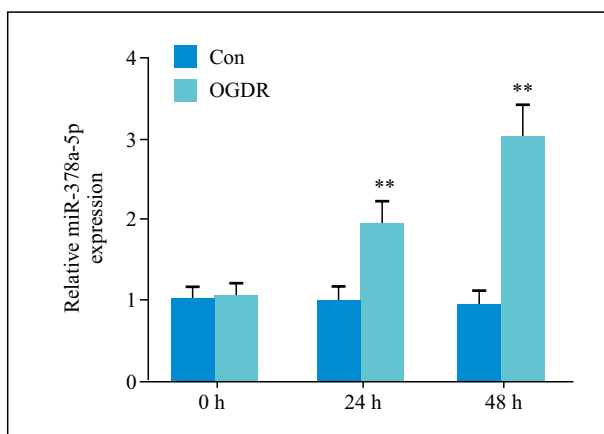

Figure 1. Expression of miR-378a-5p was upregulated in primary hippocampal neurons after OGDR. Primary hippocampal neurons were cultured in glucose-free DMEM in an atmosphere of 1% O_2, 94% N_2 and 5% CO_2 (hypoxic condition) at 37°C for 3 h. Thereafter, the neurons were cultured in normal DMEM in an atmosphere of 95% air and 5% CO_2 (normoxic condition) for 48 h. Neurons cultured in normal medium under normoxic condition were used as control group. Relative expression of miR-378a-5p after OGDR was detected by qRT-PCR as described in Methods. **$p < 0.01$ vs.* control group. Abbrev.: Con — control; OGDR — oxygen-glucose deprivation/reoxygenation.

Inhibition of miR-378a-5p promoted cell proliferation and suppressed cell apoptosis induced by OGDR

To investigate the role of miR-378a-5p in OGDR-induced neuron dysfunction, miR-378a-5p inhibitors were used to knockdown the expression of miR-378a-5p. qRT-PCR results demonstrated that the expression of miR-378a-5p was lower in cells transfected with miR-378a-5p inhibitors than that in control group (Fig. 2A). After OGDR, cell viability was significantly reduced compared with the normoxic group and the reduction of cell viability was restored by miR-378a-5p inhibitors (Fig. 2B). mir-378a-5p inhibitor had no significant effects on the cell viability under normoxic condition (Fig. 2B). After OGDR, cell survival was significantly decreased compared with the normoxic group and this reduction of cell survival was attenuated by miR-378a-5p inhibitors (Fig. 2C). Mir-378a-5p inhibitor had no effects on the cell survival under normoxic condition (Fig. 2C). After OGDR, protein expressions of Bax and cleaved caspase-3 were upregulated compared with normoxic group and this upregulation of protein expression was attenuated by miR-378a-5p inhibitors (Fig. 2D). There was no significant change of Bax and cleaved caspase-3 expression between cell transfected with miR-378a-5p inhibitors and its negative controls under normoxic condition (Fig. 2D). After OGDR, cell apoptosis was significantly induced compared with the normoxic group and this induction of cell apoptosis was restored by miR-378a-5p inhibitors (Fig. 2E). Mir-378a-5p inhibitor did not show any effects on the cell apoptosis under normoxic condition (Fig. 2E).

CAMKK2 is the direct target of miR-378a-5p

Prediction results from TargetScan (www.targetscan.org) demonstrated that there was a complementary sequence between 3'-UTR of CAMKK2 and miR-378a-5p (Fig. 3A). Luciferase assay results showed that luciferase activity was significantly reduced in cells co-transfected with CAMKK2-WT plasmid and miR-378a-5p mimics while no change was observed in cells co-transfected with CAMKK2-MUT plasmid and miR-378a-5p mimics (Fig. 3B). The expression of miR-378a-5p was increased by miR-378a-5p mimics and decreased by miR-378a-5p inhibitors (Fig. 3C). The expression of CAMKK2 mRNA was downregulated by miR-378a-5p mimics and upregulated by miR-378a-5p inhibitors (Fig. 3D). Protein expression of CAMKK2 was also downregulated by miR-378a-5p mimics and upregulated by miR-378a-5p inhibitors (Fig. 3E). These results suggested that CAMKK2 is the direct target of miR-378a-5p.

Effects of miR-378a-5p on primary hippocampal neurons were mediated by the inhibition of CAMKK2

After OGDR for 48 H, the relative expression of CAMKK2 was reduced compared with control group. This reduction was prevented by miR-378a-5p inhibitors and further reduced in cells transfected with shCAMKK2, which was reversed by miR-378a-5p inhibitors (Fig. 4A). Cell viability was also decreased after OGDR, and this decrease was suppressed by miR-378a-5p inhibitors and enhanced in cells transfected with shCAMKK2 (Fig. 4B). Inhibition of cell viability by shCAMKK2 was prevented in cells co-transfected with shCAMKK2 and miR-378a-5p inhibitors (Fig. 4B). Cell survival was also reduced after OGDR, and this reduction was suppressed by miR-378a-5p inhibitors and enhanced in cells transfected with shCAMKK2 (Fig. 4C). Inhibition of cell viability by shCAMKK2 was prevented in cells co-transfected with shCAMKK2 and miR-378a-5p inhibitors (Fig. 4C). The expressions of CAMKK2 and phosphorylation of AMPK were downregulated after OGDR, which were reversed by miR-378a-5p inhibitors (Fig. 4D). shCAMKK2 further reduced expression of CAMKK2 and phosphorylation of AMPK, which was inhibited by dual-inhibition of CAMKK2 and miR-378a-5p (Fig. 4D). Upregulation of Bax and cleaved caspase-3 was observed after OGDR and miR-378a-5p inhibitors repressed the upregulation of Bax and cleaved caspase-3 induced by OGDR (Fig. 4D). Expression of Bax and cleaved caspase-3 was further increased in cells transfected with shCAMKK2 and dual repression of CAMKK2 whereas miR-378a-5p prevented the overexpression of Bax and cleaved caspase-3 induced by shCAMKK2 (Fig. 4D). Cell apoptosis was also induced after OGDR, and this induction was suppressed by miR-378a-5p inhibitors while enhanced by transfection with shCAMKK2 (Fig. 4E). Inhibition of cell viability by shCAMKK2 was prevented in cells co-transfected with shCAMKK2 and miR-378a-5p inhibitors (Fig. 4E).

Discussion

Oxygen-glucose deprivation (OGD) is an *in vitro* ischemia-reperfusion model which is usually used to mimic ischemic cell damage [18]. Sustained OGD (lasting more than 1 hour) followed by re-oxygenation (OGDR) has been proved to induce mitochondria dysfunction, ROS production, and cell necrosis [18]. In this study, the expression of miR-378a-5p was significantly increased after OGDR in primary rat hippocampal neurons. Overexpression of miR-378a-5p inhibited cell viability and promoted cell apoptosis
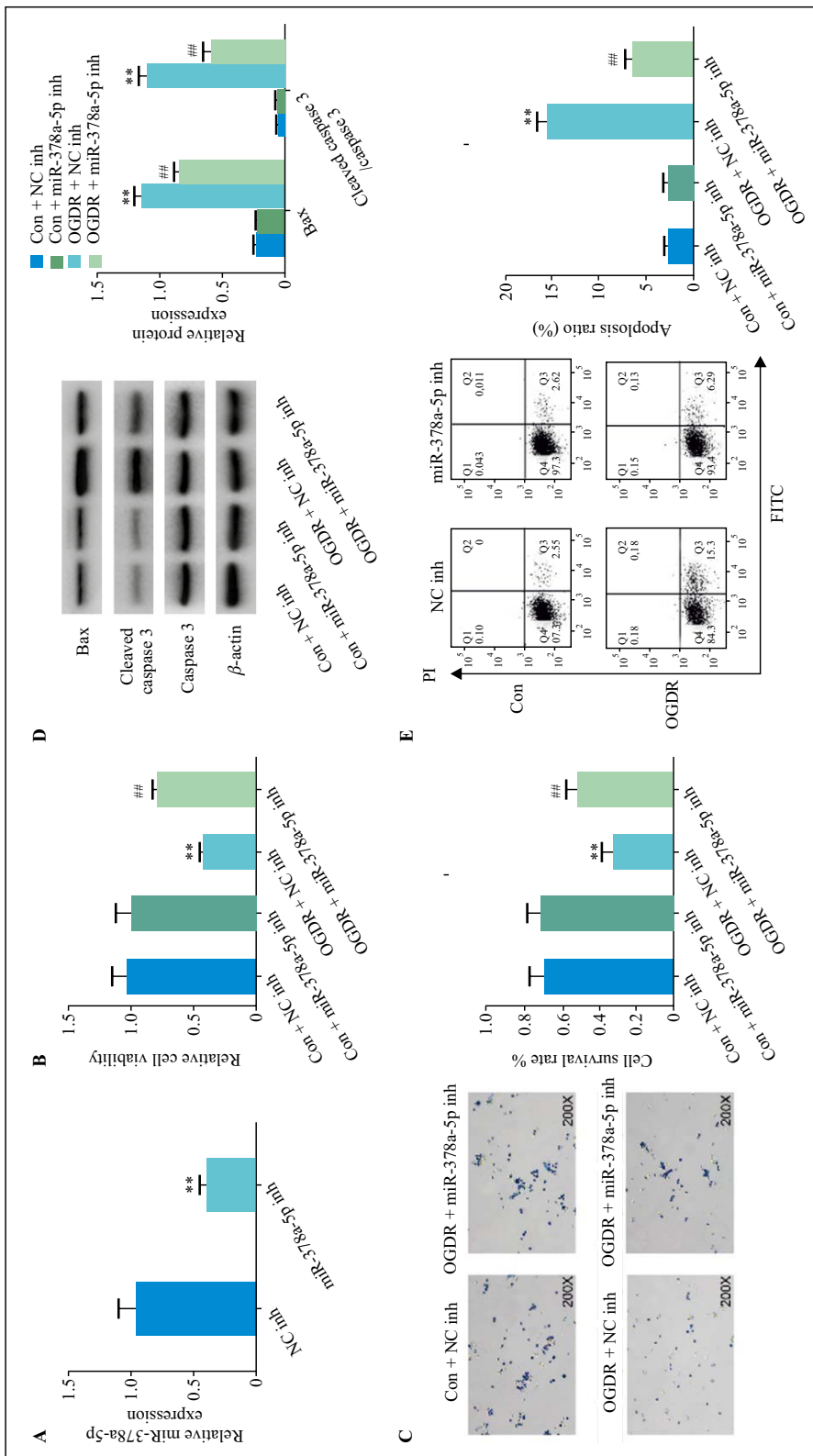
Figure 2. Inhibition of miR-378a-5p promoted neuronal cells' proliferation and suppressed cell apoptosis induced by OGDR. Incubation conditions were the same as described in the legend to Figure 1. **A.** miR-378a-5p expression was downregulated by miR-378a-5p inhibitors 48 h after OGDR. **B.** miR-378a-5p inhibitors prevented the reduction of cell viability after OGDR. **C.** miR-378a-5p inhibitors prevented the reduction of cell survival after OGDR. **D.** Western blotting revealed that miR-378a-5p inhibitors inhibited the upregulation of Bax and cleaved caspase-3 induced by OGDR. **E.** miR-378a-5p inhibitors prevented the induction of cell apoptosis after OGDR. **p < 0.01 *vs.* control cells + NC inh; ##p < 0.01 *vs.* OGDR + NC inh. Abbrev.: as in the legend to Figure 1 plus NC inh, negative control of miR-378a-5p inhibitors.
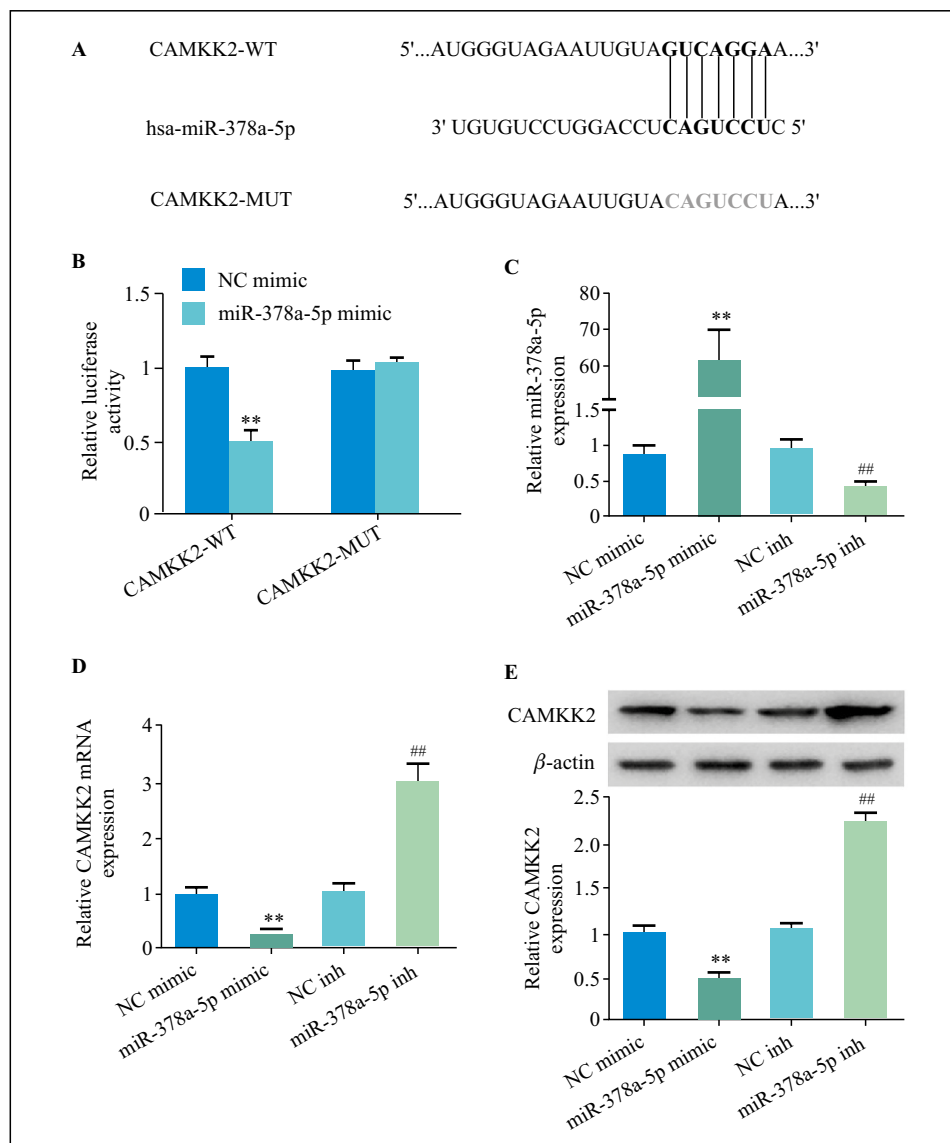
Figure 3. Calmodulin-dependent protein kinase kinase-2 (CAMKK2) is the direct target of miR-378a-5p in hippocampal neurons. Primary hippocampal neurons were incubated in the same conditions as described in the legend to Figure 1. **A.** Predicting binding site of miR-378a 5p to 3'-UTR of CAMKK2. **B.** miR-378a-5p reduced the luciferase activity in CAMKK2 amplified cells. **C.** Expression of miR-378a-5p was increased by miR-378a-5p mimics and decreased by miR-378a-5p inhibitors 48 h after OGDR. **D.** Expression of CAMKK2 mRNA was downregulated by miR-378a-5p mimics and upregulated by miR-378a-5p inhibitors. **E.** Expression of CAMKK2 protein was downregulated by miR-378a-5p mimics and upregulated by miR-378a-5p inhibitors. **$p < 0.01$ *vs*. NC mimic; ##$p < 0.01$ *vs*. NC inh. Abbrev.: NC mimic — negative control of miR-378a-5p mimic. WT: 3'-UTR of CAMKK2 with wild type sequence, MUT: 3'-UTR of CAMKK2 with mutant sequence.

through directly targeting 3'-UTR of CAMKK2 by activation of AMPK signaling pathway. Suppression of miR-378a-5p and overexpression of CAMKK2 could promote neuron viability and inhibit cell apoptosis, providing a new mechanism and biomarker for diagnosis and treatment of CIR injury.

Various miRNAs have been found to be involved in CIR injury. For example, elevation of miR-125-induced cell apoptosis and increased ROS production in PC-12 cells after OGDR were found to act *via* inhibition of casein kinase 2α (CK2α)/NADPH oxidase signaling pathway [19]. miR-182-5p, which was downregulated after OGD in microglial cells, could prevent CIR injury by direct binding to Toll-like receptor 4, demonstrating a neuroprotective effect [20]. In this study, the expression of miR-378a-5p was increased after OGDR, resulting in the suppression of cell proliferation and induction of cell apoptosis which may contribute to cerebral IR injury. Inhibition of miR-378a-5p prevented neuronal apoptosis
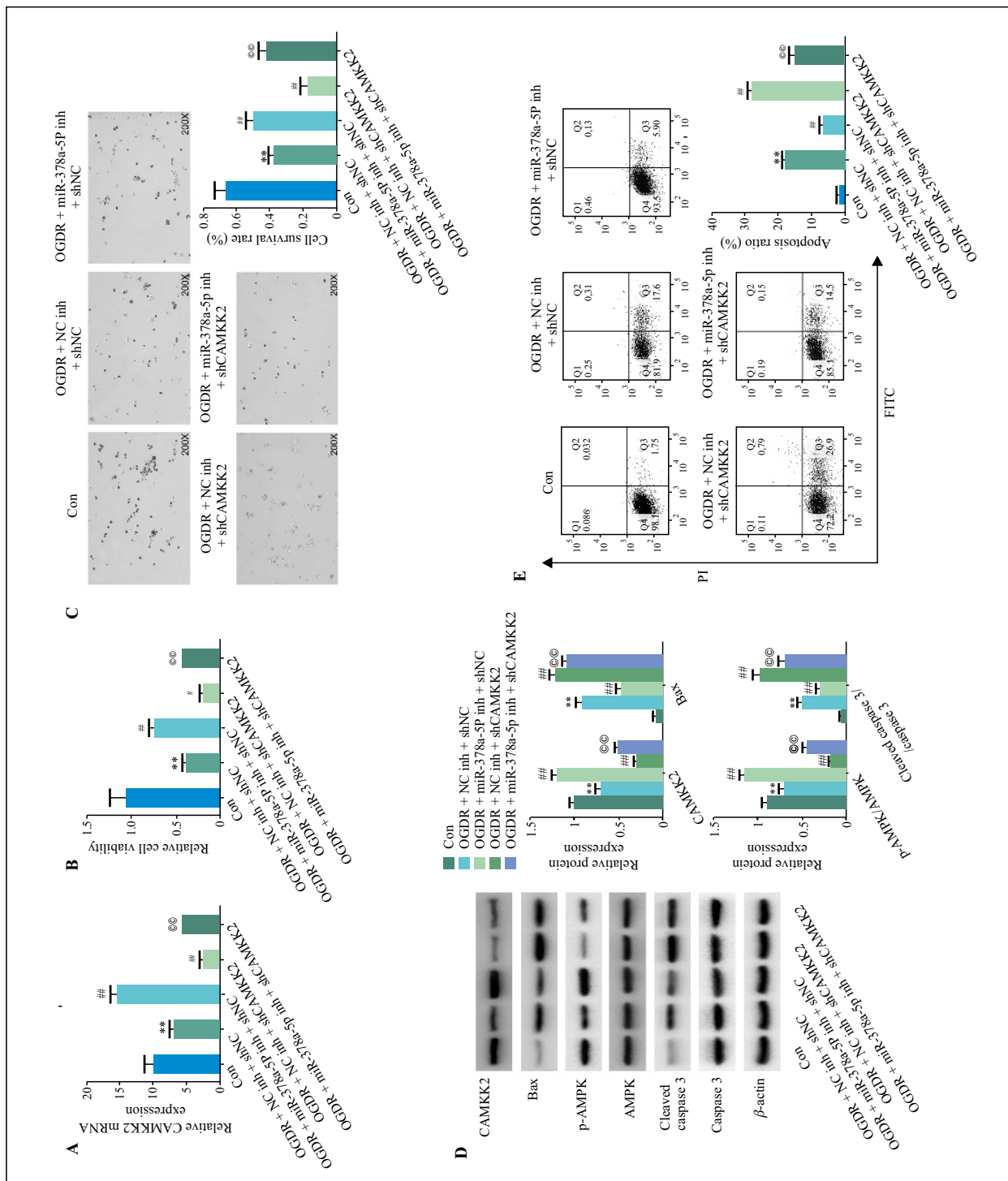
Figure 4. Effects of miR-378a-5p on primary hippocampal neurons was mediated by the inhibition of CAMKK2. The primary hippocampal neurons were cultured in glucose-free DMEM in an atmosphere of 1% O_2, 94% N_2 and 5 % CO_2 (hypoxic condition) at 37°C for 3 h. Thereafter, the neurons were cultured in normal DMEM in an atmosphere of 95% air and 5% CO_2 (normoxic condition) for 48 h. Neurons cultured in normal medium under normoxic condition were used as control group. **A.** Changes of CAMKK2 mRNA expression after treatment and transfection 48 h after OGDR. **B.** Change of cell viability after treatment and transfection 48 h after OGDR. **C.** Change of cell survival assessed by trypan blue staining after treatment and transfection. **D.** Change of CAMKK2, Bax, p-AMPK and cleaved caspase 3 protein expression after treatment and transfection. **E.** Cell apoptosis was measured by flow cytometry after treatment and transfection as described in Methods. **p < 0.01 *vs.* con; ##*p* < 0.01 *vs*. OGDR + NC inh + shNC; @@*p* < 0.01 *vs*. OGDR + NC inh + shCAMKK2. Abbrev.: shCAMKK2 — shRNA of CAMKK2; shNC — negative control of shCAMKK2.

induced by OGDR, which provides a new insight for the treatment of CIR injury.

miR-378a-5p is encoded by *Ppargc1b* gene and has been reported to act as a tumor suppressor because it could inhibit cell proliferation and induce cell apoptosis [21]. For example, by binding to the 3'-UTR of suppressor of fused homolog (SUFU), miR-378a-5p promoted cell apoptosis in triple negative breast cancer [22]. In oral squamous cell carcinoma, miR-378a-5p was shown to be negatively associated with the cell proliferation and inhibited angiogenesis through binding to kallikrein-related peptidase 4 (KLK4), inhibiting tumorigenesis and tumor metastasis [23]. Therefore, the overexpression of miR-378a-5p improves the prognosis of cancer patients. However, the inhibitory effects of miR-378a-5p on cell survival play a negative role in cerebral IR injury. In this study, overexpression of miR-378a-5p reduced cell survival after OGDR, which worsens the prognosis of cerebral IR injury. Therefore, downregulation of miR-378a-5p could prevent cerebral IR injury.

As mentioned before, miRNA could bind to 3'-UTR of target mRNA to induce translational repression. There are target regions called "seed regions", which refer to the 7 nucleotides at 2 to 8 at the 5" end of miRNA [12]. The "seed region" is the key sequence to recognize the target of miRNAs [12]. The prediction results in this study from TargetScan indicated that there was a complementary sequence between 3'-UTR of CAMKK2 and 2 to 8 at the 5" end of miR-378a-5p in compliance with Watson-Crick match [24], suggesting that calmodulin-dependent protein kinase kinase-2 was the direct target of miR-378a-5p. Luciferase activity was significantly reduced in cells co-transfected with CAMKK2-WT plasmid and miR-378a-5p mimics while no change was observed in cells co-transfected with CAMKK2-MUT plasmid and miR-378a-5p mimics, further confirming that CAMKK2 was a direct target of miR-378a-5p.

CAMKK2 is a Ca^{2+}/calmodulin-dependent serine-threonine protein kinase which could couple calcium transients to regulate cell proliferation, survival and metabolism [25]. Activation of CAMKK2 by phosphorylation of AMPK on Thr172, results in inhibition of protein and lipid synthesis, and suppression of cell growth [8, 9]. Data of this study show that inhibition of CAMKK2 prevented cell growth induced by the downregulation of miR-378a-5p, indicating that inhibition of miR-378a-5p could prevent neuronal apoptosis during CIR injury. Furthermore, inhibition of CAMKK2 reduced the phosphorylation of AMPK. All these effects were attenuated by dual-inhibition of miR-378a-5p and CAMKK2, suggesting that miR-378a is involved in CIR through regulation of CAM-KK2-AMPK signaling pathway and that CAMKK2 showed an neuroprotective effect during CIR injury. In conclusion, data of this study show that miR-378a-5p was significantly overexpressed after OGDR in primary rat hippocampal neurons, providing a new biomarker for cerebral IR injury. miR-378a-5p could inhibit cell proliferation and induce cell apoptosis through regulation of CAMKK2/AMPK pathway, providing a new therapeutic target for CIR injury. However, the findings of this study should be confirmed in clinical practice and future drug discovery could focus on the activation of CAMKK2/AMPK pathway.

Competing interests

The authors state that there are no conflicts of interest to disclose.

Ethics approval

See material and methods section.

Statement of Informed Consent

Not applicable.

Authors' contributions

Yun Zhang designed the study, supervised the data collection, analyzed the data, Peilan Zhang interpreted the data and prepare the manuscript for publication, Chunying Deng supervised the data collection, analyzed the data and reviewed the draft of the manuscript. All authors have read and approved the manuscript.

Availability of data and materials

All data generated or analyzed during this study are included in this published article.

References

1. Sarkar S, Chakraborty D, Bhowmik A, et al. Cerebral ischemic stroke: cellular fate and therapeutic opportunities. Front Biosci (Landmark Ed). 2019; 24: 435–450, indexed in Pubmed: 30468665.

2. Turley KR, Toledo-Pereyra LH, Kothari RU. Molecular mechanisms in the pathogenesis and treatment of acute ischemic stroke. J Invest Surg. 2005; 18(4): 207–218, doi: 10.1080/08941930591004449, indexed in Pubmed: 16126632.

3. Yang J, Chen M, Cao RY, et al. The Role of Circular RNAs in Cerebral Ischemic Diseases: Ischemic Stroke and Cerebral Ischemia/Reperfusion Injury. Adv Exp Med Biol. 2018; 1087: 309–325, doi: 10.1007/978-981-13-1426-1_25, indexed in Pubmed: 30259377.

4. Wu MY, Yiang GT, Liao WT, et al. Current mechanistic concepts in ischemia and reperfusion injury. Cell Physiol Biochem. 2018; 46(4): 1650–1667, doi: 10.1159/000489241, indexed in Pubmed: 29694958.

5. Wang JF, Mei ZG, Fu Y, et al. Puerarin protects rat brain against ischemia/reperfusion injury by suppressing autophagy the AMPK-mTOR-ULK1 signaling pathway. Neural Regen Res. 2018; 13(6): 989–998, doi: 10.4103/1673-5374.233441, indexed in Pubmed: 29926825.

6. Curry DW, Stutz B, Andrews ZB, et al. Targeting AMPK Signaling as a neuroprotective strategy in Parkinson's disease. J Parkinsons Dis. 2018; 8(2): 161–181, doi: 10.3233/JPD-171296, indexed in Pubmed: 29614701.

7. Woods A, Johnstone SR, Dickerson K, et al. LKB1 is the upstream kinase in the AMP-activated protein kinase cascade. Curr Biol. 2003; 13(22): 2004–2008, doi: 10.1016/j.cub.2003.10.031, indexed in Pubmed: 14614828.

8. Hawley SA, Pan DA, Mustard KJ, et al. Calmodulin-dependent protein kinase kinase-beta is an alternative upstream kinase for AMP-activated protein kinase. Cell Metab. 2005; 2(1): 9–19, doi: 10.1016/j.cmet.2005.05.009, indexed in Pubmed: 16054095.

9. Penfold L, Woods A, Muckett P, et al. CAMKK2 promotes prostate cancer independently of AMPK via increased lipogenesis. Cancer Res. 2018; 78(24): 6747–6761, doi: 10.1158/0008-5472.CAN-18-0585, indexed in Pubmed: 30242113.

10. Ma C, Wang X, Xu T, et al. Qingkailing injection ameliorates cerebral ischemia-reperfusion injury and modulates the AMPK/NLRP3 inflammasome signalling pathway. BMC Complement Altern Med. 2019; 19(1): 320, doi: 10.1186/s12906-019-2703-5, indexed in Pubmed: 31747940.

11. Du S, Deng Y, Yuan H, et al. Safflower yellow B protects brain against cerebral ischemia reperfusion injury through AMPK/NF-kB pathway. Evid Based Complement Alternat Med, 2019; 2019: 1–11, doi: 10.1155/2019/7219740, indexed in Pubmed: 30854014.

12. Liu Xi, Chen L, Liu Y, et al. Tangeretin sensitises human lung cancer cells to TRAIL induced apoptosis via ROS-JNK/ERK-CHOP pathway mediated up-regulation of death receptor 5. Tropical J Pharmac Res. 2017; 16(1): 17, doi: 10.4314/tjpr.v16i1.4.

13. Di Yu, Lei Y, Yu F, et al. MicroRNAs expression and function in cerebral ischemia reperfusion injury. J Mol Neurosci. 2014; 53(2): 242–250, doi: 10.1007/s12031-014-0293-8, indexed in Pubmed: 24696166.

14. Liu S, Yang Y, Jiang S, et al. Corrigendum: MiR-378a-5p regulates proliferation and migration in vascular smooth muscle cell by targeting CDK1. Front Genet. 2019; 10: 193, doi: 10.3389/fgene.2019.00193, indexed in Pubmed: 30930936.

15. Gao W, Zhou X, Lin R. miR-378a-5p and miR-630 induce lens epithelial cell apoptosis in cataract via suppression of E2F3. Braz J Med Biol Res. 2020; 53(5): e9608, doi: 10.1590/1414-431x20209608, indexed in Pubmed: 32348429.

16. Li L, Liu Z, Jiang YY, et al. Acetylcholine suppresses microglial inflammatory response via α7nAChR to protect hippocampal neurons. J Integr Neurosci. 2019; 18(1): 51–56, doi: 10.31083/j.jin.2019.01.114, indexed in Pubmed: 31091848.

17. Council NR. Guide for the care and use of laboratory animals: eighth edition. 2010. 327(3): 963–965.

18. Zheng K, Zhang Q, Lin G, et al. Activation of Akt by SC79 protects myocardiocytes from oxygen and glucose deprivation (OGD)/re-oxygenation. Oncotarget. 2017; 8(9): 14978–14987, doi: 10.18632/oncotarget.14785, indexed in Pubmed: 28122357.

19. Liang Y, Xu J, Wang Yu, et al. Inhibition of MiRNA-125b decreases cerebral ischemia/reperfusion injury by targeting CK2α/NADPH oxidase signaling. Cell Physiol Biochem. 2018; 45(5): 1818–1826, doi: 10.1159/000487873, indexed in Pubmed: 29510389.

20. Wang Ji, Xu Z, Chen X, et al. MicroRNA-182-5p attenuates cerebral ischemia-reperfusion injury by targeting Toll-like receptor 4. Biochem Biophys Res Commun. 2018; 505(3): 677–684, doi: 10.1016/j.bbrc.2018.09.165, indexed in Pubmed: 30292407.

21. Machado IF, Teodoro JS, Palmeira CM, et al. miR-378a: a new emerging microRNA in metabolism. Cell Mol Life Sci. 2020; 77(10): 1947–1958, doi: 10.1007/s00018-019-03375-z, indexed in Pubmed: 31748917.

22. Zheng S, Li M, Miao K, et al. lncRNA GAS5-promoted apoptosis in triple-negative breast cancer by targeting miR-378a-5p/SUFU signaling. J Cell Biochem. 2020; 121(3): 2225–2235, doi: 10.1002/jcb.29445, indexed in Pubmed: 31692053.

23. Cui Z, Liu QL, Sun SQ, et al. MiR-378a-5p inhibits angiogenesis of oral squamous cell carcinoma by targeting KLK4. Neoplasma. 2020; 67(1): 85–92, doi: 10.4149/neo_2019_190306N191, indexed in Pubmed: 31829025.

24. Varani G, McClain WH. The G x U wobble base pair. A fundamental building block of RNA structure crucial to RNA function in diverse biological systems. EMBO Rep. 2000; 1(1): 18–23, doi: 10.1093/embo-reports/kvd001, indexed in Pubmed: 11256617.

25. Racioppi L, Nelson ER, Huang W, et al. CaMKK2 in myeloid cells is a key regulator of the immune-suppressive microenvironment in breast cancer. Nat Commun. 2019; 10(1): 2450, doi: 10.1038/s41467-019-10424-5, indexed in Pubmed: 31164648.

ORIGINAL PAPER

VIA MEDICA

Naringenin promotes SDF-1/CXCR4 signaling pathway in BMSCs osteogenic differentiation

Yipei Wang[1, 2], Shulin Bai[1, 2], Qian Cheng[1, 2], Yang Zeng[1, 2], Xiaomei Xu[1, 2], Guangzhao Guan[3]

[1]Department of Orthodontics, The Affiliated Stomatology Hospital of Southwest Medical University, Luzhou, Sichuan 646000, P.R. China

[2]Oral and Maxillofacial Reconstruction and Regeneration Laboratory, Southwest Medical University, Luzhou, P.R. China

[3]Department of Oral Diagnostic and Surgical Sciences, Faculty of Dentistry, University of Otago, Dunedin, New Zealand

Abstract

Introduction. Naringenin, a dihydro-flavonoid compound that shows chemotactic activity, may have a good application prospect in repairing bone tissue, but its specific mechanism in bone regeneration, especially the osteogenic differentiation of stem cells, needs for a further study. The aim of this study was to investigate the effect of naringenin on the osteogenic differentiation and its roles in the C-X-C chemokine receptor type 4/stromal cell-derived factor 1 (SDF-1/CXCR4) signal pathway of bone marrow-derived mesenchymal stem cells (BMSCs).

Material and methods. BMSCs were harvested from the femurs and tibias of 4-to-6-week-old male Sprague-Dawley rats. Cell Counting kit-8 assay was used to determine cytotoxicity of naringenin. Alkaline phosphatase (ALP) activity was measured in cell's precipitates and alizarin-red staining was performed to determine the osteogenic differentiation capacity of the BMSCs. Real-time polymerase chain reaction, enzyme-linked immunosorbent assay and western blotting were adopted to determine the expression of genes and proteins.

Results. The cellular morphology was spindle-shaped, and arranged in radial and whorled patterns. The flow cytometric analysis have confirmed the presence of characteristic surface proteins in the harvested BMSCs. Different concentrations (0–200 μg/ml) of naringenin have no influence on the viability and proliferation rate of the BMSCs. The highest ALP activity was found at culture day 7 and 9 when the concentration of naringenin was 75 and 100 μg/ml. Positive red or dark red stained cells with mineralized nodules can be observed on day 14. The expression of ALP, Runt-related transcription factor 2, CXCR4 and SDF-1α at the gene and protein levels in naringenin-treated cells were significantly higher than those in the control cells. Moreover, AMD3100, an inhibitor of CXCR4, suppressed the expression of the studied genes and proteins.

Conclusions. Naringenin does not show toxic effect on BMSCs. Naringenin promotes the expression of the SDF-1α gene and protein via the SDF-1/CXCR4 signaling pathway. A better understanding of the mechanisms of naringenin action would be helpful for developing specific therapeutic strategies to improve bone regeneration after injuries. *(Folia Histochemica et Cytobiologica 2021, Vol. 59, No. 1, 66–73)*

Key words: bone marrow-derived mesenchymal stem cells; cell viability; naringenin; alizarin red; SDF-1; CXCR4; RT-qPCR

Correspondence address: Xiaomei Xu,
Department of Orthodontics, The Affiliated Stomatology
Hospital of Southwest Medical University, 2 Jiangyang South
Road, Luzhou, Sichuan 646000, P.R. China
e-mail: xuxiaomei@hotmail.com

Introduction

Bone has a remarkable capacity of spontaneous repairing and regeneration. The process of spontaneous bone regeneration using bone marrow stroma-derived

stem cells (BMSCs) holds a great potential, which would greatly affect the human health by a way of providing the possibility to repair tissues injury [1, 2]. BMSCs, the first important components and regulators to be found in bone marrow, produce hematopoietic-supporting stromal cells and form the hematopoietic niches for hematopoietic stem cells [3, 4]. Chemokines are the important regulators of BMSCs. The SDF-1/CXCR4 signaling pathway appears important in maintaining proliferation and survival of BMSCs by improving cellular migration, remodeling and survival in response to stress [5, 6]. In bone remodeling, the SDF-1/CXCR4 signaling pathway regulates the osteogenic differentiation of the BMSCs, the expression of osteogenic protein such as ALP, OCN and OSX and the formation of osteoblasts. It is also closely related to bone morphogenic protein 2 signaling [7]. CXCR4-knockout mice showed the reduction in bone formation and the osteogenic differentiation of BMSCs [8, 9]. The osteogenic effect of SDF-1/ CXCR4 signaling can be further enhanced by other molecules such as hypoxia-inducible factor (HIF) family members, resulting in strong synergistic effects on the bone remodeling and regeneration [10].

Although chemokines can be synthesized chemically, the expensive cost limits their clinical application. Naringenin (4',5-7 trihydroxydihydroflavone, Fig. 1), widely present in fruits such as orange, pomelo, and drynaria, is a dihydro-flavonoid compound that shows chemotactic activity [11] and other biological effects such as anti-inflammatory, antioxidative, anticancer and antiadipogenic activities [12–15], and is also shown to have anti-osteoporotic and anti-osteolytic effects [16]. Several experiments have shown that naringenin could reduce the osteolytic activities of osteoclasts, and improve the osteogenic differentiation and mineralization effects of the osteoblasts in osteolysis-related diseases [16–20]. The aim of the study was to investigate the effect of naringenin on the osteogenic differentiation of BMSCs and its role in the SDF-1/CXCR4 signaling pathway.

Materials and methods

Isolation, culture and identification of BMSCs. All experiments with the use of animals were conducted under the Guidelines for Animal Experimentation and were approved by the Ethics Committee of Southwest Medical University (Luzhou, China, Certificate No.201812-25). BMSCs were harvested from the femurs and tibias of 4-to-6-week-old rats as previously reported [21]. Briefly, rats were killed with chloral hydrate, and the tibia and femur were obtained. The bilateral epiphyseal end of the bone was cut by scissors, and then the D-Hank's solution (Solarbio, Beijing, China) containing 10% fetal bovine serum (FBS, Sijiqing, Hangzhou, China) was extracted by syringe to wash the bone marrow cavity.

Cells were incubated in F-12 medium (Gibco, Grand Island, NY, USA) with 10% FBS and 1% antibiotics (100 U/mL penicillin and 100 μg/mL streptomycin, HyClone, South Logan, UT, USA) in a 37°C humidified atmosphere with 5% CO_2 in air. When the monolayer reached approximately 80% confluence, cells were passaged. Then, the passages 2 through 3 (P2–P3) cells were used for this study.

After the second passage, cells were characterized by flow cytometry for the expression of the BMSCs surface antigens, such as CD29, CD34, CD45 and CD90. After that the cells cultured with lipogenic induction medium (α-MEM, FBS, penicillin-streptomycin solution, IBMX, dexamethasone, indometacin, insulin (all from SigmaAldrich, St. Louis, MO, USA) were stained with Oil Red O at day 12 to identify lipid vacuoles, and the cells cultured with osteogenic induction medium (α-MEM, FBS, penicillin-streptomycin solution, sodium β-glycerophosphate, vitamin C and dexamethasone; all from SigmaAldrich) were stained with Alizarin Red on day 14 to characterize osteogenic activities.

Cell Counting kit-8 (CCK-8) viability assay. To detect the potential cytotoxicity of naringenin on the BMSCs, the CCK-8 assay was performed [22]. A set of classic osteogenesis inducers group was used as positive control. The culture medium was used as negative control. BMSCs were incubated with different naringenin concentrations of 0, 6.25, 12.5, 25, 50, 75, 100, 200 μg/ml. Rat BMSCs at passage 2 were transferred to 96-well plates at 1×10^4/well density. When the cells reached 80% confluence, different reagents were added by categorization. On day 2, 10 μl of CCK-8 reagents (Dojindo-Kumamoto, Japan) were added to each well. The optical density (OD) at 450 nm wavelength was measured by a Varioskan Flash enzyme-labeled instrument (Thermo Fisher, Waltham, MA, USA). Cell viability was then calculated based on OD values.
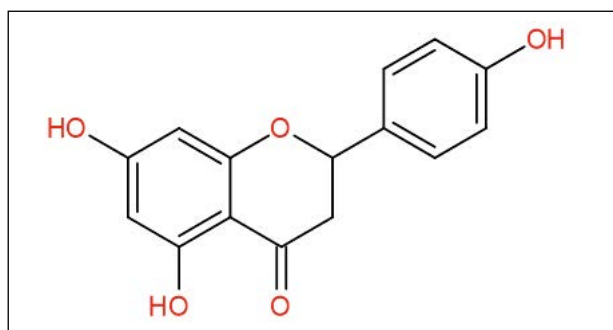

Figure 1. The chemical structure of naringenin [38].

Quantification of alkaline phosphatase (ALP) activity.
ALP quantification assay was performed to determine the
osteogenic differentiation capacity of BMSCs in the control
and experimental groups on day 3, 5, 7 and 9 [23]. BMSCs
were placed in 24-well plates at a cell density of 5×10^4/
/well. After being cultured for the indicated time, the cells
were centrifuged in a centrifuge tube and lysed by 0.1% Tri-
tonX-100 (Beyotime, Shanghai, China). After the cells were
sufficiently lysed, the cells were centrifuged at 13,000 rpm
for 5 min. Then the supernatant was proceeded according
to the manufacturer's instruction of ALP activity assay kit
(Nanjing Jiancheng Bioengineering Institute, Nanjing, Chi-
na). The OD value was measured at the 520 nm wavelength.

Alizarin red staining. BMSCs were placed in 35 mm Petri
dishes at a cell density of 5×10^5/well. When the cells
reached 80% confluence, the culture medium was trans-
ferred to the control groups, 100 μg/ml naringenin group,
100 μg/ml naringenin + AMD3100 antagonist group and
classical osteogenic induction group. 14 days later, cells were
stained with alizarin red dye (Sangon, Shanghai, China).

Real-time polymerase chain reaction (RT-qPCR). Induction
cells in each group were digested with trypsin and centri-
fuged, and the precipitates were collected on day 7. The
total RNA was extracted by Trizol reagent (Ambion, Austin,
TX, USA) and converted to cDNA (TAKARA, Mountain
View, CA, USA). Real-time RT-PCR was performed using
a SYBR Green PCR Kit (Kapa Biosystems, Wilmington,
MA, USA). The primer sequences were shown in Table 1.

Enzyme-linked immunosorbent assay (ELISA). The concen-
trations of SDF-1α and CXCR4 proteins in the cell superna-
tants were measured by ELISA (Bioswamp, Wuhan, China)
according to the manufacturer's instructions on day 1, 3, 5 and 7.

Western blotting. The cells in each group were lysed with
RIPA lysis buffer (Beyotime, Shanghai, China), after induced

Table 1. The primers sequences used for RT-qPCR

Gene	Primer Sequence
SDF-1α-F	TTGTCTCAACCCTGAAGCCC
SDF-1α-R	TGCCCGTTGAGGTACAGGAG
CXCR4-F	CCTCCTCCTGACTATCCCTGA
CXCR4-R	CGAACTCACATCCTTGCTTG
ALP-F	CTACCACTCGGGTGAACCA
ALP-R	AGCTGATATGCGATGTCCTT
Runx2-F	AACTTCCTGTGCTCCGTGCT
Runx2-R	TCGTTGAACCTGGCTACTTGG
GAPDH-F	CAAGTTCAACGGCACAG
GAPDH-R	CCAGTAGACTCCACGACAT

for 7 days to obtain the total protein. Then, the BCA protein
test kit was used to measure the total protein concentration.
Equal amounts of cell extracts (20 μg/lane) separated by 10%
SDS-PAGE and proteins were transferred to PVDF mem-
branes. After being sealed with 5% skim milk overnight at
4°C, the membranes were incubated with primary antibodies
overnight at room temperature. The antibodies used were as
following: rabbit anti-Alkaline Phosphatase (1: 1000, Abcam,
Cambridge, MA, USA), mouse anti-Runt-related transcrip-
tion factor 2 (RUNX2) (1: 1000, Abcam), rabbit anti-SDF-1/
/CXCL12 (1: 1000, CST, Danvers, MA, USA), rabbit an-
ti-CXCR4 polyclonal antibody (1: 1000, Invitrogen, Carls-
bad, CA, USA), rabbit anti-GAPDH (1:1000, Bioswamp).
Horseradish peroxidase (HRP)-goat anti-rabbit IgG
(1: 20000, Bioswamp) and HRP-rabbit anti-mouse IgG
antibody (1: 20000, Bioswamp) were used as secondary anti-
bodies for one hour at room temperature. We used glyceral-
dehyde 3-phosphate dehydrogenase as the internal control.

Statistical analysis. All the experimental data were expressed
as mean ± standard deviation (SD) from three independent
experiments. Analysis of variance (ANOVA) is used for data
analysis by the SPSS software (SPSS Inc., Chicago, IL, USA),
p values < 0.05 were defined as statistically significant.

Results

Culture and identification of BMSCs
The cells appeared in sphere shape during the first
two days. At day 6, the cells were spindle-shaped and
bipolar, occasionally multipolar (Fig. 2A). After pas-
sage of the cells, cellular morphology became uniform,
spindle-shaped, and arranged in radial and whorled
patterns (Fig. 2B).
The phenotypic cells of BMSCs were identified by
flow cytometry. BMSC-associated markers such as
CD29 (99.08%) and CD90 (96.06%) were positive.
The cells lacked the expression of hematopoietic
markers (CD45 and CD34) (Fig. 2C). In the cell cycle
assay, G1 cells accounted for 87.91% of all cells, and
S-phase cells fraction was 8.22%, given the ratio G2/
/G1 equaled to 1.90. This indicated that most of the
cells were at rest, which was one of the characteristics
of stem cells (Fig. 2D).
At day 14, the alizarin-red positively stained red
or dark-red cells with mineralized nodules can be
observed (Fig. 2E). At day 12, large lipid vacuoles
stained with Oil Red O were observed in the BMSCs
cultures (Fig. 2F). Thus, after 2 weeks of culture
BMSCs showed both osteogenic and adipogenic dif-
ferentiation potential. Experimental results showed
that the cells obtained are BMSCs, which are of high
purity, and meet the requirements of subsequent
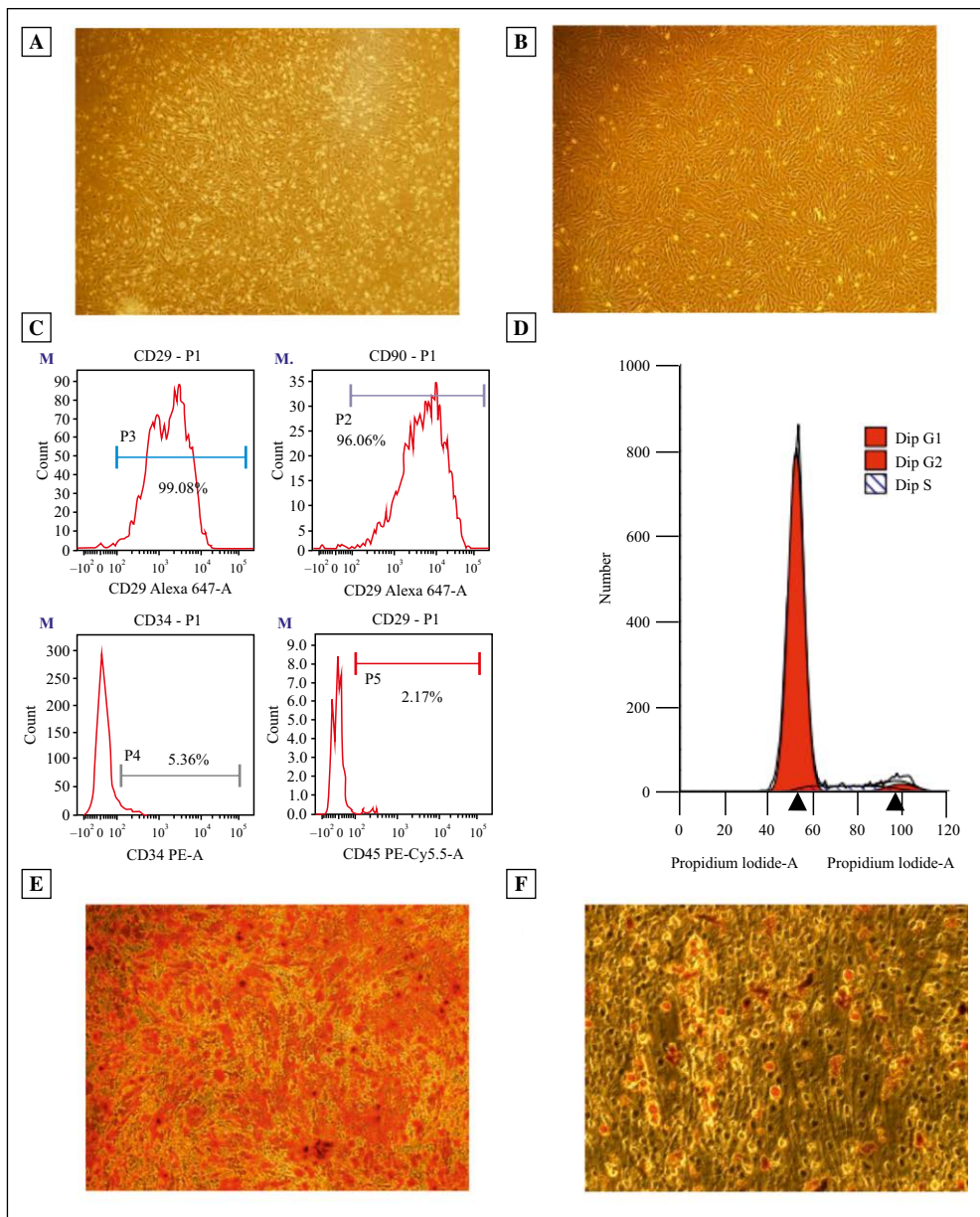experiments.

Figure 2. Culture, identification and characterization of rat BMSCs. **A.** BMSCs morphology on day 6 (40×). **B.** The morphology of the cells became uniform, spindle-shaped, with well-defined cytoplasm after passage 2 (40×). **C.** Flow cytometry results showed that the cells were positive for MSCs specific markers (CD29, CD90), and negative for hematopoietic markers (CD34, CD45). **D.** In the cell cycle assay by flow cytometry, G1 cells accounted for 87.91%, and S-phase cells fraction was 8.22%, given the ratio G2/G1 equaled to 1.90. **E.** Alizarin Red staining was used to demonstrate mineralized nodules in BMSCs cultured with osteogenic induction fluid on day 14 (40×). **F.** Large lipid vacuoles were observed in BMSCs cultured with lipogenic induction medium at day 12 *via* Oil Red O assay (100×).

Cell viability and osteogenic differentiation of BMSCs
To explore the possible naringenin toxicity, the cellular viability was quantified for different concentrations of naringenin. In the experimental groups, no significant difference in cell viability was found between 6.25–200 μg/ml at day 2 (Fig. 3A). Thus, different concentrations of naringenin did not influence the viability and proliferation rate of the BMSCs.

Within the experimental groups, the trend of each group at different time points was the same, and it showed a time-dependent increase on days 3, 5, 7 and 9. The ALP activities in cell's precipitates of 75, 100 μg/ml naringenin group were the highest at each time points, and the difference between the two groups was not statistically significant (Fig. 3B).
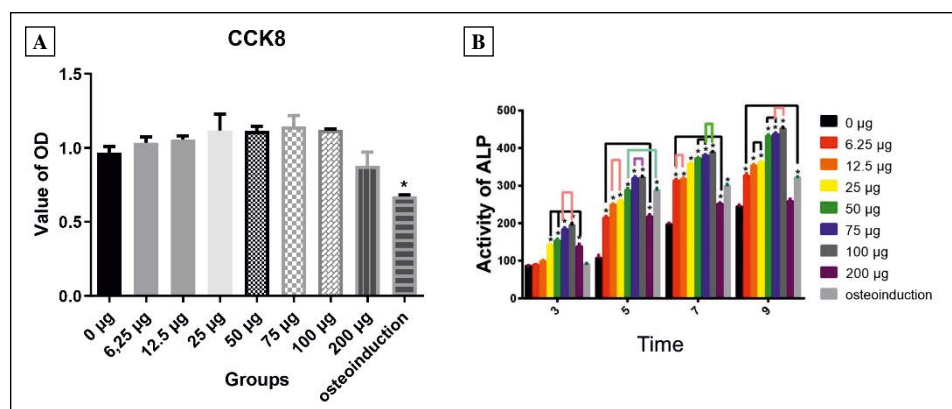
Figure 3. Cell viability and osteogenic differentiation of BMSCs. **A.** Different concentrations of naringenin have no influence on the viability and proliferation rate of the BMSCs as measured by CCK-8 assay. **B.** High ALP activity was found at the concentration of 75 and 100 μg/ml of naringenin on days 3, 5, 7, and 9. Results are means ± standard deviation (SD), and similar data were obtained from three independent experiments (n = 3). The activity of ALP was measured in arbitrary units as described in Methods. *$p < 0.05$ *vs.* the culture medium group (one-way ANOVA followed by Tukey's test).

The role of naringenin in the SDF-1/CXCR4 signaling pathway

To explore the effects of naringenin on the SDF-1/CXCR4 signaling pathway, CXCR4 antagonist AMD3100 was added to BMSCs incubated with 100 μg/ml naringenin. More mineralization nodules were noted in 100 μg/ml naringenin group when compared with the classic osteogenic induction and culture medium groups (negative control). However, the alizarin red staining was suppressed in AMD3100 + 100 μg/ml naringenin group when compared with 100 μg/ml naringenin and classic osteogenic induction groups (Fig. 4A).

The expression of ALP, RUNX2, CXCR4 and SDF-1α genes in cells incubated with naringenin, measured by RT-qPCR, were significantly higher than those in the cells of negative control. However, after adding AMD3100 to naringenin-treated cells, the expression of these genes were significantly suppressed (Fig. 4B). Similar results of SDF-1α and CXCR4 proteins by ELISA were found at different time lines, such as those on day 1, 3, 5, and 7 (Fig. 4C, D). The results of the expression of ALP, RUNX2, CXCR4 and SDF-1α proteins measured by western blot were similar to the expression of their respective genes (Fig. 4E).

Discussion

Naringenin has many pharmacological activities, and has become one of the flavonoids concerned by scientists in many areas of biological and biomedical studies. With the further study of naringenin, it is found that naringenin has obvious effect on bone defect repair. Kaczmarczyk-Sedlak *et al.* [16] found that adding naringenin to the diet of Wistar rats could improve the symptoms of osteoporosis and the morphological manifestations of bone tissue after ovarian removal showing that naringenin has obvious anti-osteoporosis and anti-osteolysis effects in bone tissue repair. In addition, naringenin, the aglycone of naringin, is the most common form in serum after oral administration of naringin because naringin can be metabolized into absorbable naringenin by intestinal flora [24]. It is also reported that naringenin exhibited higher antioxidant capacity and hydroxyl and superoxide radical scavenger efficiency than naringin [12]. SDF-1/CXCR4 signaling pathway plays an important role in preserving the bone marrow stem cells in bone marrow and regulating the release of stem cells from bone marrow to peripheral circulation [25]. CXCR4 signals the stem cells migration during fracture healing. It participates in bone repair and regeneration by inducing cellular migration and regulating differentiation [9]. SDF-1 is induced in the periosteum of injured bone, and it promotes endochondral bone repair and regeneration by recruiting BMSCs to the site of injury [26, 27]. However, the role of the SDF-1/CXCR4 signaling pathway in osteogenic differentiation induced by naringenin is unknown.

It was previously shown that the highest ALP activity was found after day 8 in the naringenin group, which was confirmed by our results [28]. Cellular viability assay showed no significant toxicity among the experimental groups at concentration between 0~200 μg/ml. Guo-Yong Y *et al.* [29] reported that treatment at the optimal concentration (50 μg/mL) for rat BMSCs increased mRNA levels of osteogenic genes (ALP, BSP, and cbfa1). In our study, the highest ALP activity value was found at day 7 and 9 at the naringenin concentration of 75 and 100 μg/ml. Therefore, we chose 100 μg/ml over 7 days for our subsequent experiments.
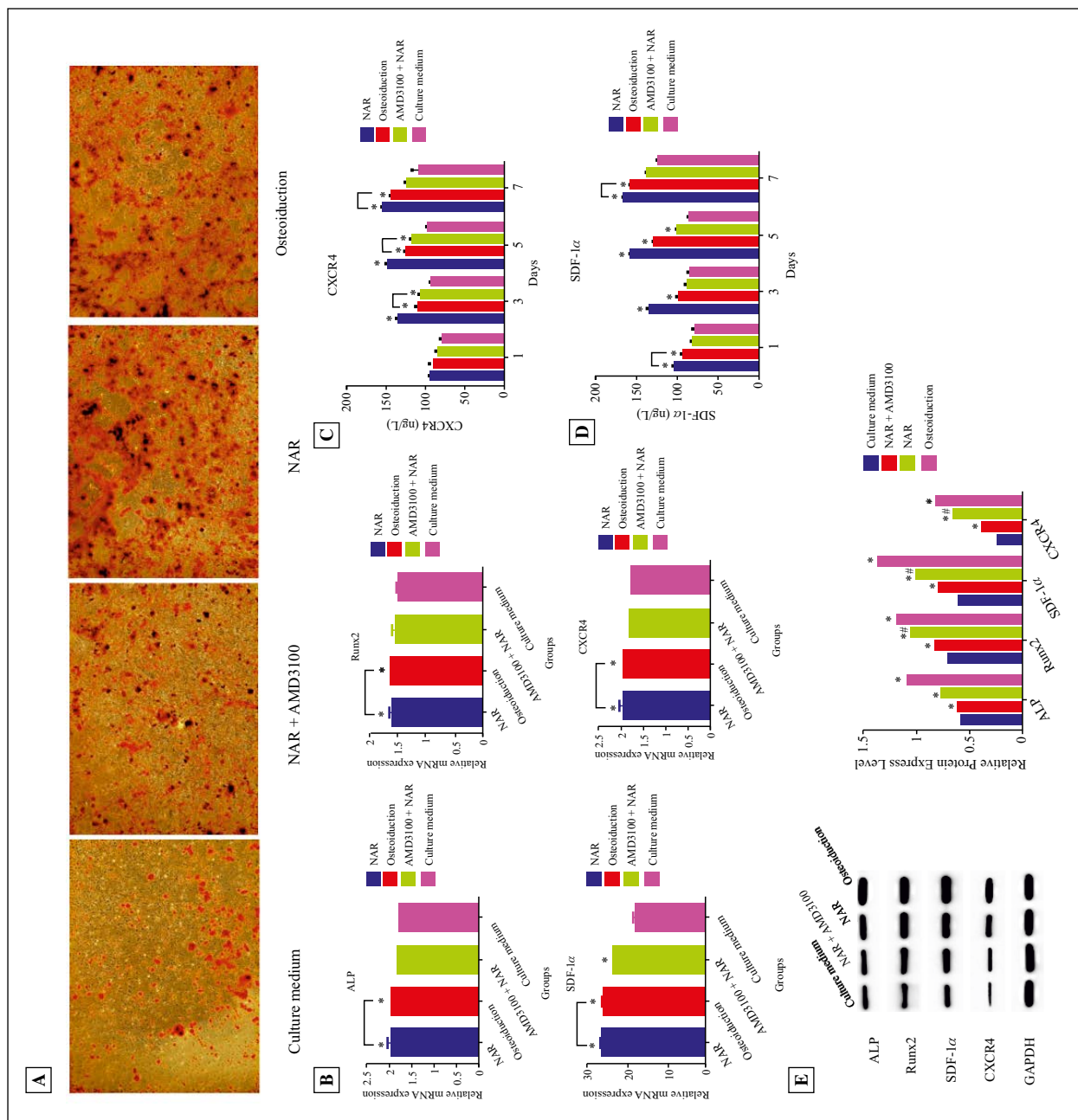
Figure 4. The role of naringenin in the SDF-1/CXCR4 signal pathway. **A.** Each group was stained with Alizarin Red on day 14. (40×). **B.** The expression of osteogenic genes in naringenin groups was upregulated at the mRNA level as assessed by RT-qPCR when compared with culture medium group (p < 0.05). **C.** The expression of CXCR4 protein in BMSCs induced by naringenin was higher than the culture medium group as measured by ELISA (p < 0.05). **D.** The expression of SDF-1α protein measured by ELISA in supernatants of naringenin-induced BMSCs was suppressed as compared with culture medium group. **E.** Suppression of ALP, RUNX2, SDF-1α, and CXCR4 proteins in BMSCs induced by naringenin were detected by Western blotting. Results are means ± standard deviation (SD), n = 3; *p < 0.05 *vs.* culture medium group, #p < 0.05 *vs*. NAR + AMD3100 group. Abbreviations: NAR — naringenin; AMD3100, an antagonist of SDF-1/CXCR4 signaling.

This study further examined the role of SDF-1/ /CXCR4 signaling pathway in the BMSCs osteogenic differentiation by using the CXCR4 antagonist AMD3100. CXCR4 antagonists include AMD3100 and T140 [30, 31]. AMD3100 inhibits the binding of CXCR4 to SDF-1, and blocks signal transduction along the SDF-1/CXCR4 axis.

In this study, the mineralized nodules were significantly decreased after adding AMD3100 to BMSCs treated with naringenin, when compared with the

osteogenic induction group and naringenin group. It suggested that AMD3100 might suppress the effect of naringenin in osteogenic differentiation by blocking the SDF-1/CXCR4 signaling pathway in BMSCs. The measurements of the expression of CXCR4 and SDF-1α genes and proteins showed that it increased over the induction time in the experimental groups. Naringenin promoted the expression the SDF-1α gene and synthesis of protein in the early stage of osteogenic differentiation in BMSCs. Study has showed that the SDF-1 was upregulated at the fracture site and ischemic site after femoral bone transplantation in a mice model [32]. Kawakami *et al.* [5] found that bone healing was delayed by decreasing the callus formation in CXCR4-deficient mice. An in vitro study showed that overexpression of SDF-1α in human BMSCs might promote osteogenic differentiation and osteoblastic angiogenesis by upregulating the osteogenic-related proteins, such as ALP, RUNX2, osteocalcin, and p-Smadl/5, and angiogenesis-related protein such as CD31 [33]. In the present study, naringenin regulated the SDF-1/CXCR4 signaling pathway by increasing the expression of SDF-1, and increased osteogenic differentiation of BMSCs. SDF-1 and CXCR4 activate a series of downstream signaling pathways, including extracellular signal-regulated kinases (ERK) 1/2 [34] and phosphoinositide 3-kinases/protein kinase B (PI3K/AKT) [35]. Naringin was shown to enhance osteogenic differentiation by activating ERK signaling pathway in human BMSCs [36] and PI3K/AKT signaling pathway in osteoblasts [37]. Naringenin might act on the same pathway and regulate the downstream pathways (ERK1/2 and PI3K/AKT) to induce osteogenesis. In addition, it was found that naringenin exerted its protective effects by inhibiting osteoclastogenesis and osteoclast bone resorption [19, 20]. Therefore, naringenin might have therapeutic potentials for a range of bone diseases such as osteoporosis, repairing of bone defects, alveolar bone resorption and other.

In summary, we found that naringenin does not have toxic effects on BMSCs. Naringenin promoted the expression of the ALP, RUNX2, SDF-1α and CXCR4 genes and proteins via the SDF-1/CXCR4 signaling pathway. A better understanding of the molecular mechanisms of naringenin activity will be beneficial in developing specific therapeutic strategies to improve bone repair after injuries.

Conflict of interests

The authors declare that they have no conflict of interest.

References

1. Hokugo A, Saito T, Li A, et al. Stimulation of bone regeneration following the controlled release of water-insoluble oxysterol from biodegradable hydrogel. Biomaterials. 2014; 35(21): 5565–5571, doi: 10.1016/j.biomaterials.2014.03.018, indexed in Pubmed: 24731715.

2. Fong ELS, Chan CK, Goodman SB. Stem cell homing in musculoskeletal injury. Biomaterials. 2011; 32(2): 395–409, doi: 10.1016/j.biomaterials.2010.08.101, indexed in Pubmed: 20933277.

3. Sha Y, Lv Y, Xu Z, et al. MGF E peptide pretreatment improves the proliferation and osteogenic differentiation of BMSCs via MEK-ERK1/2 and PI3K-Akt pathway under severe hypoxia. Life Sci. 2017; 189: 52–62, doi: 10.1016/j.lfs.2017.09.017, indexed in Pubmed: 28927682.

4. Wu J, Zhang W, Ran Q, et al. The differentiation balance of bone marrow mesenchymal stem cells is crucial to hematopoiesis. Stem Cells Int. 2018; 2018: 1540148, doi: 10.1155/2018/1540148, indexed in Pubmed: 29765406.

5. Kawakami Y, Ii M, Matsumoto T, et al. SDF-1/CXCR4 axis in Tie2-lineage cells including endothelial progenitor cells contributes to bone fracture healing. J Bone Miner Res. 2015; 30(1): 95–105, doi: 10.1002/jbmr.2318, indexed in Pubmed: 25130304.

6. Peyvandi AA, Roozbahany NA, Peyvandi H, et al. Critical role of SDF-1/CXCR4 signaling pathway in stem cell homing in the deafened rat cochlea after acoustic trauma. Neural Regen Res. 2018; 13(1): 154–160, doi: 10.4103/1673-5374.224382, indexed in Pubmed: 29451220.

7. Zhu W, Liang G, Huang Z, et al. Conditional inactivation of the CXCR4 receptor in osteoprecursors reduces postnatal bone formation due to impaired osteoblast development. J Biol Chem. 2011; 286(30): 26794–26805, doi: 10.1074/jbc.M111.250985, indexed in Pubmed: 21636574.

8. Herberg S, Kondrikova G, Hussein KA, et al. Mesenchymal stem cell expression of stromal cell-derived factor-1β augments bone formation in a model of local regenerative therapy. J Orthop Res. 2015; 33(2): 174–184, doi: 10.1002/jor.22749, indexed in Pubmed: 25351363.

9. Toupadakis CA, Wong A, Genetos DC, et al. Long-term administration of AMD3100, an antagonist of SDF-1/CXCR4 signaling, alters fracture repair. J Orthop Res. 2012; 30(11): 1853–1859, doi: 10.1002/jor.22145, indexed in Pubmed: 22592891.

10. Liles W, Broxmeyer H, Rodger E, et al. Mobilization of hematopoietic progenitor cells in healthy volunteers by AMD3100, a CXCR4 antagonist. Blood. 2003; 102(8): 2728––2730, doi: 10.1182/blood-2003-02-0663, indexed in Pubmed: 12855591.

11. Joshi R, Kulkarni YA, Wairkar S. Pharmacokinetic, pharmacodynamic and formulations aspects of Naringenin: An update. Life Sci. 2018; 215: 43–56, doi: 10.1016/j.lfs.2018.10.066, indexed in Pubmed: 30391464.

12. Cavia-Saiz M, Busto MD, Pilar-Izquierdo MC, et al. Antioxidant properties, radical scavenging activity and biomolecule protection capacity of flavonoid naringenin and its glycoside naringin: a comparative study. J Sci Food Agric. 2010; 90(7): 1238–1244, doi: 10.1002/jsfa.3959, indexed in Pubmed: 20394007.

13. Li YR, Chen DY, Chu CL, et al. Naringenin inhibits dendritic cell maturation and has therapeutic effects in a murine model of collagen-induced arthritis. J Nutr Biochem. 2015; 26(12): 1467–1478, doi: 10.1016/j.jnutbio.2015.07.016, indexed in Pubmed: 26350255.

14. Pinho-Ribeiro FA, Zarpelon AC, Fattori V, et al. Naringenin reduces inflammatory pain in mice. Neuropharmacology. 2016; 105: 508–519, doi: 10.1016/j.neuropharm.2016.02.019, indexed in Pubmed: 26907804.

15. Yi LT, Li CF, Zhan X, et al. Involvement of monoaminergic system in the antidepressant-like effect of the flavonoid naringenin in mice. Prog Neuropsychopharmacol Biol Psychiatry. 2010; 34(7): 1223–1228, doi: 10.1016/j.pnpbp.2010.06.024, indexed in Pubmed: 20603175.

16. Kaczmarczyk-Sedlak I, Wojnar W, Zych M, et al. Effect of dietary flavonoid naringenin on bones in rats with ovariectomy-induced osteoporosis. Acta Pol Pharm. 2016; 73(4): 1073–1081, indexed in Pubmed: 29648734.

17. Swarnkar G, Sharan K, Siddiqui JA, et al. A naturally occurring naringenin derivative exerts potent bone anabolic effects by mimicking oestrogen action on osteoblasts. Br J Pharmacol. 2012; 165(5): 1526–1542, doi: 10.1111/j.1476-5381.2011.01637.x, indexed in Pubmed: 21864313.

18. Wang X, Zhen L, Zhang Ge, et al. Osteogenic effects of flavonoid aglycones from an osteoprotective fraction of Drynaria fortunei-an in vitro efficacy study. Phytomedicine. 2011; 18(10): 868–872, doi: 10.1016/j.phymed.2011.01.022, indexed in Pubmed: 21377852.

19. Wang W, Wu C, Tian Bo, et al. The inhibition of RANKL-induced osteoclastogenesis through the suppression of p38 signaling pathway by naringenin and attenuation of titanium-particle-induced osteolysis. Int J Mol Sci. 2014; 15(12): 21913–21934, doi: 10.3390/ijms151221913, indexed in Pubmed: 25464380.

20. Wang W, Li M, Luo M, et al. Naringenin inhibits osteoclastogenesis through modulation of helper T cells-secreted IL-4. J Cell Biochem. 2018; 119(2): 2084–2093, doi: 10.1002/jcb.26370, indexed in Pubmed: 28834554.

21. Azizi SA, Stokes D, Augelli BJ, et al. Engraftment and migration of human bone marrow stromal cells implanted in the brains of albino rats-similarities to astrocyte grafts. Proc Natl Acad Sci U S A. 1998; 95(7): 3908–3913, doi: 10.1073/pnas.95.7.3908, indexed in Pubmed: 9520466.

22. Yin Y, Li F, Li S, et al. TLR4 influences hepatitis B virus related hepatocellular carcinoma by regulating the Wnt/β-catenin pathway. Cell Physiol Biochem. 2017; 42(2): 469–479, doi: 10.1159/000477594, indexed in Pubmed: 28578348.

23. Zhang X, Du Yu, Ling J, et al. Dickkopf-related protein 3 negatively regulates the osteogenic differentiation of rat dental follicle cells. Mol Med Rep. 2017; 15(4): 1673–1681, doi: 10.3892/mmr.2017.6165, indexed in Pubmed: 28259940.

24. Fang T, Wang Y, Ma Y, et al. A rapid LC/MS/MS quantitation assay for naringin and its two metabolites in rats plasma. J Pharm Biomed Anal. 2006; 40(2): 454–459, doi: 10.1016/j.jpba.2005.07.031, indexed in Pubmed: 16406442.

25. Hübel K, Liles W, Broxmeyer H, et al. Leukocytosis and mobilization of CD34+ hematopoietic progenitor cells by AMD3100, a CXCR4 antagonist. Supportive Cancer Therapy. 2004; 1(3): 165–172, doi: 10.3816/sct.2004.n.008, indexed in Pubmed: 18628138.

26. Toupadakis CA, Wong A, Genetos DC, et al. Long-term administration of AMD3100, an antagonist of SDF-1/CXCR4 signaling, alters fracture repair. J Orthop Res. 2012; 30(11): 1853–1859, doi: 10.1002/jor.22145, indexed in Pubmed: 22592891.

27. Kitaori T, Ito H, Schwarz EM, et al. Stromal cell-derived factor 1/CXCR4 signaling is critical for the recruitment of mesenchymal stem cells to the fracture site during skeletal repair in a mouse model. Arthritis Rheum. 2009; 60(3): 813–823, doi: 10.1002/art.24330, indexed in Pubmed: 19248097.

28. Ming LG, Ge BF, Wang MG, et al. Comparison between 8-prenylnarigenin and narigenin concerning their activities on promotion of rat bone marrow stromal cells' osteogenic differentiation in vitro. Cell Prolif. 2012; 45(6): 508–515, doi: 10.1111/j.1365-2184.2012.00844.x, indexed in Pubmed: 23106298.

29. Yu GY, Zheng GZ, Chang Bo, et al. Naringin stimulates osteogenic differentiation of rat bone marrow stromal cells via activation of the notch signaling pathway. Stem Cells Int. 2016; 2016: 7130653, doi: 10.1155/2016/7130653, indexed in Pubmed: 27069482.

30. Tamamura H, Kuroda M, Masuda M, et al. A comparative study of the solution structures of tachyplesin I and a novel anti-HIV synthetic peptide, T22 ([Tyr5,12, Lys7]-polyphemusin II), determined by nuclear magnetic resonance. Biochim Biophys Acta. 1993; 1163(2): 209–216, doi: 10.1016/0167-4838(93)90183-r, indexed in Pubmed: 8490053.

31. Nakashima H, Masuda M, Murakami T, et al. Anti-human immunodeficiency virus activity of a novel synthetic peptide, T22 ([Tyr-5,12, Lys-7]polyphemusin II): a possible inhibitor of virus-cell fusion. Antimicrob Agents Chemother. 1992; 36(6): 1249–1255, doi: 10.1128/aac.36.6.1249, indexed in Pubmed: 1384424.

32. Kitaori T, Ito H, Schwarz EM, et al. Stromal cell-derived factor 1/CXCR4 signaling is critical for the recruitment of mesenchymal stem cells to the fracture site during skeletal repair in a mouse model. Arthritis Rheum. 2009; 60(3): 813–823, doi: 10.1002/art.24330, indexed in Pubmed: 19248097.

33. Yang F, Xue F, Guan J, et al. Stromal-cell-derived factor (SDF) 1-alpha overexpression promotes bone regeneration by osteogenesis and angiogenesis in osteonecrosis of the femoral head. Cell Physiol Biochem. 2018; 46(6): 2561–2575, doi: 10.1159/000489684, indexed in Pubmed: 29758548.

34. Wang S, Zhou C, Zheng H, et al. Chondrogenic progenitor cells promote vascular endothelial growth factor expression through stromal-derived factor-1. Osteoarthritis Cartilage. 2017; 25(5): 742–749, doi: 10.1016/j.joca.2016.10.017, indexed in Pubmed: 27989872.

35. Chen HT, Tsou HK, Hsu CJ, et al. Stromal cell-derived factor-1/CXCR4 promotes IL-6 production in human synovial fibroblasts. J Cell Biochem. 2011; 112(4): 1219–1227, doi: 10.1002/jcb.23043, indexed in Pubmed: 21312239.

36. Wang H, Li C, Li J, et al. Naringin enhances osteogenic differentiation through the activation of ERK signaling in human bone marrow mesenchymal stem cells. Iran J Basic Med Sci. 2017; 20(4): 408–414, doi: 10.22038/IJBMS.2017.8582, indexed in Pubmed: 28804610.

37. Wu JB, Fong YC, Tsai HY, et al. Naringin-induced bone morphogenetic protein-2 expression via PI3K, Akt, c-Fos/c-Jun and AP-1 pathway in osteoblasts. Eur J Pharmacol. 2008; 588(2-3): 333–341, doi: 10.1016/j.ejphar.2008.04.030, indexed in Pubmed: 18495116.

38. Hernández-Aquino E, Muriel P. Beneficial effects of naringenin in liver diseases: Molecular mechanisms. World J Gastroenterol. 2018; 24(16): 1679–1707, doi: 10.3748/wjg.v24.i16.1679, indexed in Pubmed: 29713125.

INSTRUCTIONS FOR AUTHORS

MANUSCRPIT SUBMISSION

Folia Histochemica et Cytobiologica accepts manuscripts (original articles, short communications, review articles) from the field of histochemistry, as well as cell and tissue biology. Each manuscript is reviewed by independent referees. Book reviews and information concerning congresses, symposia, meetings etc., are also published.

All articles should be submitted to FHC electronically online at www.fhc.viamedica.pl where detailed instruction regarding submission process will be provided.

AUTHOR'S STATEMENT

The manuscript must be accompanied by the author's statement that it has not been published (or submitted to publication) elsewhere.

GHOSTWRITING

Ghostwriting and guest-authorship are forbidden. In case of detecting ghost written manuscripts, their actions will be taking involving both the submitting authors and the participants involved.

The corresponding author must have obtained permission from all authors for the submission of each version of the paper and for any change in authorship. Submission of a paper that has not been approved by all authors may result in immediate rejection.

COST OF PUBLICATION

The cost of publication of accepted manuscript is 800 Euro.

OFFPRINTS

PDF file of each printed paper is supplied for the author free of charge. Orders for additional offprints should be sent to the Editorial Office together with galley proofs.

ORGANIZATION OF MANUSCRIPT

The first page must include: the title, name(s) of author(s), affiliation(s), short running head (no more than 60 characters incl. spaces) and detailed address for correspondence including e-mail. Organization of the manuscript: 1. Abstract (not exceeding one typed page — should consist of the following sections: Introduction, Material and methods, Results, Conclusions); 2. Key words (max. 10); Introduction; Material and methods; Results; Discussion; Acknowledgements (if any); References; Tables (with legends); Figures; Legends to figures.

In a short communication, Results and Discussion should be written jointly. Organization of a review article is free.

TECHNICAL REQUIREMENTS

Illustrations (line drawings and halftones) — either single or mounted in the form of plates, can be 85 mm, 125 mm, or 175 mm wide and cannot exceed the size of 175 × 250 mm. The authors are requested to plan their illustrations in such a way that the printed area is eco-nomically used. Numbers, inscriptions and abbreviations on the figures must be about 3 mm high. In case of micrographs, magnification (*e.g.* × 65 000) should be given in the legend. Calibration bars can also be used. For the best quality of illustrations please provide images in one of commonly used formats e.g. *.tiff, *.png, *pdf (preferred resolution 300 dpi). Tables should be numbered consecutively in Arabic numerals and each table must be typed on a separate page. The authors are requested to mark the places in the text, where a given table or figure should appear in print. Legends must begin on a new page and should be as concise as necessary for a self-sufficient explanation of the illustrations. PDF file of each paper is supplied free of charge.

CITATIONS

In References section of article please use following American Medical Association 9th Ed. citation style. Note, that items are listed numerically in the order they are cited in the text, not alphabetically. If you are using a typewriter and cannot use italics, then use underlining.

Authors: use initials of first and second names with no spaces. Include up to six authors. If there are more than six, include the first three, followed by et al. If no author is given, start with the title. **Books:** include the edition statement (ex: 3rd ed. or Rev ed.) between the title and place if it is not the first edition. **Place:** use abbreviations of states, not postal codes. **Journals:** abbreviate titles as shown in *Index Medicus*. If the journal does not paginate continuously through the volume, include the month (and day). **Websites:** include the name of the webpage, the name of the entire website, the full date of the page (if available), and the date you looked at it. The rules concerning a title within a title are *not* displayed here for purposes of clarity. See the printed version of the manual for details. For documents and situations not listed here, see the printed version of the manual.

EXAMPLES

Book:
1. Okuda M, Okuda D. *Star Trek Chronology: The History of the Future.* New York: Pocket Books; 1993.

Journal or Magazine Article (with volume numbers):
2. Redon J, Cifkova R, Laurent S et al. Mechanisms of hypertension in the cardiometabolic syndrome. *J Hypertens.* 2009; 27(3):441–451. doi: 10.1097/HJH.0b013e32831e13e5.

Book Article or Chapter:
3. James NE. Two sides of paradise: the Eden myth according to Kirk and Spock. In: Palumbo D, ed. *Spectrum of the Fantastic*. Westport, Conn: Greenwood; 1988:219–223.

When the manufacturers of the reagents etc. are mentioned for the first time, town, (state in the US) and country must be provided wheras for next referral only the name of the firm should be given.

Website:
4. Lynch T. DSN trials and tribble-ations review. Psi Phi: Bradley's Science Fiction Club Web site. 1996. Available at: http://www.bradley.edu/campusorg/psiphi/DS9/ep/503r.htm. Accessed October 8, 1997.

Journal Article on the Internet:
5. McCoy LH. Respiratory changes in Vulcans during pon farr. *J Extr Med* [serial online]. 1999;47:237–247. Available at: http://infotrac.galegroup.com/itweb/nysl_li_liu. Accessed April 7, 1999.